CalVal Jason-2

Jason-2 validation and cross calibration activities (Annual report 2016)

Contract No 160182-14026/00 Lot 1.6.3

Nomenclature : SALP-RP-MA-EA-23058-CLS

Issue : 1rev 2

Date : February 24, 2017

CLS - 8-10 Rue Hermès - Parc Technologique du Canal - 31520 Ramonville St-Agne - FRANCE
Telephone 33 5 61 39 47 00 / Fax 33 5 61 75 10 14

Chronology Issues:		
Issue:	Date:	Reason for change:
1rev0	November 21, 2016	Creation
1rev1	January 31, 2017	Delivery version
1rev2	February 24, 2017	Revision after comments from J-D. Desjonqueres.

People involved in this issue :	AUTHORS	COMPANY	DATE	INITIALS
Written by:	H. Roinard M. Lievin	CLS CLS		
Checked by:		CLS		
Approved by:		CLS CLS		
Application authorised by:				

Index Sheet :	
Context:	
Keywords:	
Hyperlink:	

Distribution:		
Company	Means of distribution	Names
CLS/DOS	electronic copy	G.DIBARBOURE V.ROSMORDUC
CNES	electronic copy	thierry.guinle@cnes.fr emilie.bronner@cnes.fr jean-damien.desjonqueres@cnes.fr nicolas.picot@cnes.fr aqgp_rs@cnes.fr dominique.chermain@cnes.fr delphine.vergnoux@cnes.fr

List of tables and figures

List of Tables

1 *Planned events* . . . 5
2 *Missing pass status* . . . 10
3 Edited measurement status . . . 13
4 Models and standards adopted for the Jason-2 version "T" and "c" products. Adapted from [69] . . . 15
5 Models and standards adopted for the Jason-2 version "d" products. Adapted from [69] . . . 18
6 Models and standards adopted for the Jason-2 product version "T", and "d" . . . 21
7 Editing criteria . . . 25
8 Seasonal variations of Jason SLA (cm) for years 2008 to 2016 . . . 70
9 *Correlation and rms of the differences between Jason-2 and Argo DHA referenced to 900 dbar over the period Aug. 2008 - Jul. 2016. Analyses performed for altimeter standards 2014 and 2018* . . . 75

List of Figures

1 *Percentage of missing measurements over ocean and land for JA2 and JA1* . . . 22
2 *Map of percentage of available measurements over land for Jason-2 on cycle 154 (left) and for Jason-1 on cycle 511 (right)* . . . 23
3 *Cycle per cycle percentage of missing measurements over ocean (top left), without anomalies (top right), without anomalies and with geographical selections (bottom).* . . . 24
4 *Cycle per cycle percentage of eliminated measurements during selection of ocean/lake measurements.* . . . 26
5 *Percentage of edited measurements by ice flag criterion. Left: Cycle per cycle monitoring. The blue curve shows the trend of edited measurements after adjusting for annual and semi-annual signals. Right: Map over a one year period (cycles 267 to 303).* . . . 27
6 *Percentage of edited measurements by altimeter rain flag criterion (all figures computed after iced flagged points remove). Map over a one year period (cycles 267 to 303). Left: rejected measurements where rain flag is also activated . Right: valid measurements where rain flag is activated. Bottom: All points where rain flag is activated.* . . . 28
7 *Cycle per cycle percentage of edited measurements by threshold criteria. The blue curve shows the trend of edited measurements after adjusting for annual and semi-annual signals.* . . . 29
8 *Percentage of edited measurements by 20-Hz measurements number criterion. Left: Cycle per cycle monitoring. The blue curve shows the trend of edited measurements after adjusting for annual and semi-annual signals. Right: Map over a one year period (cycles 267 to 303).* . . . 29
9 *Percentage of edited measurements by 20-Hz measurements standard deviation criterion. Left: Cycle per cycle monitoring. The blue curve shows the trend of edited measurements after adjusting for annual and semi-annual signals. Right: Map over a one year period (cycles 267 to 303).* . . . 30

10 *Percentage of edited measurements by SWH criterion. Left: Cycle per cycle monitoring. The blue curve shows the trend of edited measurements after adjusting for annual and semi-annual signals. Right: Map over a one year period (cycles 267 to 303).* . . . 31
11 *Percentage of edited measurements by Sigma0 criterion. Left: Cycle per cycle monitoring. The blue curve shows the trend of edited measurements after adjusting for annual and semi-annual signals. Right: Map over a one year period (cycles 267 to 303).* . . . 32
12 *Percentage of edited measurements by 20 Hz Sigma0 standard deviation criterion. Left: Cycle per cycle monitoring. The blue curve shows the trend of edited measurements after adjusting for annual and semi-annual signals. Right: Map over a one year period (cycles 267 to 303).* . . . 33
13 *Percentage of edited measurements by radiometer wet troposphere criterion. Left: Cycle per cycle monitoring. The blue curve shows the trend of edited measurements after adjusting for annual and semi-annual signals. Right: Map over a one year period (cycles 267 to 303).* . . . 34
14 *Percentage of edited measurements by dual frequency ionosphere criterion. Left: Cycle per cycle monitoring. The blue curve shows the trend of edited measurements after adjusting for annual and semi-annual signals. Right: Map over a one year period (cycles 267 to 303).* . . . 34
15 *Percentage of edited measurements by square off-nadir angle criterion. Left: Cycle per cycle monitoring. The blue curve shows the trend of edited measurements after adjusting for annual and semi-annual signals. Right: Map over a one year period (cycles 267 to 303).* . . . 35
16 *Cycle per cycle percentage of edited measurements by sea state bias criterion (left). The blue curve shows the trend of edited measurements after adjusting for annual and semi-annual signals. Right: Map of percentage of edited measurements by sea state bias criterion over a one year period (cycles 267 to 303).* . . . 36
17 *Percentage of edited measurements by altimeter wind speed criterion. Left: Cycle per cycle monitoring.The blue curve shows the trend of edited measurements after adjusting for annual and semi-annual signals. Right: Map over a one year period (cycles 267 to 303).* . . . 37
18 *Percentage of edited measurements by ocean tide criterion. Left: Cycle per cycle monitoring. The blue curve shows the trend of edited measurements after adjusting for annual and semi-annual signals. Right: Map over a one year period (cycles 267 to 303).* . . . 38
19 *Percentage of edited measurements by sea surface height criterion. Left: Cycle per cycle monitoring. The blue curve shows the trend of edited measurements after adjusting for annual and semi-annual signals. Right: Map over a one year period (cycles 267 to 303).* . . . 39
20 *Percentage of edited measurements by sea level anomaly criterion. Left: Cycle per cycle monitoring. The blue curve shows the trend of edited measurements after adjusting for annual and semi-annual signals. Right: Map over a one year period (cycles 267 to 303).* . . . 39
21 *Map of 20 Hz Ku-band (left) and C-band (right) MQE for Jason-2 cycle 157. Note that the color scales are different for the two maps.* . . . 41
22 *Cyclic monitoring of number of elementary 20 Hz range measurements for Jason-1 and Jason-2 for Ku-band (left) and C-band (right).* . . . 42

23 *Daily monitoring of mean and standard deviation of Jason-1 - Jason-2 differences for number of elementary 20 Hz Ku-band range measurements (left) and map showing mean of Jason-1 - Jason-2 differences over cycles 1 to 20.* . . . 42
24 *Daily monitoring of mean and standard deviation of Jason-1 - Jason-2 differences for number of elementary 20 Hz C-band range measurements (left) and map showing mean of Jason-1 - Jason-2 differences over cycles 1 to 20.* . . . 43
25 *Cyclic monitoring of rms of elementary 20 Hz range measurements for Jason-1 and Jason-2 for Ku-band (left) and C-band (right).* . . . 43
26 *Daily monitoring of mean and standard deviation of Jason-1 - Jason-2 differences for the rms of elementary 20 Hz Ku-band range measurements (left) and map showing mean of Jason-1 - Jason-2 differences over cycles 1 to 20 (right).* . . . 43
27 *Daily monitoring of mean and standard deviation of Jason-1 - Jason-2 differences for rms of elementary 20 Hz C-band range measurements (left) and map showing mean of Jason-1 - Jason-2 differences over cycles 1 to 20 (right).* . . . 44
28 *Square of the off-nadir angle deduced from waveforms (deg^2) for Jason-1 and Jason-2: Daily monitoring (left), histograms for Jason-2 cycle 157 (Jason-1 cycle 513/514).* 45
29 *Histograms of Jason-2 mispointing after retracking with different antenna beamwidth (from [101]): 1.26° (blue), 1.28° (light blue), 1.30° (dark blue).* . . . 45
30 *Cyclic monitoring of Sigma0 for Jason-1 and Jason-2 for Ku-band (left) and C-band (right). Daily monitoring of Jason-1 - Jason-2 differences (bottom), a 10 day filter is applied.* . . . 47
31 *Daily monitoring of mean and standard deviation of Jason-1 - Jason-2 differences for Ku-band Sigma0 (left) and map showing mean of Jason-1 - Jason-2 differences over cycles 1 to 20.* . . . 47
32 *Daily monitoring of mean and standard deviation of Jason-1 - Jason-2 differences for C-band Sigma0 (left) and map showing mean of Jason-1 - Jason-2 differences over cycles 1 to 20.* . . . 48
33 *Cyclic monitoring of SWH for Jason-1 and Jason-2 for Ku-band (left) and C-band (right). Daily monitoring of Jason-1 - Jason-2 differences (bottom), a 10 day filter is applied.* . . . 49
34 *Daily monitoring of mean and standard deviation of Jason-1 - Jason-2 differences for Ku-band SWH (left) and map showing mean of Jason-1 - Jason-2 differences over cycles 1 to 20.* . . . 50
35 *Daily monitoring of mean and standard deviation of Jason-1 - Jason-2 differences for C-band SWH (left) and map showing mean of Jason-1 - Jason-2 differences over cycles 1 to 20.* . . . 50
36 *Daily monitoring of mean and standard deviation of Jason-1 - Jason-2 differences for dual-frequency ionospheric correction (left) and map showing mean of Jason-1 - Jason-2 differences over cycles 1 to 20.* . . . 51
37 *Diagram of dispersion of Jason-1 (GDR-E) - Jason-2 versus Jason-2 dual-frequency ionosphere correction for Jason-2 cycle 15. Left: non-filtered, right: filtered.* . . . 52
38 *Cyclic monitoring of dual-frequency ionosphere for Jason-1 and Jason-2 (right). Daily monitoring of Jason-1 - Jason-2 differences (left), a 10 day filter is applied.* . 52
39 *Cycle per cycle monitoring of filtered altimeter ionosphere correction minus GIM ionosphere correction for Jason-1 and Jason-2. Left: Mean, right: standard deviation.* 53
40 *Cycle per cycle monitoring of filtered altimeter ionosphere minus GIM correction computed per local hour time intervals. A one-year smooth is applied.* . . . 53

41 *Daily monitoring of mean and standard deviation (left) of Jason-1 - Jason-2 radiometer wet troposphere correction. Map showing mean of Jason-1 - Jason-2 differences over cycles 1 to 20.* . . . 54
42 *Cycle per cycle monitoring of mean (left) and standard deviation (right) of radiometer minus ECMWF model wet troposphere correction over 2016 (until cycle 303) for Jason-2 O/I/GDR.* . . . 55
43 *Left: Daily monitoring of radiometer and ECMWF model wet troposphere correction differences for Jason-1 (blue) and Jason-2 (red). Right: daily monitoring for Jason-2 GDRs (red) and IGDRs (pink). Vertical green lines correspond to ECMWF model version changes, black lines correspond to AMR calibration coefficients changes on GDR products also impacting IGDR product (but later). Bottom: Daily monitoring for Jason-2 GDRs (red) for 2016. Vertical green lines correspond to ECMWF model version changes, black lines correspond to AMR calibration coefficients changes on GDR products. They impact also IGDR products (but later). Vertical gray bands correspond to yaw maneuvers on Jason-2.* . . . 56
44 *Map (**left**) and monitoring (**right**) of difference of variance at crossovers , neural approach for wet troposphere minus GDR product wet troposphere.* . . . 57
45 *Daily monitoring of mean and standard deviation (left) of Jason-1 - Jason-2 altimeter wind speed. Map showing mean of Jason-1 - Jason-2 differences over cycles 1 to 20.* . . . 58
46 *Cycle per cycle monitoring of mean (left) and standard deviation (right) of altimeter wind speed over 2016 (until cycle 303) for Jason-2 O/I/GDR.* . . . 58
47 *Daily monitoring of mean and standard deviation (left) of Jason-1 - Jason-2 sea state bias over cycles 1 to 20. DMap showing mean of Jason-1 - Jason-2 sea state bias differences over cycles 1 to 20. using SSB from Jason-1 GDR-E and updated (2012) SSB for Jason-2 (map centered around +0.34 cm) (right).* . . . 59
48 *Top: Monitoring of mean of SSH crossover differences for Jason-2 and Jason-1 using Jason-2 (red), Jason-1 GDR-E (blue), Jason-2 GDR-D Upd with GOT4.10 + POE-E + Tran2012 SSB (pink). Bottom: Monitoring of mean of SSH crossover differences for different data types of Jason-2: OGDR (blue), IGDR (green), GDR (red): over 2016 (left) and over 4 years (right).* . . . 61
49 *Left: Map of mean of SSH crossovers differences for Jason-2 cycle 1 to 303. note that for cycles 1 to 253, GDR orbit is POE-D. GDR have been available with orbit POE-E since cycle 254. Right: Map of mean of SSH crossovers differences for Jason-2 cycle 1 to 253 using final POE-E orbit solution.* . . . 62
50 *Cycle by cycle standard deviation of SSH crossover differences for Jason-2 and Jason-1. Only data with abs(latitude) < 50°, bathymetry < -1000m and low oceanic variability were selected.* . . . 63
51 *Monitoring (left) and periodogram (right) of pseudo time-tag bias estimated cycle by cycle from GDR products for Jason-2 and Jason-1* . . . 63
52 *Cycle by cycle monitoring of SSH bias between Jason-1 and Jason-2 before and after Jason-1 ground-track change (black curve and dots) and SSH bias without applying corrections in SSH calculation for both missions only during the tandem phase (gray curve).* . . . 65
53 ***Top left:** Maps of SLA (orbit (POE-E) - range - geophysical corrections - MSS 2011 (ref20)) mean differences between Jason-1 and Jason-2 during tandem phase (cycles 1 to 20), using Jason-2 updated GDR-D and Jason-1 GDR-E (the map is centered around the mean of 0.2 cm).**Top right:** without applying geophysical corrections. **Bottom:** using GSFC09 orbits without applying geophysical corrections* . . . 66

54 *Cycle by cycle monitoring of SLA standard deviation for Jason-1 and Jason-2.* . . . 67
55 *MSL evolution calculated from T/P, Jason-1 and using Jason-2 data from October 2008 onwards. GIA (-0.3 mm/yr, [90]) is applied.* . . . 72
56 *Global MSL trend evolution calculated for Jason-2 (top left). MSL trend evolution when separating in ascending and descending passes (top right) , Seasonal signal (annual and semi-annual) is adjusted for top figures. Bottom: Difference of MSL slopes (MSL ascending passes - MSL descending passes) for Jason-2. Slopes are computed for 2 month filtered data. GIA correction is not applied. Bottom right: periodogram of MSL difference (MSL ascending passes - MSL descending passes)* . . 73
57 *Maps of regional MSL slopes for Jason-2 cycles 1 to 303, seasonal signal removed.* . 73
58 Time series of global average differences between Jason-2 and tide gauges, with (58a) and without the seasonnal cycle (58b). The red points represent the raw data while the blue curve is obtained after applying a two months running mean filter 74
59 *Left : EOF mode 2 of the orbit differences and the contour defining areas of significant positive and negative difference. Right : SSH differences (cm) between altimeter and Argo data for Jason-2 computed with the GEOC-VERT (top) and POE-E (bottom) orbit solutions.* . . . 75
60 SLA spectra for Jason-2/Jason-3 and SARAL Altika from respectively 20 Hz and 40 Hz measurements . . . 77
61 Editing procedure adapted to high rate measurements for Jason-2/Jason-3 and SARAL/Altika missions . . . 78
62 Map of SLA variance reduction applying new editing and Zaron's method (V1) compared to data processed with classical 1-Hz editing procedure (V0), after filtering out along-track data lower than 200 km. . . . 79
63 *SLA spectra applying new editing and Zaron's method (V1) compared to data processed with classical 1-Hz editing procedure (V0) : classical power spectral density spectra with theoretical spectra superimposed (dashed lines) on left and spectra differences between classical and theoretical spectra on right. Theoretical spectrum is defined from the oceanic slope (as observed by model) and the white noise level (plateau).* 79
64 Map of the mean difference of SSH at crossovers . . . 80
65 *On left : GSFC12 - Rigth : GSFC15- Bottom: GDR E* . . . 81

List of items to be defined or to be confirmed

Applicable documents / reference documents

Contents

1. Introduction **1**

2. Processing status **3**
2.1. **Processing** . . . 3
2.2. **CAL/VAL status** . . . 3
2.2.1. List of events . . . 3
2.2.2. Missing measurements . . . 6
2.2.3. Edited measurements . . . 11
2.3. **Models and Standards History** . . . 13

3. Data coverage and edited measurements **22**
3.1. **Missing measurements** . . . 22
3.1.1. Over land and ocean . . . 22
3.1.2. Over ocean . . . 23
3.2. **Edited measurements** . . . 24
3.2.1. Editing criteria definition . . . 24
3.2.2. Selection of measurements over ocean and lakes . . . 25
3.2.3. Flagging quality criteria: Ice flag . . . 27
3.2.4. Flagging quality criteria: Rain flag . . . 27
3.2.5. Threshold criteria: Global . . . 28
3.2.6. Threshold criteria: 20-Hz measurements number . . . 29
3.2.7. Threshold criteria: 20-Hz measurements standard deviation . . . 30
3.2.8. Threshold criteria: Significant wave height . . . 31
3.2.9. Backscatter coefficient . . . 32
3.2.10. Backscatter coefficient: 20 Hz standard deviation . . . 32
3.2.11. Radiometer wet troposphere correction . . . 33
3.2.12. Dual frequency ionosphere correction . . . 34
3.2.13. Square off-nadir angle . . . 34
3.2.14. Sea state bias correction . . . 36
3.2.15. Altimeter wind speed . . . 37
3.2.16. Ocean tide correction . . . 38
3.2.17. Sea surface height . . . 38
3.2.18. Sea level anomaly . . . 39

4. Monitoring of altimeter and radiometer parameters **40**
4.1. **Methodology** . . . 40
4.2. **20 Hz Measurements** . . . 40
4.2.1. 20 Hz measurements number in Ku-Band and C-Band . . . 41
4.2.2. 20 Hz measurements standard deviation in Ku-Band and C-Band . . . 42
4.3. **Off-Nadir Angle from waveforms** . . . 45
4.4. **Backscatter coefficient** . . . 46
4.5. **Significant wave height** . . . 49
4.6. **Dual-frequency ionosphere correction** . . . 51
4.7. **AMR Wet troposphere correction** . . . 54
4.7.1. Overview . . . 54
4.7.2. Comparison with the ECMWF model . . . 55
4.7.3. Neural approach for wet tropospheric correction . . . 56
4.8. **Altimeter wind speed** . . . 58

4.9. **Sea state bias** . . . 59

5. SSH crossover analysis **60**
5.1. **Overview** . . . 60
5.2. **Mean of SSH crossover differences** . . . 60
5.3. **Standard deviation of SSH crossover differences** . . . 62
5.4. **Estimation of pseudo time-tag bias** . . . 63

6. Sea Level Anomalies (SLA) Along-track analysis **64**
6.1. **Overview** . . . 64
6.2. **Mean of SLA differences between Jason-2 and updated Jason-1** . . . 64
6.3. **Standard deviation of SLA differences between Jason-2 and Jason-1** . . . 67
6.4. **Sea level seasonal variations** . . . 67

7. Mean Sea Level (MSL) calculation **71**
7.1. **Altimeter Mean Sea Level evolution** . . . 71
7.1.1. Mean sea level (MSL) calculation of reference time serie . . . 71
7.1.2. Regional and global mean sea level trend for Jason-2 . . . 72
7.2. **External data comparisons** . . . 74
7.2.1. Comparison with tide gauges . . . 74
7.2.2. Altimeter calibration and validation by comparison with Argo in-situ measurements . . . 74

8. Investigations **76**
8.1. **Altimetry errors for submesoscale** . . . 76
8.1.1. Error Description . . . 76
8.1.2. Expected Improvements . . . 77
8.2. **Assessment of orbit quality through the SSH calculation towards POE-E standards** . . . 80
8.2.1. Quality of the current CNES POE orbits . . . 80
8.2.2. Quality of the GSFC orbits . . . 81
8.2.3. Impact on orbits of the geocenter position change . . . 81

9. Appendix **82**
9.1. **Jason-2 performance assessment: from meso-scale to climate** . . . 82

10. References **84**

1. Introduction

This document presents the synthesis report concerning validation activities of Jason-2 GDRs under SALP contract (N° 160182-14026/00 Lot 1.6.3) supported by CNES at the CLS Space Oceanography Division. It covers several points: CAL/VAL Jason-2 activities, Jason-2 / Jason-1 cross-calibration (until mid-2013), particular studies and investigations.
The OSTM/Jason-2 satellite was successfully launched on June, 20th 2008. Since July, 4th, Jason-2 is on its operational orbit. Until January 2009, it was flying in tandem with **Jason-1**, only 55s apart. Note that from May 2012 onwards, Jason-1 was on a geodetic orbit (see note on Jason-1 geodetic mission [9]). Jason-1 sent its last measurement on 21st June 2013, after about 11.5 years in orbit. Jason-2 was moved from its original groundtrack to its new interleaved groundtrack on October 2016: October 2nd at 11 :53 UTC (end of cycle 303) the Poseidon-3 altimeter is put in WAIT mode. During move to interleaved ground track, there is no more measurement until the end of the orbit change nominal sequence scheduled until 13-10-2016 at 20:00:00 (cycle 305, pass 164). Since the beginning of the mission, Jason-2 data have been analyzed and monitored in order to assess the quality of Jason-2 products. Cycle per cycle reports are available on AVISO webpage (http://www.aviso.altimetry.fr/en/data/calval/systematic-calval.html).
This present report assesses the Jason-2 data quality. Missing and edited measurements are monitored. Furthermore relevant parameters derived from instrumental measurements and geophysical corrections are analyzed.
During 2012, the whole Jason-2 mission was reprocessed in GDR-D standard. For more details, please refer to the reprocessing report ([17]), spanning the reprocessing period (cycles 001 to 145), which contains comparisons between previous GDR-T and current GDR-D standard, as well as comparison between Jason-2 GDR-D and Jason-1 and Envisat data. Another report ([16]) focuses on the comparison of Jason-2 GDR-T and GDR-D with Jason-1 data during the first 20 Jason-2 cycles (the tandem phase, when both satellites were on the same ground-track only 55s apart).

Hereafter, analyzes focus on Jason-1/Jason-2 cross-calibration. During the tandem configuration (4th July 2008 to 26th January 2009) both satellites were on the same ground track. This allowed to precisely assess parameter discrepancies between both missions in order to detect geographically correlated biases, jumps or drifts. The SLA performances and consistency with Jason-1 are also described. But even during the formation flight phase (after the end of the tandem phase), and after Jason-1 moved to its geodetic orbit, comparison were still possible until the end of the Jason-1 mission in June 2013. Even if only low order statistics are mainly presented here, other analyzes including histograms, plots and maps are continuously produced and used in the quality assessment process. As Jason-1 data were reprocessed recently, the new GDR-E version of Jason-1 data are used and presented in this report (for more information about Jason-1 GDR-E data, see [13])
It is now well recognized that the usefulness of any altimeter data only makes sense in a multi-mission context, given the growing importance of scientific needs and applications, in particular for operational oceanography. One major objective of the Jason-2 mission is to continue the Jason-1 and T/P high precision altimetry and to allow combination with other missions (ENVISAT, Jason-1, SARAL/AltiKa). This kind of comparisons between different altimeter missions flying together provides a large number of estimations and consequently efficient long term monitoring of instrument measurements.
An ISRO (Indian Space Research Organization)/CNES satellite, SARAL (Satellite with ARgos and ALtika), embarks the **AltiKa** altimeter (working in Ka-band, 35 GHz), built by CNES, as well as a DORIS and an Argos instruments. The launch of this mission on 25th of February 2013 allows

to complete the altimetry constellation from 2013 onwards, re-occupying the long-term ERS and Envisat ground track. Comparisons between AltiKa and Jason-2 data are available in [28].
Jason-3 was launched on 2016, January 17th. By continuing long-term operational oceanography observations, Jason-3 will be a key element of the constellation of altimetry satellites in the years ahead. Succeeding Jason-2, it boasts a number of enhancements to its systems and in processing of the data it will deliver [21]. Cross-calibration analyzes between Jason-2 and Jason-3 are also performed, but shown in annual report of Jason-3 (see [21]).
Finally, **Sentinel-3** was launched on 2016, February 16th. The Sentinel-3 satellite fits into the Copernicus program, a joint project between Esa and European Union. It is dedicated to Earth monitoring and operational oceanography. This project is the European answer to the needs still growing related to the global environment.

2. Processing status

In this report, GDR-D from cycle 1 to 303(until 02/10/2016) and IGDR until cycle 309(26/11/2016) are considered.

2.1. Processing

End of 2008 Jason-2 data were already available to end users in OGDR (3h data latency) and IGDR (1-2 days data latency). They were first released in version T and switched at cycle 015 to version C. They stayed in this version till cycle 149 (till 2012/07/31 12:01:59 for OGDR). GDR data were released in version T during August 2009. During 2012 the whole GDR dataset was reprocessed in GDR-D version.

A description of the different Jason-2 products is available in the OSTM/Jason-2 Products handbook ([69]). Note that since 5th of April 2013 (cycle 175), platform moduleB has been used. During cycle 226 and 227, the precise orbit ephemeris (orbit in GDR) was based on DORIS and SLR only due to payload GPS unavailability. Since cycle 228, GPS-B (instead of GPS-A) is operational. The purpose of this document is to report the major features of the data quality from the Jason-2 mission. As Jason-2 was in tandem with Jason-1 (only 55 s apart) until January 2009, this report also uses results from intercalibration with Jason-1 (please note that GDR-E Jason- data are used in this report. For more details concerning Jason-1 reprocessing in GDR-E standards, see [13]).

2.2. CAL/VAL status

2.2.1. List of events

The following table shows the major planned events during the Jason-2 mission.

Dates	Events	Impacts
4 July 2008 5h57	Start of Jason-2 Cycle 0	
4 July 2008 12h15	Start of Poseidon3 altimeter. Tracking mode : autonomous acquisition, median	Start of level2 product generation.
04 July 2008 13:47:52 to 04 July 2008 14:13:36	Poseidon3 altimeter. Tracking mode : Diode acquisition, median	
04 July 2008 14:14:39 to 17 July 2008 15:30:22	Poseidon3 altimeter. Tracking mode : Diode acquisition, SGT	
8 July 2008 4h45 - 5h25	Poseidon3 altimeter. Dedicated period for validation of tracking mode performances	small data gaps on corresponding passes [Cycle 0]
		.../...

Dates	Events	Impacts
11 July 2008 13h00-13h01 and 13h04-13h12	Poseidon3 altimeter. Tracking mode : Diode-DEM (functional)	Functional test of DIODE-DEM tracking mode while onboard DEM was not correct, leading to wrong waveforms and so impacts on altimeter retracking outputs.
12 July 2008 1h20	Start of Jason-2 Cycle 1	
16 July 2008 7h10-17h08	upload Poseidon-3 - DEM	Data gap on corresponding passes [Cycle 1, Pass 108-144]
17 July 2008 7h29-11h30	upload Poseidon-3 - DEM	Data gap on corresponding passes [Cycle 1, Pass 108-144]
17 July 2008 15:30:22 to 31 July 2008 21:17:08 UTC	Poseidon-3 altimeter. Tracking mode : Diode acquisition, median	
21 July 2008 23h18	Start of Jason-2 Cycle 2	
31 July 2008 21:17:09 to 10 August 2008 19:15:39	Jason-2 Cycle 3: Poseidon3 altimeter. Tracking mode : Diode-DEM	
10 August 2008 19:15:40 to 20 August 2008 17:14:10	Jason-2 Cycle 4: Poseidon3 altimeter. Tracking mode : Diode acquisition, median	
20 August 2008 17:14:11 to 30 August 2008 15:12:43	Jason-2 Cycle 5: Poseidon3 altimeter. Tracking mode : Diode-DEM	
30 August 2008 15:12:43 to 9 September 2008 13:11:15	Jason-2 Cycle 6: Poseidon3 altimeter. Tracking mode : Diode acquisition, median	
9 September 2008 13:11:15 to 19 September 2008 11:09:47	Jason-2 Cycle 7: Poseidon3 altimeter. Tracking mode : Diode-DEM	
19 September 2008 11:09:47 to 29 September 2008 09:08:19	Jason-2 Cycle 8: Poseidon3 altimeter. Tracking mode : Diode acquisition, median	
11 Mai 2009 12:09 to 14 Mai 2009 13:09	Upload Poseidon-3 (new DEM)	data gaps (northern hemisphere) for passes 154 to 231

.../...

Dates	Events	Impacts
2 February 2009 06:55:11 to 15:58:05	software upload to Poseidon-3	data gap between passes 204 and 213
4 June 2009 06:31:27 to 14 June 2008 04:29:59	Jason-2 Cycle 34: Poseidon3 altimeter. Tracking mode : Diode-DEM	
12 February 2010	Upload of Doris V8.0 flight software	improved OGDR orbit accuracy
16 September 2010	Jason-2 Cycle 81: Upload of DEM patch for Gavdos transponder calibration	data gap for passes 087 and 237
17 February 2011	GPSP OBS revert upload	
12-14 September 2012	DORIS OBS upload (DORIS restart on 19th September)	OGDR data gap (during the DORIS restart)
15 May 2013	update on Usingen receiver was done on 15-May-2013 at 11:05Z in order to solve a problem with the TM receiver	
5-15 March 2014	Tracking mode : Diode-DEM	gain of available measurements on earth
18 March 2014	Update of TRIODE software (for OGDR).	Reduction of 14days signal in OGDR SLA.
22 June-2 July 2014	Tracking mode : Diode-DEM	gain of available measurements on earth
9 September 2014	cycle 228: switch to GPS-B (instead of GPS-A)	
25 May 2015	cycle 254: orbit standard switches to POE-E from this cycle onwards.	
5-6 April 2016	cycle 285: upload of new GPS On Board software	Data gap: no scientific products have been processed between April, 5 at 13:35:10 and April, 6 at 12:02:40.
2-13 October 2016	from cycle 304 pass 001 to cycle 305 pass 163: move to interleaved ground track	Data gap: Poseidon-3 altimeter is put in WAIT mode.
4-6 October 2016	upload of a new DEM	

Table 1 – Planned events

2.2.2. Missing measurements

This section presents a summary of major satellite or ground segment events that occurred from cycle 0 to 303. Table 2 gives a status about the number of missing passes (or partly missing) for GDRs, as well as the associated events for each cycle.

During 2016, cycles 271 to 303 were analyzed. Few altimetry data were missing due to technical or operator problems. Except these cases, missing measurements are mostly due to scheduled events (like altimeter expert calibrations performed every 6 month or software upload).
The following table gives an overview over missing data and why it is missing.

Jason-2 Cycles/Pass	Dates	Events
000/222-224	10/07/2008 - 18:28:02 to 20:25:04	Missing telemetry (Usingen station pb)
000/232	11/07/2008 - 03:57:08 to 04:30:30	Partly missing due to altimeter calibration (long LPF)
000/235	11/07/2008 - 07:01:28 to 07:27:41	Partly missing due to altimeter calibration (CNG step)
001/44-46	13/07/2008 - 17:40:00 to 19:37:30	Missing telemetry (Usingen station pb)
001/48-50	13/07/2008 - 21:37:02 to 23:30:00	Missing telemetry (NOAA station pb)
001/108-144		several passes partly missing due to upload of new DEM (planned unavailability)
003/032-035	02/08/2008 - 02:23:45 to 05:46:30	Passes 32 and 35 are partly missing, passes 33 and 34 are completely missing due to missing telemetry (Usingen)
005/236-241	29/08/2008 - 21:44:56 to 30/08/2008 02:52:07	Missing telemetry (Usingen station pb): passes 237 to 240 completely missing, passes 236 and 241 partly missing
006/232	08/09/2008 - 15:48:00 to 16:21:22	pass 232 partially missing due to altimeter calibration (long LPF)
006/235	08/09/2008 - 18:53:00 to 19:19:10	pass 235 partially missing due to altimeter calibration (CNG step)
016/73	10/12/2008 - 15:11:19 to 15:13:27	pass 73 partially missing due to 1) upload of correction for low signal tracking anomaly and 2) memory dumps (planned unavailability)
		.../...

Jason-2 Cycles/Pass	Dates	Events
026/33	18/03/2009 - 05:09:15 to 05:10:44	pass 33 has approximately 90 seconds of missing ocean measurements in gulf of guinea (probably due to missing telemetry)
029/209-210	23/04/2009 - 20:18:36 to 20:35:11	data gap over land (on transition between passes 209 and 210) due to missing telemetry
031/154-231	11/05/2009 12:09 to 14/05/2009 13:09	Upload of new DEM leading to missing portions (northern hemisphere) for passes 154 to 231
033/204-213	02/06/2009 - 06:55:11 to 15:58:05	Passes 205 to 212 are completely missing. Passes 204 and 213 are partly missing with respectively 100% and 96% of missing measurements over ocean. This is due to software upload to Poseidon-3.
034/232	13/06/2009 - 07:07:03 to 07:40:23	Due to long calibration, pass 232 is partly missing with 65% of missing measurements over ocean.
034/235	13/06/2009 - 10:11:41 to 10:37:50	Due to calibration CNG step, pass 235 is partly missing with 8% of missing measurements over ocean.
037/54	06/07/2009 - 02:33:12 to 02:34:33	pass 054 has a small data gap due to missing PLTM
053/57	11/12/2009 - 20:38:19 to 21:29:43	passes 57 and 58 have a data gap due to Gyro calibration
053/232	18/12/2009 - 16:39 to 17:12	pass 232 has a data gap due to CAL2 calibration
053/235	18/12/2009 - 19:43	pass 235 has a 26 minutes data gap due to CNG calibration (mostly over land)
072/199	23/06/2010 - 19:15:37 to 19:16:59	pass 199 has small data gap due to missing telemetry
073/232	05/07/2010 - 00:09:33 to 00:42:54	pass 232 has a data gap due to CAL2 calibration
073/235	05/07/2010 - 03:14:11 to 03:40:20	pass 235 has a data gap due to CNG calibration (mostly over land)
081/087	16/09/2010 - 16:40:22 to 16:52:48	pass 087 has a data gap due to upload of DEM update (for GAVDOS transponder calibration)
081/237	22/09/2010 - 13:07:27 to 13:18:12	pass 237 has a data gap due to upload of DEM update (for GAVDOS transponder calibration)
084/031	14/10/2010 - 06:02 to 06:11:15	Calibration (I2 and Q2)

.../...

Jason-2 Cycles/Pass	Dates	Events
084/031-032	14/10/2010 - 06:12 to 06:21:15	Calibration (I and Q)
084/043	14/10/2010 - 17:00:57 to 17:02:39	pass 043 has a small data gap due to missing PLTM
094/231	29/01/2011 - 04:50 to 04:55	Calibration CAL1 (14% of missing ocean data)
094/232	29/01/2011 - 05:38 to 06:11	Calibration CAL2 (65% of missing ocean data)
094/235	29/01/2011 - 08:37 to 09:03	Calibration CNG (mostly over land, 9% of missing ocean data)
101/133-135	04/04/2011 - 18:49:08 to 21:03:48	Telemetry outage at Usingen, passes 133 to 135 have respectively 23%, 100%, and 91% of missing ocean data
110/158-159	04/07/2011 - 00:27:29 to 01:27:29	Gyro calibration. Passes 158 and 159 have respectively 18% and 88% of missing ocean data
115/232	25/08/2011 - 11:07:35 to 11:40:56	Calibration CAL2: 65% of missing ocean data
115/235	25/08/2011 - 14:12 to 14:38	Calibration CNG: mostly over land, 8% of missing ocean data
132/232	10/02/2012 - 00:42:26 to 01:14:03	Calibration CAL2: 65% of missing ocean data
132/235	10/02/2012 - 03:47:11 to 04:13:20	Calibration CNG: mostly over land, 8% of missing ocean data
135/105	05/03/2012 - 19:54:49 to 20:26:14	technical problem and operator error: 25% of missing ocean data
136/191	19/03/2012 - 02:15:18 to 02:50:11	problem of ACK: 56% of missing ocean data
145/143	14/06/2012 - 11:41:15 to 11:42:58	pass 143 has a small data gap due to missing telemetry
145/248	18/06/2012 - 13:20:10 to 13:21:29	pass 248 has a small data gap
147/022	29/06/2012 - 13:45:30 to 13:49:46	pass 022 has a small data gap due to missing telemetry (8% of missing ocean data)
147/134	03/07/2012 - 22:41:25 to 22:43:58	pass 134 has a small data gap due to operator error (5% of missing ocean data)

.../...

Jason-2 Cycles/Pass	Dates	Events
154/210	14/09/2012 - 07:45:08 to 07:46:07	pass 210 has a small portion of missing data in central Pacific
156/232	05/10/2012 - 00:07:08 to 00:40:30	Calibration CAL2: 66% of missing ocean data
156/235	05/10/2012 - 03:11:47 to 03:37:57	Calibration CNG: mostly over land, 9% of missing ocean data
168/158-159	29/01/2013 - 03:08:20 to 04:02:37	Gyro calibration. Passes 158 and 159 have respectively 14% and 100% of missing ocean data
172/96-97	07/03/2013 - 08:18:37 to 09:30:49	Operator error. Passes 96 and 97 have respectively 72% and 52% of missing ocean data
174/43-161	25/03/2013 - 02:42 to 29/03/2013 17:53	First Safe Hold Mode. Pass 43 has 63% of missing ocean data and passes 44 to 161 are entirely missing
174-191/175-83	30/03/2013 - 21:57 to 05/04/2013 14:49	Second Safe Hold Mode. About cycle 174, pass 191 has 9% of missing ocean data and passes 192 to 254 are entirely missing. About cycle 175, passes 1 to 82 are entirely missing and pass 83 has 90% of missing measurements over ocean.
178/234		Due to a problem with TM receiver, pass 234 is partly missing (north of pacific) and has 10% of missing measurements over ocean
179/ 38		Due to a problem with TM receiver, pass 38 has 6.8% of missing measurements over ocean
182/235	19/06/2013 from 22 :33 :29 to 22 :59 :37	pass 235 has a data gap due to CNG calibration (mostly over land)
190/185 - 191/116	05/09/2013 at 07 :44 :17 to 12/09/2013 at 12 :25 :52	Third Safe Hold Mode. Concerning cycle 190, pass 185 has 10.2% of missing measurements over sea and passes 186 to 254 are entirely missing. Concerning cycle 191, passes 1 to 115 are missing.
197/035	07/11/2013 - 20:45	Pass 35 has a small data gap.
198/235	25/11/2013 - 14:04:02 to 14:37:35	Calibration (I and Q) with 8% of missing ocean data
207/178	20/02/2014 - 14:30:33 to 14:43:50	24.6% of global missing data and 11.8% missing data over ocean due to DEM upload
208/027	24/02/2014 - 14:38:26 to 14:52:07	40.7% missing data over ocean due to recurring network problems between Fairbanks and SOCC

.../...

Jason-2 Cycles/Pass	Dates	Events
218/235	11/06/2014 - 21:34:36 to 22:13:13	Poseidon3/Jason2 special calibration. 9% missing data over ocean
222/114	16/07/2014 - between 20:05:19 and 20:10:34 and between 20:23:21 and 20:34:51	Gyro calibration. Pass 114 has 73% of missing ocean data
226/235	07/12/2014 - 09:13:54 TU (26 minutes and 10 seconds)	Poseidon3/Jason2 special calibration. Only 8.3% of missing measurements over ocean (most of the missing measurements are over land.)
247/227-228		Passes 227 and 228 are partly missing due to telemetry dropouts during pass and ack sent by mistake at ground station. 13.91% of pass 228 is missing (over land only). 80.37% of pass 227 is missing (76.69% over sea).
256/235	23/06/2015 16:44:28 TU (26 minutes and 10 seconds)	Poseidon3/Jason2 special calibration. Only 8.3% of missing measurements over ocean (most of the missing measurements are over land.)
275/235	29/12/2015 02:16:30 TU (26 minutes and 10 seconds)	Poseidon3/Jason2 special calibration. Only 8.3% of missing measurements over ocean (most of the missing measurements are over land.)
285/217-241	05/04/2016 13:35:10 to 06/04/2016 12:02:40	Upload of new GPS On Board software.
287/024	17/04/2016 20:15:50 to 20:39:41	Data dropout at Fairbanks (pass 024 is partly missing)
294/211	03/07/2016 - 13:26:00 TU (26 minutes and 10 seconds)	Poseidon3/Jason2 special calibration.
297/123	29/07/2016	cycle 297 pass 123 has dotted line of missing measurements : 66 points over ocean
304/001-305/164	02/10/2016 11:53:32 to 13/10/2016 20:00:00	move to interleaved ground track. Data gap: Poseidon-3 altimeter is put in WAIT mode.

Table 2 – Missing pass status

2.2.3. Edited measurements

Table 3 indicates particular high editing periods (see section 3.2.1.). Most of the occurrences correspond to radiometer wet troposphere correction at default value (due to AMR unavailability) or altimeter low signal tracking anomaly (AGC anomaly), though the latter concerns only few measurements and was corrected during cycle 16.
There are three AMR anomaly events between cycle 271 and cycle 303.

Jason-2 Cycles/Passes	Date	Comments
000/89	05/07/08 - 14:22:07 to 14:23:38	Partly edited by several parameters out of threshold (AGC anomaly)
000/134	07/07/08 - 08:06:37 to 08:28:57	Partly edited by several parameters out of threshold (AGC anomaly)
000/156	08/07/08 - 04:35:12 to 05:31:01	rain flag is set (dotted), probably related to start/stop sequence (from 04:45 to 05:24)
000/234	11/07/08 - 05:45:12 to 05:49:03	Partly edited by several parameters out of threshold (AGC anomaly)
000/241	11/07/08 - 13:04:27 to 13:09:11	Partly edited by ice flag (number of elementary Ku-band measurements at 0, AGC=16.88) due to test of altimeter DEM mode
001/		several passes partly edited by several parameters out of threshold (AGC anomaly)
002/		several passes partly edited by several parameters out of threshold (AGC anomaly)
004/		several passes partly edited by several parameters out of threshold (AGC anomaly)
006/		several passes partly edited by several parameters out of threshold (AGC anomaly)
008/		several passes partly edited by several parameters out of threshold (AGC anomaly)
009/		several passes partly edited by several parameters out of threshold (AGC anomaly)
010/		several passes partly edited by several parameters out of threshold (AGC anomaly)
011/		several passes partly edited by several parameters out of threshold (AGC anomaly)
		.../...

Jason-2 Cycles/Passes	Date	Comments
012/		several passes partly edited by several parameters out of threshold (AGC anomaly)
013/		several passes partly edited by several parameters out of threshold (AGC anomaly)
014/		several passes partly edited by several parameters out of threshold (AGC anomaly)
015/		several passes partly edited by several parameters out of threshold (AGC anomaly)
019/024-042	07/01/ 11:00:35 to 08/01/2009 03:23:34	radiometer wet troposphere correction at default value due to AMR unavailability
019/119-161	11/01/ 03:56:38 to 12/01/2009 19:26:14	radiometer wet troposphere correction at default value due to AMR unavailability
110/047	29/09/2011 16:14 to 16:20	a portion of pass 47 is edited by radiometer wet troposphere correction out of threshold or at default values (radio-frequency interference from a ground based source)
168/141-144	28/01/2013 10:50 to 13:22	radiometer wet troposphere correction at default value due to AMR unavailability
169/176-181	08/02/2013 17:37 to 22:44	radiometer wet troposphere correction at default value due to AMR unavailability
174/162-163	29/03/2013 17:53 to 29/03/2013 19:36	radiometer wet troposphere correction at default value after first Safe Hold Mode
175/83-85	05/04/2013 14:18 to 16:27	radiometer wet troposphere correction at default value after second Safe Hold Mode
191/116-125	12/09/2013 12:25:52 to 21:56:39	radiometer wet troposphere correction at default value after third Safe Hold Mode
194/227	16/10/2013 15:02:08 to 15:04:17	a part of pass 227 is rejected near Kamchatka Peninsula because of ice flag (linked to high radiometer minus model wet troposphere difference, and probably related to typhoon WIPHA that happened in the region between the 15th and 17th October 2013)
238/020-043	18/12/2014 19:18:48 to 19/12/2014 17:47:57	AMR unavailability: No AMR data. Passes 21 to 42 are completely edited. Passes 20 and 43 are partly edited with respectively 33.73%, and 20.28% of edited measurements.

.../...

Jason-2 Cycles/Passes	Date	Comments
269/111-115	25/10/2015 from 18:18 to 22:25	Anomaly on AMR-H leading to radiometer unavailability: Passes 112,113,114 are fully edited; Passes 111 and 115 are partially edited with respectively 15% and 93% of ocean data due to radiometer wet tropospheric correction at default values.
277/35-37	10/01/2016 02:45:05 to 05:03:03	Anomaly on AMR: passes 35, 36 and 37 have respectiveley 44%, 100% and 81% of rejected measurements
279/17-20	19/01/2016 05:58:31 to 08:21	Due to AMR reset, missing radiometer data for part of passes 17 and 20 and whole passes 18 and 19
285/85-87	31/03/2016 09:30:52 to 11:39:11	Due to AMR anomaly, missing radiometer data for part of passes 85 and 87 and whole pass 86

Table 3 – Edited measurement status

2.3. Models and Standards History

Three versions of the Jason-2 Operational Geophysical Data Records (OGDRs) and Interim Geophysical Data Records (IGDRs) have been generated up to now. These three versions are identified by the version numbers "T" (for test), "c" and "d" in the product filename. For example, version "T" IGDRs are named "JA2_IPN_2PT", version "c" IGDRs are named "JA2_IPN_2Pc", and version "d" IGDRs are named "JA2_IPN_2Pd". All three versions adopt an identical data record format as described in Jason-2 User Handbook ([69]). Versions "T" and "c" differ only slightly (names of variables are corrected and 3 variables added). Version "T" O/IGDRs were the first version released soon after launch and was disseminated only to OSTST community. Version "c" O/IGDRs were first implemented operationally from data segment 141 of cycle 15 for the OGDRs (3rd December 2008) and cycle 15 for the IGDRs. Version "c" of Jason-2 data is consistent with version "c" of Jason-1 data. Version "d" O/IGDRs were first implemented operationally from data segment 78 of cycle 150 for the OGDRs (31st July 2012) and cycle 150 for the IGDRs. GDR data switched to version "d" from cycle 146 onwards, but previous cycles 1 to 145 were reprocessed in version "d" during 2012. Therefore the whole Jason-2 mission is available in GDR version "d". The tables 4 and 5 below summarize the models and standards that are adopted for versions "T" / "c" and "d" of Jason-2 data. More details on some of these models are provided in Jason-2 User Handbook document ([69]).
Impact of GDR reprocessing can be found in the reprocessing reports [17] and [16].
Note that orbit switched to standard POE-E from GDR cycle 254 onwards.
From cycle 170 to 178, the flag "qual_inst_corr_1hz_sig0_ku" was wrongly set to one because of an out of thresholds criterion. From cycle 179 onwards, the flag "qual_inst_corr_1hz_sig0_ku" won't constantly be set as the threshold used to set this flag has been adjusted in the processing chain, in order to take into account the natural instrumental drift.

Model	Product version "T" and "c"
Orbit	Based on Doris onboard navigator solution for OGDRs. DORIS tracking data for IGDRs (DORIS + SLR tracking for cycles 20 to 78) DORIS+SLR+GPS tracking data for GDRs. Using POE-C
Altimeter Retracking	"Ocean" retracking: MLE4 fit from 2nd order Brown model: MLE4 simultaneously retrieves the following 4 parameters from the altimeter waveforms: • Epoch (tracker range offset) → altimeter range • Composite Sigma → SWH • Amplitude → Sigma0 • Trailing Edge slope → Square of mispointing angle "Ice" retracking: Geometrical analysis of the altimeter waveforms, which retrieves the following parameters: • Epoch (tracker range offset) → altimeter range • Amplitude → Sigma0
Altimeter Instrument Corrections	Consistent with MLE4 retracking algorithm.
Jason-2 Advanced Microwave Radiometer (AMR) Parameters	Using calibration parameters derived from long term calibration tool developed and operated by NASA/JPL.
Dry Troposphere Range Correction	From ECMWF atmospheric pressures and model for S1 and S2 atmospheric tides
Wet Troposphere Range Correction from Model	From ECMWF model
Ionosphere correction from model	Based on Global Ionosphere TEC Maps from JPL
Sea State Bias Model	Empirical model derived from 3 years of MLE4 Jason-1 altimeter data with version "b" geophysical models.
Mean Sea Surface Model	CLS01
Mean Dynamic Topography Model	MDT_RIO_2005
	.../...

Model	Product version “T” and “c”
Geoid	EGM96
Bathymetry Model	DTM2000.1
Inverse Barometer Correction	Computed from ECMWF atmospheric pressures after removing S1 and S2 atmospheric tides
Non-tidal High-frequency De-aliasing Correction	Mog2D high resolution ocean model on I/GDRs. None on OGDRs. Ocean model forced by ECMWF atmospheric pressures after removing S1 and S2 atmospheric tides.
Tide Solution 1	GOT00.2 + S1 ocean tide . S1 load tide ignored
Tide Solution 2	FES2004 + S1 and M4 ocean tides. S1 and M4 load tides ignored
Equilibrium long-period ocean tide model.	From Cartwright and Taylor tidal potential.
Non-equilibrium long-period ocean tide model.	Mm, Mf, Mtm, and Msqm from FES2004
Solid Earth Tide Model	From Cartwright and Taylor tidal potential.
Pole Tide Model	Equilibrium model
Wind Speed from Model	ECMWF model
Altimeter Wind Speed	Wind speed table derived from Jason-1 data (Collard, [53]).

Table 4 – Models and standards adopted for the Jason-2 version “T” and “c” products. Adapted from [69]

Model	Product version “d”
Orbit	Based on Doris onboard navigator solution for OGDRs. DORIS tracking data for IGDRs (exept for cycles 20 to 78 : DORIS + SLR tracking). Using POE-E standards from 25/05/215 onwards. DORIS+SLR+GPS-A tracking data for GDRs cycles 1 to 225. DORIS + SLR tracking for GDRs for cycles 226 and 227) DORIS+SLR+GPS-B tracking data for GDRs from cycle 228 onwards. Using POE-C standard for GDRs until cycle 254 and POE-E from cycle 254 onwards
	.../...

Model	Product version "d"
Altimeter Retracking	"Ocean MLE4" retracking: MLE4 fit from 2nd order Brown analytical model: MLE4 simultaneously retrieves the 4 parameters that can be inverted from the altimeter waveforms: • Epoch (tracker range offset) → altimeter range • Composite Sigma → SWH • Amplitude → Sigma0 • Square of mispointing angle (Ku band only, a null value is used in input of the C band retracking algorithm) "Ocean MLE3" retracking: MLE3 fit from 1st order Brown analytical model: MLE3 simultaneously retrieves the 3 parameters that can be inverted from the altimeter waveforms: • Epoch (tracker range offset) → altimeter range • Composite Sigma → SWH • Amplitude → Sigma0 "Ice" retracking: Geometrical analysis of the altimeter waveforms, which retrieves the following parameters: • Epoch (tracker range offset) → altimeter range • Amplitude → Sigma0
Altimeter Instrument Corrections	Two sets: • on set consistent with MLE4 retracking • on set consistent with MLE3 retracking
Jason-2 Advanced Microwave Radiometer (AMR) Parameters	Using calibration parameters derived from long term calibration tool developed and operated by NASA/JPL.
Dry Troposphere Range Correction	From ECMWF atmospheric pressures and model for S1 and S2 atmospheric tides
Wet Troposphere Range Correction from Model	From ECMWF model
	.../...

Model	Product version "d"
Ionosphere correction from model	Based on Global Ionosphere TEC Maps from JPL
Sea State Bias Model	Two empirical models: • MLE4 version derived from 1 year of MLE4 Jason-2 altimeter data with version "d" geophysical models • MLE3 version derived from 1 year of MLE3 Jason-2 altimeter data with version "d" geophysical models
Mean Sea Surface Model	MSS_CNES_CLS11
Mean Dynamic Topography Model	MDT_CNES-CLS09
Geoid	EGM96
Bathymetry Model	DTM2000.1
Inverse Barometer Correction	Computed from ECMWF atmospheric pressures after removing S1 and S2 atmospheric tides
Non-tidal High-frequency De-aliasing Correction	Mog2D high resolution ocean model on I/GDRs. None on OGDRs. Ocean model forced by ECMWF atmospheric pressures after removing S1 and S2 atmospheric tides.
Tide Solution 1	GOT4.8 + S1 ocean tide. S1 and M4 load tide included.
Tide Solution 2	FES2004 + S1 and M4 ocean tides. S1 and M4 load tides ignored
Equilibrium long-period ocean tide model.	From Cartwright and Taylor tidal potential.
Non-equilibrium long-period ocean tide model.	Mm, Mf, Mtm, and Msqm from FES2004
Solid Earth Tide Model	From Cartwright and Taylor tidal potential.
Pole Tide Model	Equilibrium model
Wind Speed from Model	ECMWF model
Altimeter Wind Speed	Wind speed table derived from Jason-1 data (Collard, [53]). In addition, a calibration bias of 0.32 is applied to JA2 Ku-band sigma0 prior wind speed computation.
	.../...

Model	Product version “d”
Rain flag	Derived from comparisons to thresholds of the radiometer-derived integrated liquid water content and of the difference between the measured and the expected Ku-band backscatter coefficient
Ice flag	Derived from comparison of the model wet tropospheric correction to a dual-frequency wet tropospheric correction retrieved from radiometer brightness temperatures, with a default value issued from a climatology table

Table 5 – Models and standards adopted for the Jason-2 version “d” products. Adapted from [69]

The differences between GDR-T and GDR-D products are listed in the table 6.

Model	Product Version “T”	Product Version “d”
Orbit	EIGEN-GL04S with time-varying gravity (annual and semi-annual terms up to deg/ord 50) + ITRF 2005	EIGEN-GRGS_RL02bis_MEAN_FIELD with time-varying gravity (annual, semi-annual, and drifts up to deg/ord 50) + ITRF 2008 :until cycle 254 EIGEN+GRGS.RL03-v2.MEAN-FIELD with time-varying gravity (annual, semi-annual, bias and drift terms for each year up to deg/ord 80) :from cycle 254 onwards
	DORIS+SLR+GPS	DORIS+SLR+GPS (increased weight for GPS) until cycle 254 and DORIS + GPS only from cycle 254 onwards
	Radiation pressure model: thermo-optical coefficient from pre-launch box and wing model, with smoothed Earth shadow model	Radiation pressure model: calibrated semi-empirical solar radiation pressure model.
.../...		

Model	Product Version "T"	Product Version "d"
Altimeter Retracking	MLE4 + 2nd order Brown model : MLE4 simultaneously retrieves the 4 parameters that can be inverted from the altimeter waveforms: epoch, SWH, Sigma0 and mispointing angle. This algorithm is more robust for large off-nadir angles (up to 0.8°).	Identical to version "T", in addition altimeter parameters are also available for MLE3 retracking
Altimeter Instrument Corrections	Consistent with MLE4 retracking algorithm.	One consistent with MLE4 retracking + One consistent with MLE3 retracking
Jason-2 Microwave Radiometer Parameters	Using calibration parameters derived from long term calibration tool developed and operated by NASA/JPL	Using calibration parameters derived from long term calibration tool developed and operated by NASA/JPL + enhancement in coastal regions + correction of anomaly in 34 GHz channel addition of radiometer rain and ice flag addition of radiometer 18.7 GHz/ 23.8 GHz/ 34 GHz antenna gain weighted land fraction in main beam
Dry Troposphere Range Correction	From ECMWF atmospheric pressures and model for S1 and S2 atmospheric tides.	Identical to version "T"
Wet Troposphere Range Correction from Model	From ECMWF model.	Identical to version "T"
Back up model for Ku-band ionospheric range correction.	Derived from JPL's Global Ionosphere Model (GIM) maps	Identical to version "T"
Sea State Bias Model	Empirical model derived from 3 years of Jason-1 MLE4 altimeter data with version "b" geophysical models	Empirical models derived from Jason-2 data (One consistent with MLE4 retracking + One consistent with MLE3 retracking)
Mean Sea Surface Model	CLS01	CNES_CLS_2011
Geoid	EGM96	Identical to version "T"

.../...

Model	Product Version "T"	Product Version "d"
Bathymetry Model	DTM2000.1	Identical to version "T"
Mean Dynamic Topography	Rio 2005 solution	CNES_CLS2009 solution
Inverse Barometer Correction	Computed from ECMWF atmospheric pressures after removing model for S1 and S2 atmospheric tides.	Identical to version "T"
Non-tidal High-frequency De-aliasing Correction	Mog2D high resolution ocean model. Ocean model forced by ECMWF atmospheric pressures after removing model for S1 and S2 atmospheric tides.	Identical to version "T"
Tide Solution 1	GOT00.2 + S1 ocean tide . S1 load tide ignored.	GOT4.8 (S1 ocean tide and S1 load tide are included).
Tide Solution 2	FES2004 + S1 and M4 ocean tides. S1 and M4 load tides ignored	Identical to version "T"
Equilibrium long-period ocean tide model.	From Cartwright and Taylor tidal potential.	Identical to version "T"
Non-equilibrium long-period ocean tide model.	Mm, Mf, Mtm, and Msqm from FES2004.	Mm, Mf, Mtm, and Msqm from FES2004 + correction for a bug
Solid Earth Tide Model	From Cartwright and Taylor tidal potential.	Identical to version "T"
Pole Tide Model	Equilibrium model.	Equilibrium model + correction of error which was present over lakes and enclosed seas.
Wind Speed from Model	ECMWF model	Identical to version "T"
Altimeter Wind Speed	Table derived from Jason-1 GDR data.	Table is identical to version "T", but the inputs differ.
Altimeter Rain Flag	Set to default values	Derived from Jason-2 sigma naught MLE3 values
		.../...

Model	Product Version "T"	Product Version "d"
Altimeter Ice Flag	Flag based on the comparison of the model wet tropospheric correction and of a radiometer bi frequency wet tropospheric correction (derived from 23.8 GHz and 34.0 GHz), accounting for a backup solution based on climatologic estimates of the latitudinal boundary of the ice shelf, and from altimeter wind speed.	Identical to version "T"
Update of the altimeter characterization file		PRF value is no longer truncated (2058.513239 Hz) Bias of 18.092 cm applied for Ku and C-band ranges (corrects the value of the distance between center of gravity and the reference point of the altimeter antenna). This correction is applied only to MLE-3 and MLE-4 retracking range. For ICE retracking range, this bias must still be applied by user. Antenna aperture angle (at 3 dB) changed to 1.29 deg MQE setting is applied during 20 Hz to 1 Hz compression Tracker_range_res at a more precise value
other	LTM calculated over 1 day	LTM calculated over 7 days (sliding window) and applied for one day. the origin of the constant part of the time tag bias was found and is directly corrected in the Gdr-D datation.

Table 6 – Models and standards adopted for the Jason-2 product version "T", and "d"

3. Data coverage and edited measurements

In this report, GDR-D from cycle 1 to 303(until 02/10/2016) and IGDR until cycle 309(26/11/2016) are considered.

3.1. Missing measurements

3.1.1. Over land and ocean

Determination of missing measurements relative to the theoretically expected orbit ground pattern is an essential tool to detect missing telemetry or satellite events for instance. Applying the same procedure for Jason-1 and Jason-2, the comparison of the percentage of missing measurements has been performed. Jason-2 can use several onboard tracking modes: Split Gate Tracker (ie the Jason-1 tracking mode, and used for cycle 0 and half of cycle 1), Diode/DEM (used for cycles 3, 5, 7, 34, 209 and 220) and median tracker (used for the other cycles). These different tracking modes are described by [58]. Thanks to the new modes of onboard tracking (median tracker and Diode/DEM), the data coverage over land surface was dramatically increased in comparison with Jason-1 depending on the tracker mode and the period. Figure 1 shows the percentage of missing measurements for Jason-2 and Jason-1 (all surfaces) computed with respect to a theoretical possible number of measurements. Due to differences between altimeter tracking algorithms, the number of available data is greater for Jason-2 than for Jason-1. Differences appear on land surfaces as shown in figure 2. The missing data are highly correlated with the mountains location. The monitoring shows a slight annual signal. During 2013, Jason-2 entered safe hold mode twice in March (from 25/03/2013 to 29/03/2013 and from 30/03/2013 until 05/04/2013, during cycles 174 and 175) and a third time in September (from 05/09/2013 to 12/09/2013, during cycles 190-191). During 2016, data are missing between April, 5 at 13:35:10 and April, 6 at 12:02:40 as no altimeter measurements have been performed (altimeter in wait mode) during this period to allow the upload of new GPS onboard software

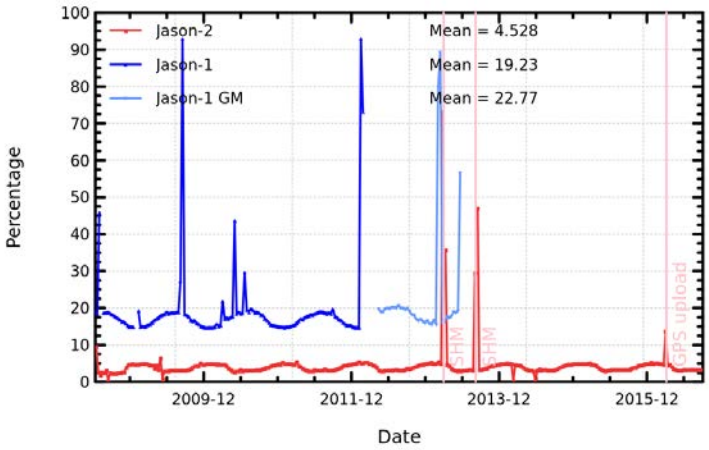

Figure 1 – Percentage of missing measurements over ocean and land for JA2 and JA1

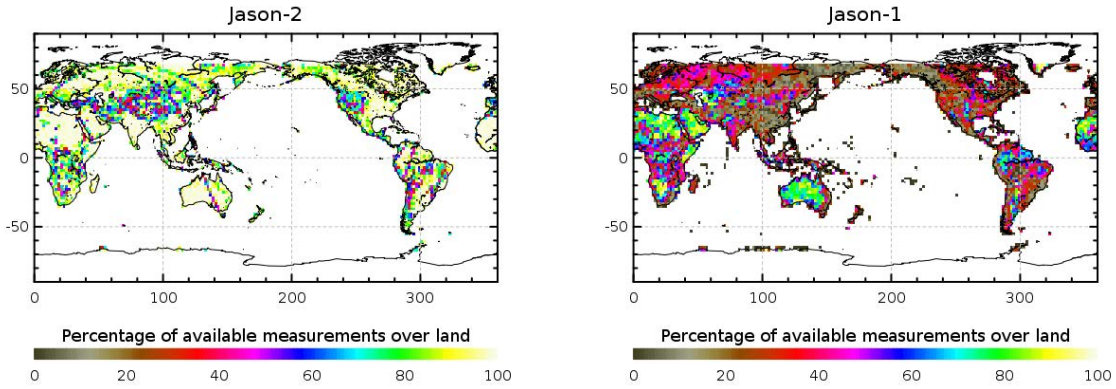

Figure 2 – Map of percentage of available measurements over land for Jason-2 on cycle 154 (left) and for Jason-1 on cycle 511 (right)

3.1.2. Over ocean

When considering ocean surface, the same analysis method leads also to an improvement of Jason-2 data coverage, as plotted on the top left figure 3. It represents the percentage of missing measurements relative to the theory, when limited to ocean surfaces. The mean value is about 0.7% for Jason-2, 4.6% for Jason-1 on its repeat ground-track and 7.7% for Jason-1 on its geodetic ground-track. Note that since Jason-1 is on a geodetic ground-track, it is roughly once per month during about 2 h in INIT mode (no science data), due to Jason-2 overflight. Even if already very low, this figure of missing measurements is not significant due to several events where the measurements are missing. All these events are described on table 2.
On figure 3 on the top right, the percentage of missing measurements is plotted without taking into account the cycles where instrumental events or other big anomalies occurred. The mean value of missing measurements lowers down to 0.03% for Jason-2 and 1.9% (2.4%) for Jason-1 (Jason-1 geodetic). These additional Jason-1 missing measurements are mainly located over sea ice and near the coasts and are related to the altimeter tracking method. Indeed, selecting latitudes lower than 50° and bathymetry area lower than -1000m (see bottom of figure 3), the Jason-1 percentage becomes very weak (close to 0.02%) which represents less than 100 missing measurements per cycle over open ocean. For Jason-2, the same statistic is smaller with around 0.006% of missing measurements over open ocean. This weak percentage of missing measurements is mainly explained by the rain cells and sigma0 blooms. These sea states can disturb significantly the Ku band waveform shape leading to an altimeter lost of tracking.

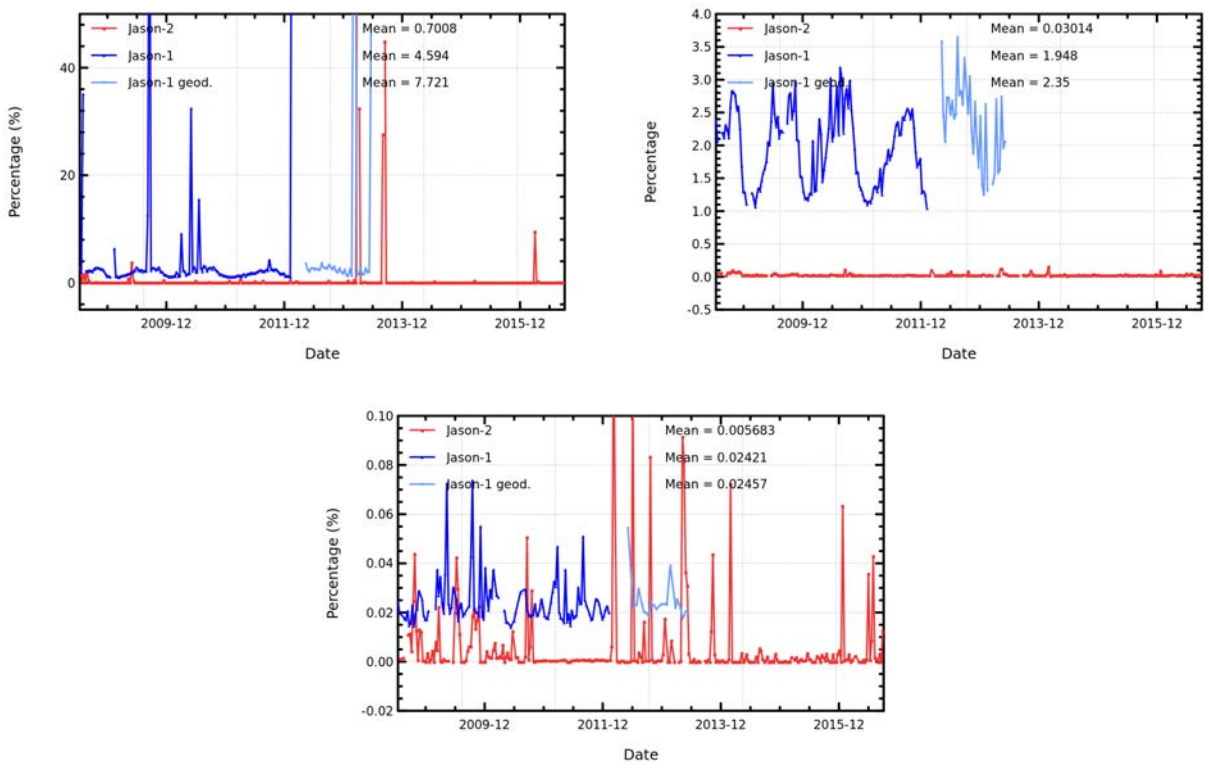

Figure 3 – Cycle per cycle percentage of missing measurements over ocean (top left), without anomalies (top right), without anomalies and with geographical selections (bottom).

3.2. Edited measurements

3.2.1. Editing criteria definition

Editing criteria are used to select valid measurements over ocean. The editing process is divided into 4 parts. First, only measurements over ocean and lakes are kept (see section 3.2.2.). Second, some flags are used as described in section 3.2.3.. Note that though the altimeter rain flag is now available in the current release of GDR (D), it is not used hereafter in the editing procedure. But measurements corrupted by rain are well detected by other altimeter parameter criteria. Then, threshold criteria are applied on altimeter, radiometer and geophysical parameters and are described in the table 7. Except for the dual frequency ionosphere correction, only Ku-band measurements are used in this editing procedure, as they mainly represent the end user dataset. Moreover, a spline criterion is applied to remove the remaining spurious data. For each criterion, the cycle per cycle percentage of edited measurements has been monitored. This allows detection of anomalies in the number of removed data, which could come from instrumental, geophysical or algorithmic changes.

Parameter	Min thresholds	Max thresholds	mean edited
Sea surface height	$-130\,m$	$100\,m$	0.77%
Sea level anomaly	$-10\,m$	$10.0\,m$	1.05%
Number measurements of range	10	*Not applicable*	1.04%
Standard deviation of range	0	$0.2\,m$	1.41%
Squared off-nadir angle	$-0.2\,deg^2$	$0.64\,deg^2$	0.59%
Dry troposphere correction	$-2.5\,m$	$-1.9\,m$	0.00%
Inverted barometer correction	$-2.0\,m$	$2.0\,m$	0.00%
AMR wet troposphere correction	$-0.5m$	$-0.001\,m$	0.24%
Ionosphere correction	$-0.4\,m$	$0.04\,m$	1.18%
Significant wave height	$0.0\,m$	$11.0\,m$	0.65%
Sea State Bias	$-0.5\,m$	$0.0\,m$	0.62%
Number measurements of Ku-band Sigma0	10	*Not applicable*	1.03%
Standard deviation of Ku-band Sigma0	0	$1.0\,dB$	1.95%
Ku-band Sigma0 [1]	$7.0\,dB$	$30.0\,dB$	0.61%
Ocean tide	$-5.0\,m$	$5.0\,m$	0.01%
Equilibrium tide	$-0.5\,m$	$0.5\,m$	0.00%
Earth tide	$-1.0\,m$	$1.0\,m$	0.00%
Pole tide	$-15.0\,m$	$15.0\,m$	0.00%
Altimeter wind speed	$0\,m.s^{-1}$	$30.0\,m.s^{-1}$	1.03%
All together	-	-	3.29%

Table 7 – Editing criteria

3.2.2. Selection of measurements over ocean and lakes

In order to remove data over land, a land-water mask is used. Only measurements over ocean or lakes are kept. This allows to keep data near the coasts and so to detect potential anomalies in these areas. Furthermore, there is no impact on global performance estimations since the most significant results are derived from analyzes in deep ocean areas. Figure 4 shows the cycle per

[1]The thresholds used for the Ku-band Sigma0 are the same than for Jason-1 and T/P, but the same sigma0 bias as between Jason-1 and T/P (about 2.4 dB) is applied.

cycle percentage of measurements eliminated by this selection. The signal shows mainly a seasonal cycle, due to changing properties of land reflection. But it also reveals the impact of the different altimeter tracking modes: SGT (split gate tracking), Median and DIODE/DEM (digital elevation model). SGT mode, the nominal mode for Jason-1, was used for Jason-2 during cycle 0 and half of cycle 1. This mode does not perform very well over land (as also depicted on right side of figure 2), therefore a comparable small percentage of measurements are edited over land for cycle 1 (approximately 24%). Most of Jason-2 cycles (cycles 2, 4, 6, 8 to 33, 35 to 208, 210 to 219 and from cycle 221 onwards) were operated in Median mode (also used by Envisat). This mode is more adapted for tracking over land than SGT and provides therefore more measurements over land (as also seen on left side of figure 2) and so more measurements are edited (between 25.5% and 27% depending on season) due to the ocean/land criteria. A new tracking mode, DEM, was used during cycles 3, 5, 7, 34, 209 and 220. It has been designed to provide more data over inland water surfaces and coastal areas. It provides a continuous data set over land but some are not meaningful (in areas where the DEM is not accurate enough like in the major mountains). Therefore during these cycles, almost 29% of measurements are removed by the selection. Since 10th of December, 2008 the onboard altimeter configuration was modified to correct for the low signal tracking anomaly, which led to a more strict control of acquisition gain loop (to avoid the tracking of low signal anomalies). This explains the quite steep decrease of land measurements edited around cycle 16.

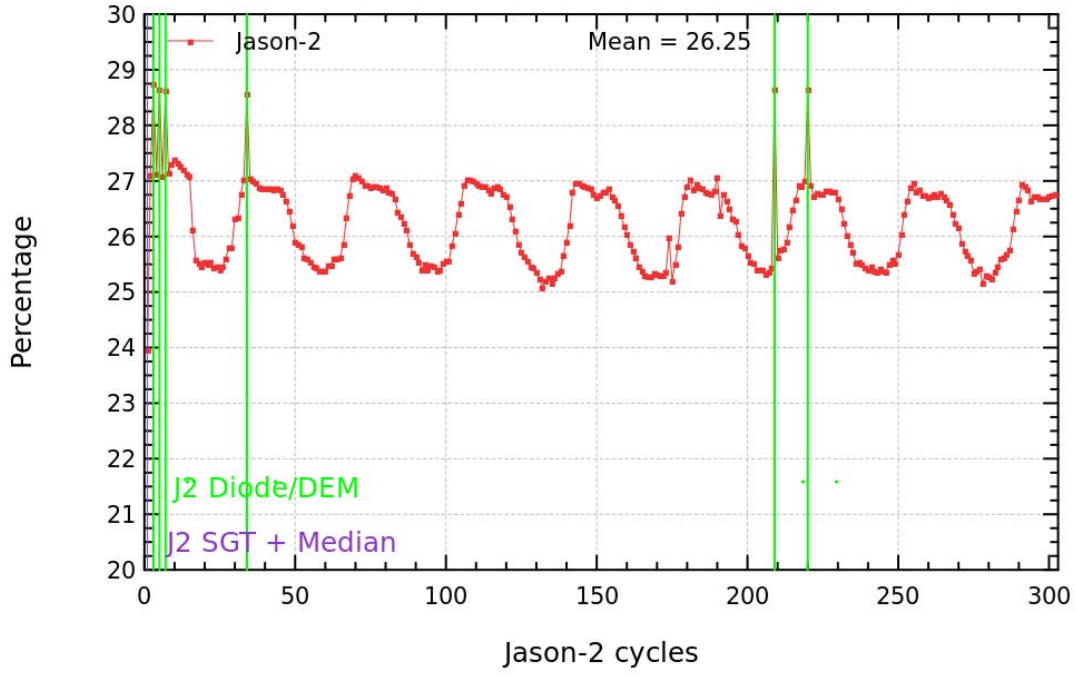

Figure 4 – Cycle per cycle percentage of eliminated measurements during selection of ocean/lake measurements.

3.2.3. Flagging quality criteria: Ice flag

The ice flag is used to remove the sea ice data. Figure 5 shows the cycle per cycle percentage of measurements edited by this criterion. Over the shown period, no anomalous trend is detected (figure 5 left) but the nominal annual cycle is visible. Indeed, the maximum number of points over ice is reached during the southern winter (i.e. July - September). As Jason-2 takes measurements between 66° north and south, it does not detect thawing of sea ice (due to global warming), which takes place especially in northern hemisphere over 66°N. A slight decrease is visible over the last year: it is also visible with SARAL/AltiKa data [28]. The percentage of measurements edited by ice flag is plotted in the right of figure 5 for a period of 1 year.

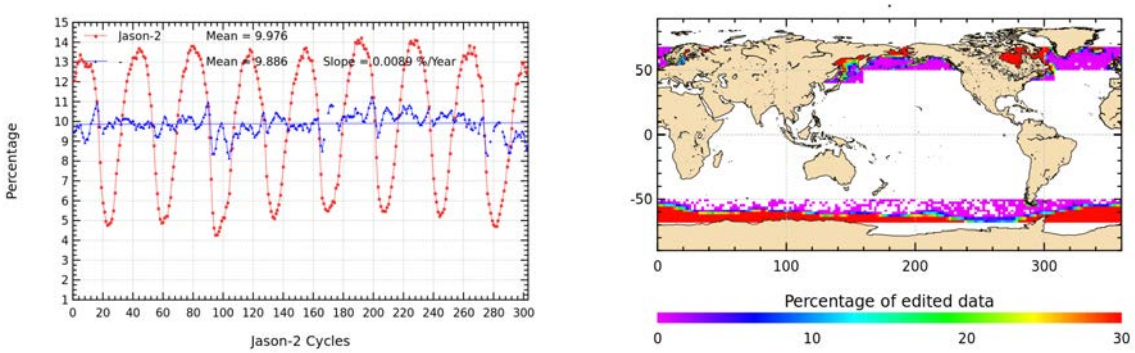

Figure 5 – Percentage of edited measurements by ice flag criterion. Left: Cycle per cycle monitoring. The blue curve shows the trend of edited measurements after adjusting for annual and semi-annual signals. Right: Map over a one year period (cycles 267 to 303).

3.2.4. Flagging quality criteria: Rain flag

Though the altimeter rain flag is now present in GDR-D release, it is not used hereafter during the editing procedure. The percentage of measurements where rain flag is set to 1 is plotted in figure 6 over cycles 267 to 303 (covering 12 months). It shows that measurements are especially edited near coasts, but also in the equatorial zone and open ocean. The altimeter rain flag seems to be slightly too strict, using it would lead to edit 6.8% of additional measurements (for location see right part of figure 6).

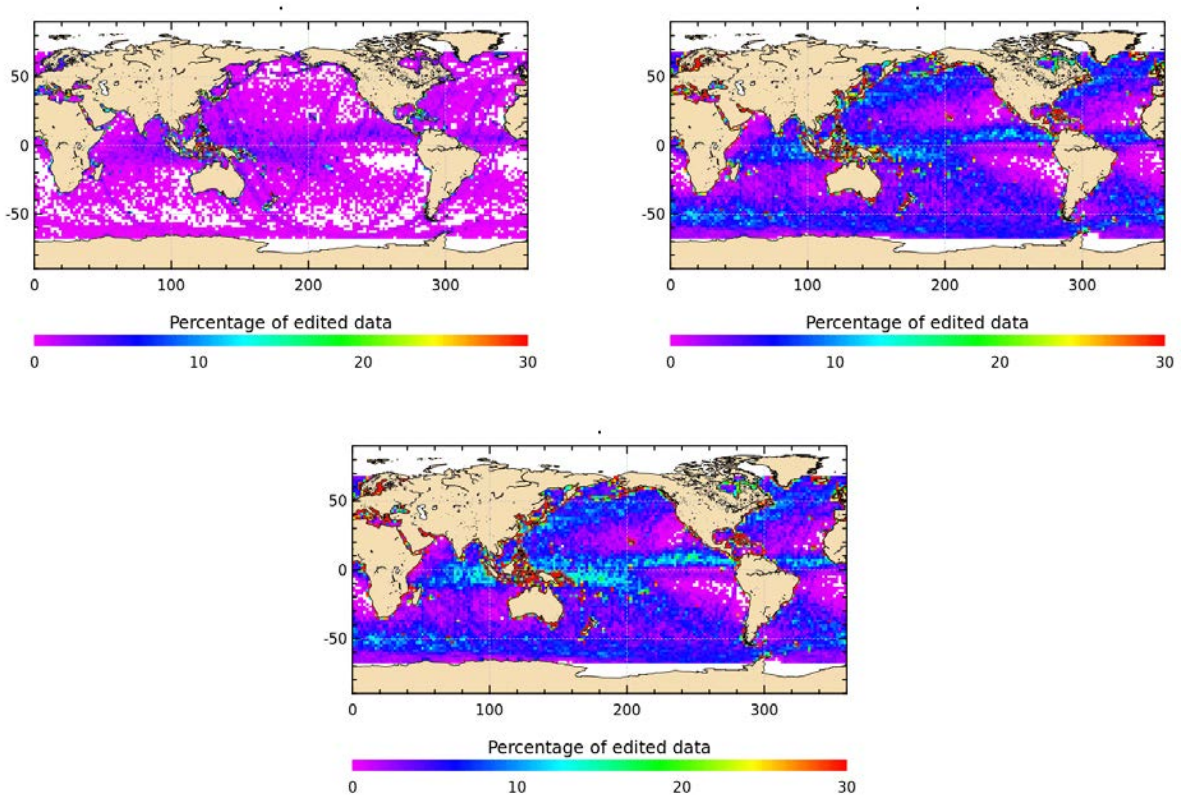

Figure 6 – Percentage of edited measurements by altimeter rain flag criterion (all figures computed after iced flagged points remove). Map over a one year period (cycles 267 to 303). Left: rejected measurements where rain flag is also activated . Right: valid measurements where rain flag is activated. Bottom: All points where rain flag is activated.

3.2.5. Threshold criteria: Global

Instrumental parameters have also been analyzed from comparison with thresholds, after having selected only ocean/lakes measurements and applied flagging quality criteria (ice flag). Therefore measurements appear not as edited by thresholds, when they were already edited by land or sea ice flag. Note that no measurement is edited by the following corrections : dry troposphere correction, inverted barometer correction (including DAC), equilibrium tide, earth and pole tide. Indeed these parameters are only verified in order to detect data at default values, which might happen during a processing anomaly.
The percentage of measurements edited using each criterion is monitored on a cycle per cycle basis (figure 7). The mean percentage of edited measurements is about 3.3%. A small annual cycle is visible. The high percentage of edited measurements of cycles 019, 168, 169,238 and 269 are explained by an AMR anomaly, which resulted in defaulted radiometer values during several passes. Concerning cycles 174 and 191, it is explained by the time lag between the altimeter restart and the radiometer restart after safe hold modes.

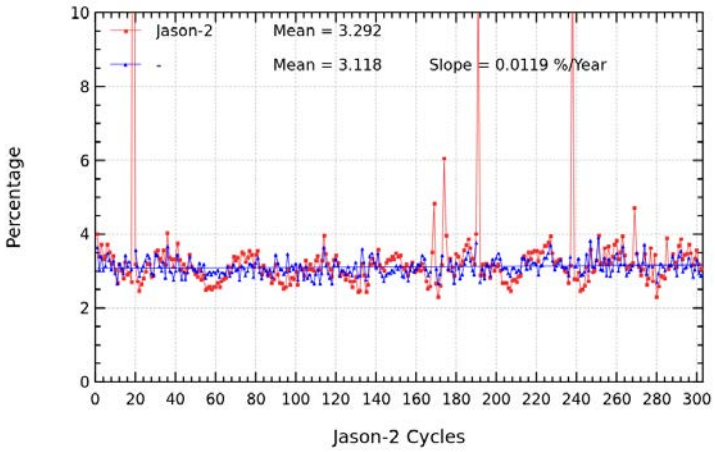

Figure 7 – Cycle per cycle percentage of edited measurements by threshold criteria. The blue curve shows the trend of edited measurements after adjusting for annual and semi-annual signals.

3.2.6. Threshold criteria: 20-Hz measurements number

The percentage of edited measurements because of a too low number of 20-Hz measurements is represented on left side of figure 8. No trend neither any anomaly has been detected.
The map of measurements edited by 20-Hz measurements number criterion is plotted on right side of figure 8 and shows correlation with heavy rain and wet areas (in general regions with disturbed sea state). Indeed waveforms are distorted by rain cells, which makes them often meaningless for SSH calculation. As a consequence, edited measurements due to several altimetric criteria are often correlated with wet areas.

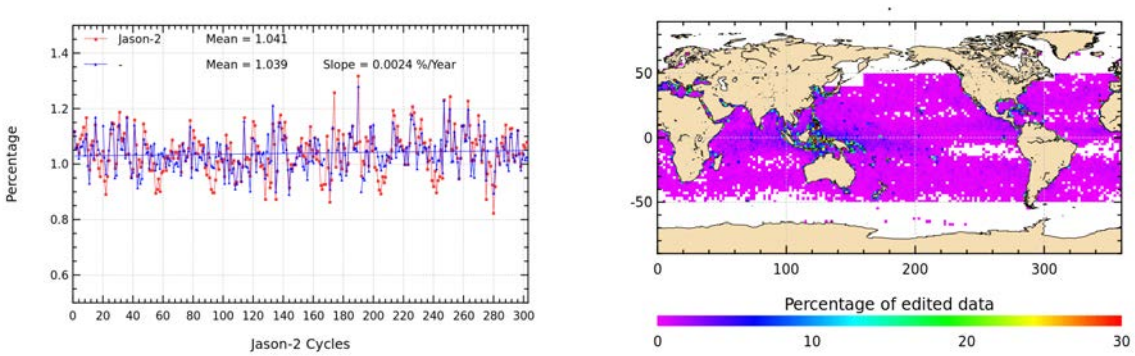

Figure 8 – Percentage of edited measurements by 20-Hz measurements number criterion. Left: Cycle per cycle monitoring. The blue curve shows the trend of edited measurements after adjusting for annual and semi-annual signals. Right: Map over a one year period (cycles 267 to 303).

3.2.7. Threshold criteria: 20-Hz measurements standard deviation

The percentage of edited measurements due to 20-Hz measurements standard deviation criterion is shown in figure 9 (left). During cycle 1, slightly more measurements are edited by 20-Hz measurements standard deviation criterion than during other cycles. This is likely due to low signal tracking anomaly which impacted especially this cycle. The right side of figure 9 shows a map of measurements edited by the 20-Hz measurements standard deviation criterion. As in section 3.2.6., edited measurements are correlated with wet areas.

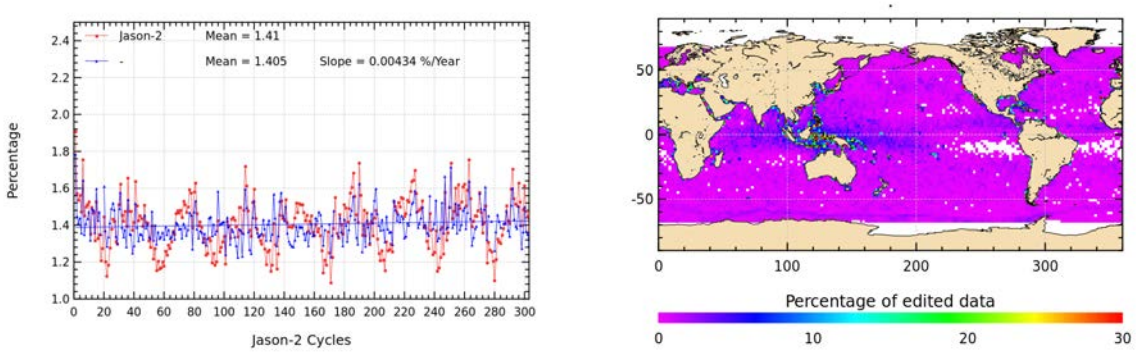

Figure 9 – Percentage of edited measurements by 20-Hz measurements standard deviation criterion. Left: Cycle per cycle monitoring. The blue curve shows the trend of edited measurements after adjusting for annual and semi-annual signals. Right: Map over a one year period (cycles 267 to 303).

3.2.8. Threshold criteria: Significant wave height

The percentage of edited measurements due to significant wave height criterion is represented in figure 10. It is about 0.65%. In the beginning of the mission, the curve of measurements edited by SWH threshold criterion is quite irregular, as low signal tracking anomalies occurred during SGT and Median tracking modes, whereas there are no low signal tracking anomalies during DEM tracking modes (cycles 3, 5, and 7). Indeed during periods of low signal tracking anomaly, parameters like significant wave height, backscatter coefficient and squared off-nadir angle from waveforms are out of thresholds and therefore edited. Figure 10 (right part) shows that measurements edited by SWH criterion are especially found near coasts in the equatorial regions and in the Mediterranean Sea.

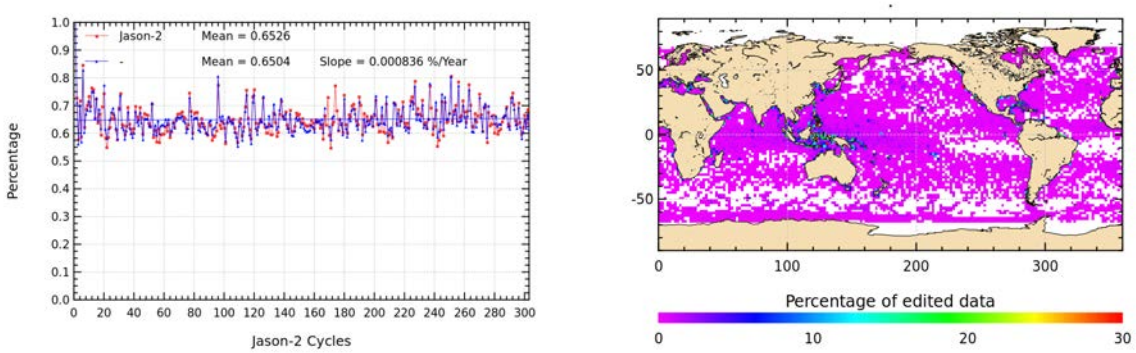

Figure 10 – Percentage of edited measurements by SWH criterion. Left: Cycle per cycle monitoring. The blue curve shows the trend of edited measurements after adjusting for annual and semi-annual signals. Right: Map over a one year period (cycles 267 to 303).

3.2.9. Backscatter coefficient

The percentage of edited measurements due to backscatter coefficient criterion is represented in figure 11. It is about 0.61%. It is also impacted by low signal tracking anomalies, especially during cycle 1. The right part of figure 11 shows that measurements edited by backscatter coefficient criterion are especially found near coasts in the equatorial regions and enclosed sea (Mediterranean).

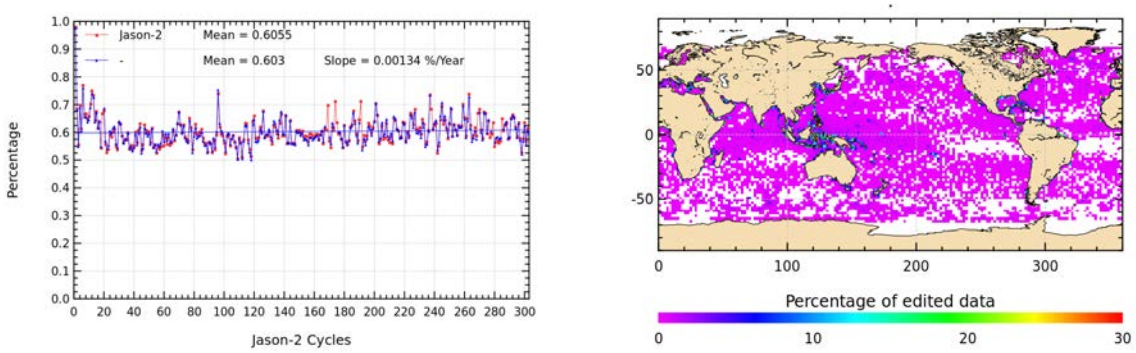

Figure 11 – Percentage of edited measurements by Sigma0 criterion. Left: Cycle per cycle monitoring. The blue curve shows the trend of edited measurements after adjusting for annual and semi-annual signals. Right: Map over a one year period (cycles 267 to 303).

3.2.10. Backscatter coefficient: 20 Hz standard deviation

The percentage of edited measurements due to 20 Hz backscatter coefficient standard deviation criterion is represented in figure 12. It is about 1.95%. The right part of figure 11 shows that measurements edited by 20 Hz backscatter coefficient standard deviation criterion are especially found in regions with disturbed waveforms.

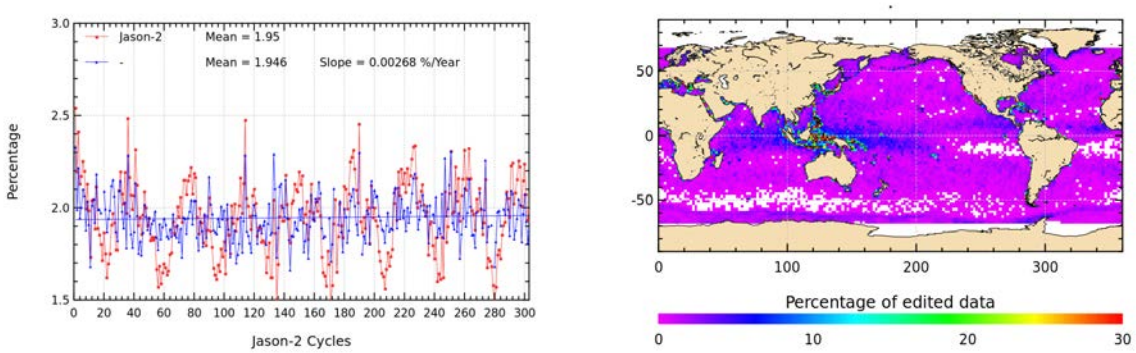

Figure 12 – Percentage of edited measurements by 20 Hz Sigma0 standard deviation criterion. Left: Cycle per cycle monitoring. The blue curve shows the trend of edited measurements after adjusting for annual and semi-annual signals. Right: Map over a one year period (cycles 267 to 303).

3.2.11. Radiometer wet troposphere correction

The percentage of edited measurements due to radiometer wet troposphere correction criterion is represented in figure 13. It is about 0.24%. When removing cycles which experienced problems, percentage of edited measurements drops to less than 0.1%. For some cycles the percentage of edited measurements is higher than usual. This is linked to radiometer wet troposphere correction at default value due to AMR unavailability in case of cycle 19, 238 and 269, AMR reset in case of cycles 168 and 169, and time lag between altimeter restart and radiometer restart after safe hold modes in case of cycles 174, 175 and 191.

On the right part of figure 13, the following unavailability periods are visible:

- there were no AMR data on 25/10/2015 from 18h18 to 22h25 (cycle 269 passes 111 to 115),
- on 10/01/2016 from 02:45:05 to 05:03:03 (impacting cycle 277 passes 035 to 037)
- on 19/01/2016 from 05:58:31 to 08:21 (cycle 279 passes 017 to 020).
- and on 31/03/2016 from 09:30:52 to 11:39:11 (cycle 285 passes 085 to 087).

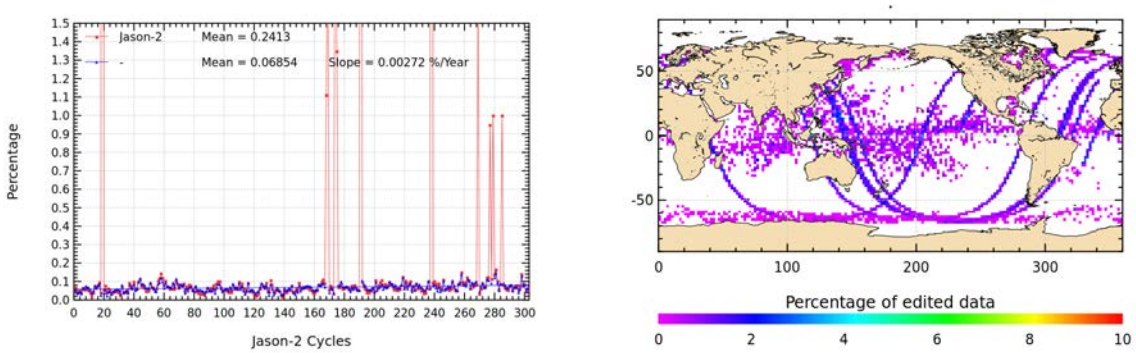

Figure 13 – Percentage of edited measurements by radiometer wet troposphere criterion. Left: Cycle per cycle monitoring. The blue curve shows the trend of edited measurements after adjusting for annual and semi-annual signals. Right: Map over a one year period (cycles 267 to 303).

3.2.12. Dual frequency ionosphere correction

The percentage of edited measurements due to dual frequency ionosphere correction criterion is represented in figure 14. It is about 1.2% and shows no drift. The map 14 shows that measurements edited by dual frequency ionosphere correction are mostly found in equatorial regions, but also near sea ice.

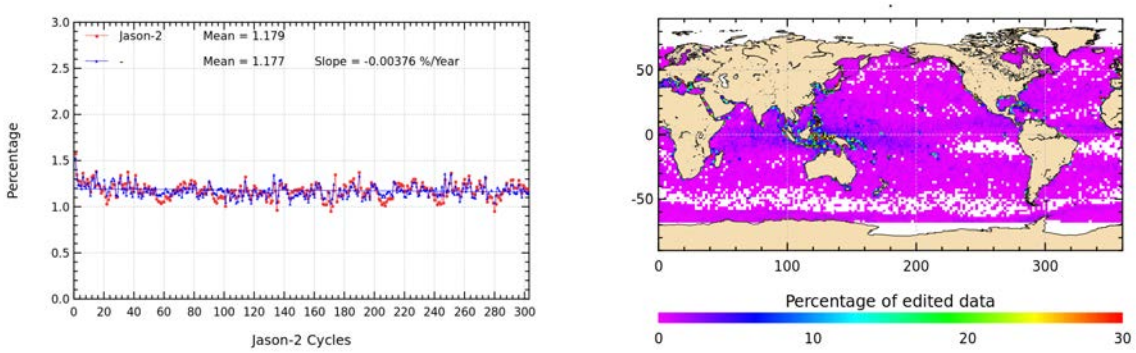

Figure 14 – Percentage of edited measurements by dual frequency ionosphere criterion. Left: Cycle per cycle monitoring. The blue curve shows the trend of edited measurements after adjusting for annual and semi-annual signals. Right: Map over a one year period (cycles 267 to 303).

3.2.13. Square off-nadir angle

The percentage of edited measurements due to square off-nadir angle criterion is represented in figure 15. It is about 0.6%. As for other parameters, impact of low signal tracking anomalies is

visible in general for the first 16 cycles and especially for cycle 1. The map 15 shows that edited measurements are mostly found in coastal regions and regions with disturbed waveforms.

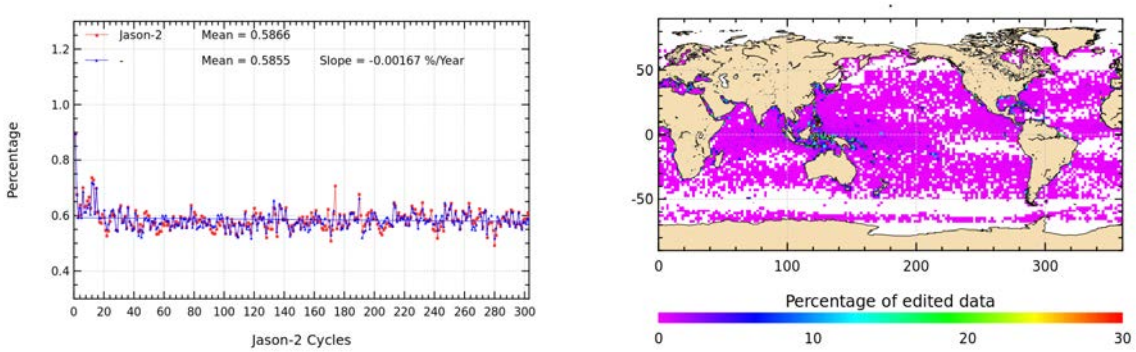

Figure 15 – Percentage of edited measurements by square off-nadir angle criterion. Left: Cycle per cycle monitoring. The blue curve shows the trend of edited measurements after adjusting for annual and semi-annual signals. Right: Map over a one year period (cycles 267 to 303).

3.2.14. Sea state bias correction

The percentage of edited measurements due to sea state bias correction criterion is represented in figure 16. The percentage of edited measurements is about 0.6% and shows no drift.
The map 16 shows that edited measurements are mostly found in equatorial regions near coasts.

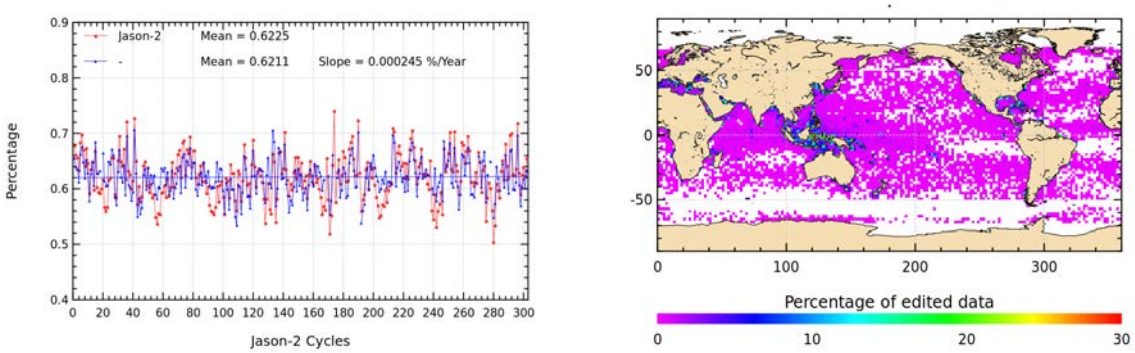

Figure 16 – Cycle per cycle percentage of edited measurements by sea state bias criterion (left). The blue curve shows the trend of edited measurements after adjusting for annual and semi-annual signals. Right: Map of percentage of edited measurements by sea state bias criterion over a one year period (cycles 267 to 303).

3.2.15. Altimeter wind speed

The percentage of edited measurements due to altimeter wind speed criterion is represented in figure 17. It is about 1.0%. The measurements are edited because they have default values. This is the case when sigma0 itself is at default value, or when it shows very high values (higher than 25 dB), which occur during sigma bloom and also over sea ice. Indeed, the wind speed algorithm (which uses backscatter coefficient and significant wave height) can not retrieve values for sigma0 higher than 25 dB.
Wind speed is also edited, when it has negative values, which can occur in GDR products. Nevertheless, sea state bias is available even for negative wind speed values. Therefore, the percentage of edited altimeter wind speed is higher than that of edited sea state bias.

The map 17 showing percentage of measurements edited by altimeter wind speed criterion is correlated with maps 16 and 10.

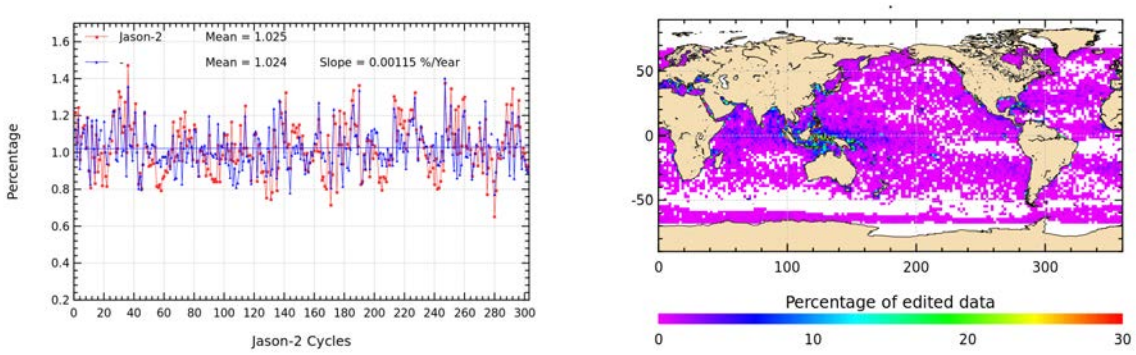

Figure 17 – Percentage of edited measurements by altimeter wind speed criterion. Left: Cycle per cycle monitoring.The blue curve shows the trend of edited measurements after adjusting for annual and semi-annual signals. Right: Map over a one year period (cycles 267 to 303).

3.2.16. Ocean tide correction

The percentage of edited measurements due to ocean tide correction criterion is represented in figure 18. It is less than 0.01% and is very stable. The ocean tide correction is a model output, there should therefore be no edited measurements. Indeed there are no measurements edited in open ocean areas, but only very few near coasts (Alaska, Kamchatka, Labrador). These measurements are mostly at default values. The percentage of measurement increases for cycle 174 and 175 (2013 safe hold mode).

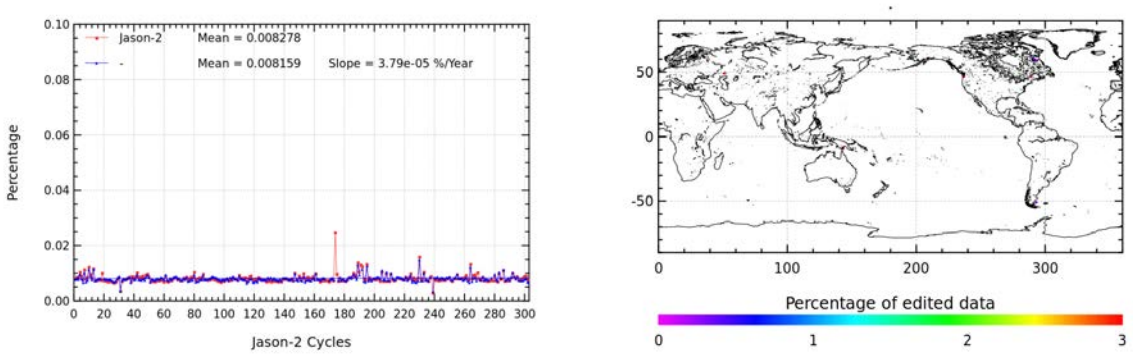

Figure 18 – Percentage of edited measurements by ocean tide criterion. Left: Cycle per cycle monitoring. The blue curve shows the trend of edited measurements after adjusting for annual and semi-annual signals. Right: Map over a one year period (cycles 267 to 303).

3.2.17. Sea surface height

The percentage of edited measurements due to sea surface height (orbit - ku-band range) criterion is represented in figure 19. It is about 0.77% and shows no drift. The measurements edited by sea surface height criterion are mostly found near coasts in equatorial regions (see map 19). The majority of the edited measurements has defaulted range values.

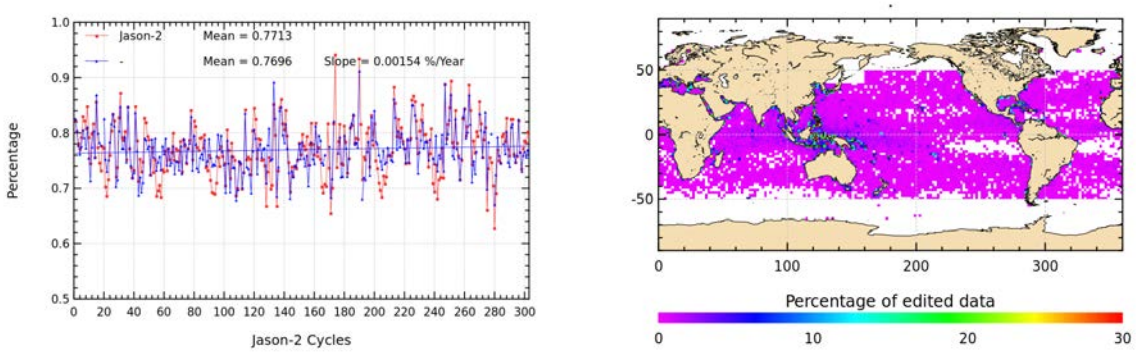

Figure 19 – Percentage of edited measurements by sea surface height criterion. Left: Cycle per cycle monitoring. The blue curve shows the trend of edited measurements after adjusting for annual and semi-annual signals. Right: Map over a one year period (cycles 267 to 303).

3.2.18. Sea level anomaly

The percentage of edited measurements due to sea level anomaly criterion is represented in figure 20. It is about 1.05% (0.9% without cycles 19,168,169,174,175,191,238 and 269) and shows no drift. The peaks are related to AMR unavailabilities (see figure 13 (showing the percentage of measurements edited by AMR)), as the SLA clip contains, among other parameters, the radiometer wet troposphere correction.
Whereas the map in figure 20 allows us to plot the measurements edited due to sea level anomaly out of thresholds (after applying all other threshold criteria). There are only very few measurements, principally located in Caspian Sea.

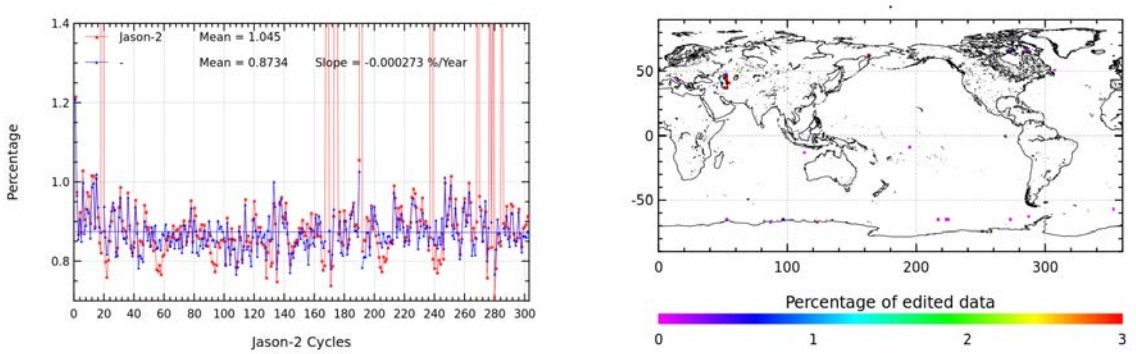

Figure 20 – Percentage of edited measurements by sea level anomaly criterion. Left: Cycle per cycle monitoring. The blue curve shows the trend of edited measurements after adjusting for annual and semi-annual signals. Right: Map over a one year period (cycles 267 to 303).

4. Monitoring of altimeter and radiometer parameters

4.1. Methodology

Both mean and standard deviation of the main parameters of Jason-2 (GDR-D) have been monitored since the beginning of the mission. Moreover, a comparison with Jason-1 (GDR-E) parameters has been performed: it allows us to monitor the bias between the parameters of the 2 missions. Two different methods have been used to compute the bias:

- Till Jason-2 cycle 20, Jason-2 and Jason-1 are on the same ground track and are spaced out about 1 minute apart (tandem phase). The mean of the Jason-1 - Jason-2 differences can be computed using a point by point repeat track analysis.
- From Jason-2 cycle 21 (Jason-1 cycle 260), a maneuver sequence was conducted (from 26th of January to 14th of February 2009) to move Jason-1 to the new formation flight mission orbit. Jason-1 has a repeat ground-track which is interleaved with Jason-2. It is the same ground-track as already used by Topex/Poseidon during its formation flight phase with Jason-1, but there is a time shift of 5 days. Geographical variations are then too strong to directly compare Jason-2 and Jason-1 parameters on a point by point basis. Therefore day per day global differences have been carried out to monitor differences between the two missions. A filter over 11 days was applied. Nevertheless the differences are still quite noisy, especially for corrections which vary rapidly in time and space. Therefore occasional small jumps might be covered by the noise of the differences. Nevertheless it should be possible to detect drifts and permanent jumps. Jason-2 and Jason-1 were in this formation flight phase from Jason-2 cycles 22 to 135 (Jason-1 cycles 262 to 374).

In February and March of 2012, Jason-1 experienced severals safe holds (anomaly on gyro3, double EDAC error in RAM memory). It was decided to move Jason-1 to a geodetic orbit (more about the Jason-1 geodetic mission can be found in [9]). Science data on the geodetic orbit are available from 7th of May 2012 onwards. Note that the first cycle on the geodetic orbit starts with cycle 500 (this corresponds to end of Jason-2 cycle 141). The last (incomplete) cycle of Jason-1 on the repeat ground-track was cycle 374. As during the formation flight phase, day per day global differences of the parameters have been carried out to monitor differences between the two missions.
Finally, after loss of telemetry on 21 June 2013 (during cycle 537), Jason-1 was passivated and decommissioned on 01 July 2013, with the last command sent at 16:37:40 UTC. Note that differences are done over Jason-2 cycles 1 to 183, corresponding to Jason-1 cycles 240 to 537.

4.2. 20 Hz Measurements

The monitoring of the number and standard deviation of 20 Hz elementary range measurements used to derive 1 Hz data is presented here. These two parameters are computed during the altimeter ground processing. For both Jason-1 and Jason-2, before performing a regression to derive the 1 Hz range from 20 Hz data, a MQE (mean quadratic error) criterion is used to select valid 20 Hz measurements. This first step of selection consists in verifying that the 20 Hz waveforms can be approximated by a Brown echo model (Brown, 1977 [46]) (Thibaut et al. 2002 [99]). Then, through an iterative regression process, elementary ranges too far from the regression line are discarded until convergence is reached. Thus, monitoring the number of 20 Hz range measurements and the standard deviation computed among them is likely to reveal changes at instrumental level.

The Jason-1 MQE threshold are not applicable to Jason-2, using those thresholds would edit more measurements than necessary. Therefore, for the first GDR release of Jason-2 (GDR-T), the MQE threshold had been set to default, leading to no editing based on MQE values. Note that for Jason-2 data in version GDR-D, specific Jason-2 MQE thresholds were computed and are applied.

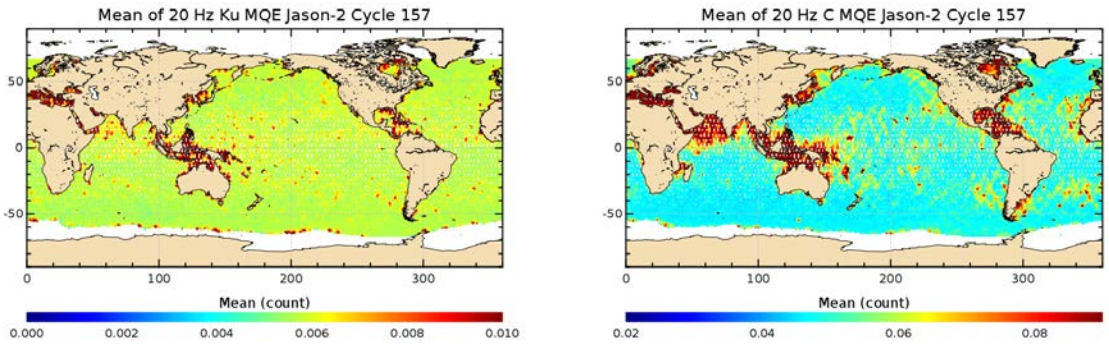

Figure 21 – Map of 20 Hz Ku-band (left) and C-band (right) MQE for Jason-2 cycle 157. Note that the color scales are different for the two maps.

4.2.1. 20 Hz measurements number in Ku-Band and C-Band

GDR-D Jason-2 number of elementary 20 Hz range measurements is very similar to Jason-1's (especially for C-band) with an average of 19.61 for Ku-band and 19.26 for C-band as shown on figure 22. For both satellites a slight annual signal is visible (especially for C-band). Figures 23 and 24 show on the left the daily monitoring of the mean and standard deviation of Jason-1 - Jason-2 differences of 20-Hz measurements number in Ku-Band and C-band during the tandem phase. Besides a slight variation, they are quite stable and do not show any anomaly. Number of 20 Hz Ku-band range measurements is slightly higher for Jason-2 than for Jason-1, since mean of Jason-1 - Jason-2 difference is slightly negative (-0.07 for Ku-band), whereas the difference for C-band is close to zero. The regions where Jason-1 has less elementary Ku-band range measurements are especially located around Indonesia, as shown on map of Jason-1 - Jason-2 differences (right side of figures 23). Indeed in regions of sigma bloom or rain, using a MQE criterion during the regression to derive 1Hz from 20Hz data, discards 20 Hz measurements and therefore reduces the value of number of the 20 Hz measurements used for the 1 Hz data. It is possible that differences in the tuning of the MQE criterion for Jason-1 and Jason-2 Ku-band explain what is observed on the right side of figure 23.

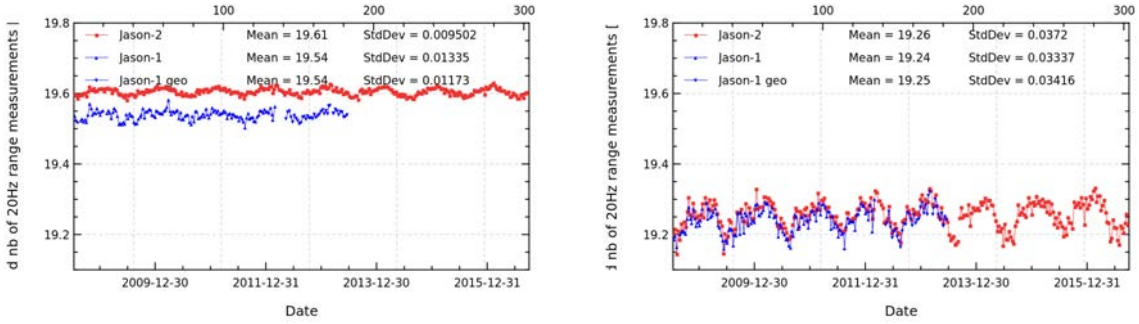

Figure 22 – Cyclic monitoring of number of elementary 20 Hz range measurements for Jason-1 and Jason-2 for Ku-band (left) and C-band (right).

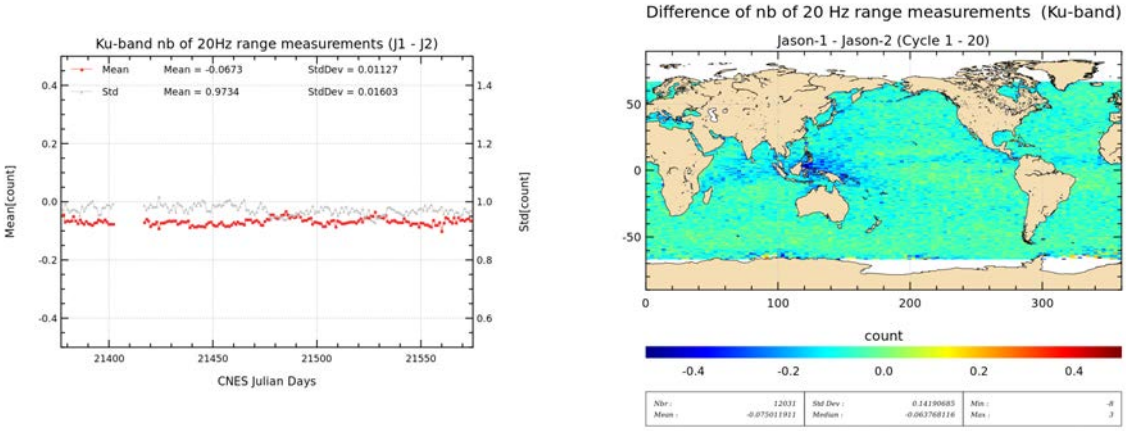

Figure 23 – Daily monitoring of mean and standard deviation of Jason-1 - Jason-2 differences for number of elementary 20 Hz Ku-band range measurements (left) and map showing mean of Jason-1 - Jason-2 differences over cycles 1 to 20.

4.2.2. 20 Hz measurements standard deviation in Ku-Band and C-Band

Jason-2 standard deviation of the 20 Hz measurements is 8.0 cm for Ku-Band and 17.4 cm for C-Band (figure 25). It is very similar to Jason-1 data. Figure 26 and 27, showing daily monitoring of Jason-1 - Jason-2 difference of standard deviation of the 20 Hz measurements in Ku-Band and C-Band (on the left), reveal no trend neither anomaly. C-Band standard deviation of the 20 Hz measurements rms is noisier than those of Ku-Band. This is directly linked to the C-band standard deviation which is higher than the Ku, as the onboard averaging is performed over less waveforms (6 Ku for 1 C) leading to an increased noise.

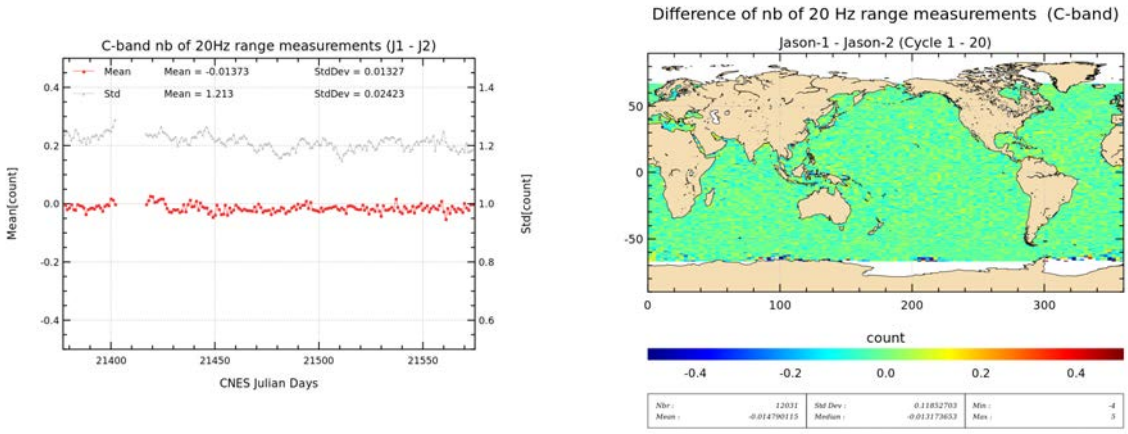

Figure 24 – Daily monitoring of mean and standard deviation of Jason-1 - Jason-2 differences for number of elementary 20 Hz C-band range measurements (left) and map showing mean of Jason-1 - Jason-2 differences over cycles 1 to 20.

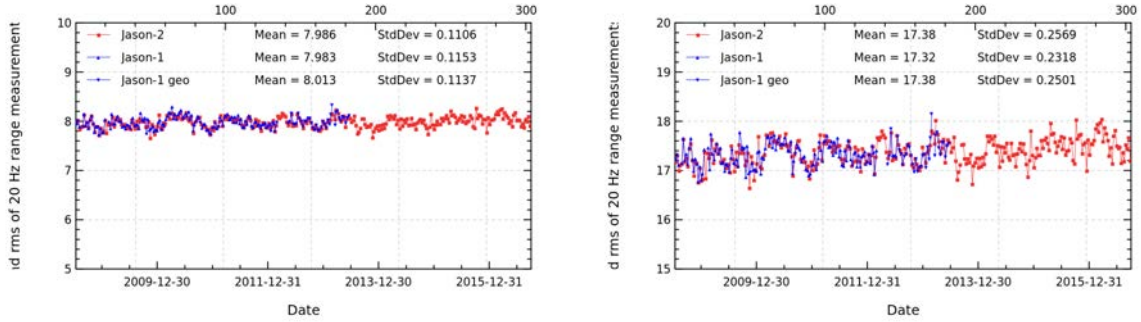

Figure 25 – Cyclic monitoring of rms of elementary 20 Hz range measurements for Jason-1 and Jason-2 for Ku-band (left) and C-band (right).

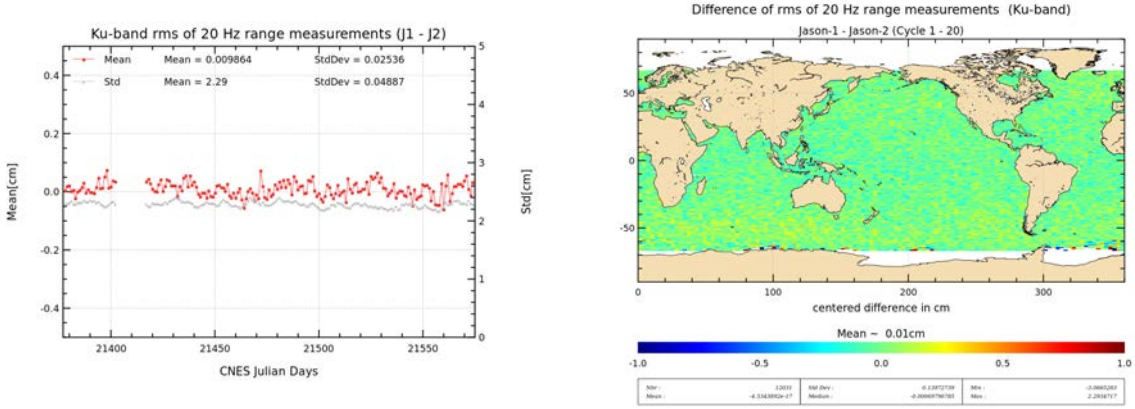

Figure 26 – Daily monitoring of mean and standard deviation of Jason-1 - Jason-2 differences for the rms of elementary 20 Hz Ku-band range measurements (left) and map showing mean of Jason-1 - Jason-2 differences over cycles 1 to 20 (right).

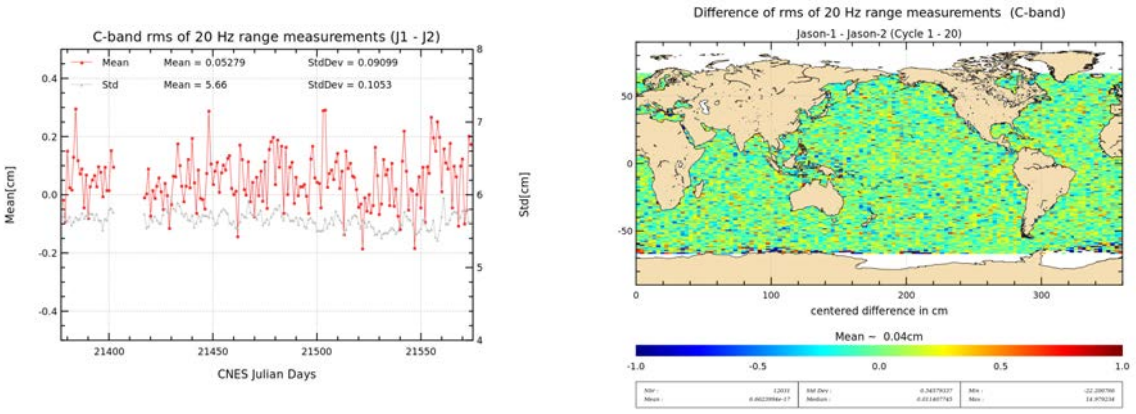

Figure 27 – Daily monitoring of mean and standard deviation of Jason-1 - Jason-2 differences for rms of elementary 20 Hz C-band range measurements (left) and map showing mean of Jason-1 - Jason-2 differences over cycles 1 to 20 (right).

4.3. Off-Nadir Angle from waveforms

The off-nadir angle is estimated from the waveform shape during the altimeter processing. The square of the off-nadir angle, averaged on a daily basis, has been plotted for Jason-1 and Jason-2 on the left side of figure 28, whereas the right side shows the histograms over one cycle. For GDR-D Jason-2 the mispointing is very stable and very close to zero (though very slightly negative). Whereas Jason-1 may show higher values (related to the reduced tracking performance of both star trackers, especially during fixed-yaw). Jason-1 experienced especially during 2010 very high mispointing values, for more information see Jason-1 validation report [11]. Jason-1 mispointing situation has been highly improved since end of 2010.
Jason-2 GDR-T mispointing was slightly positive (see also reprocessing report ([17])), which was related to the antenna aperture values used for data processing (1.26° for GDR-T, 1.29° for GDR-D). Indeed [101] shows, that retracking with different values of antenna aperture, changes the mean value of Jason-2 mispointing (see figure 29). Note that for Jason-1 1.28° is used for the antenna aperture.

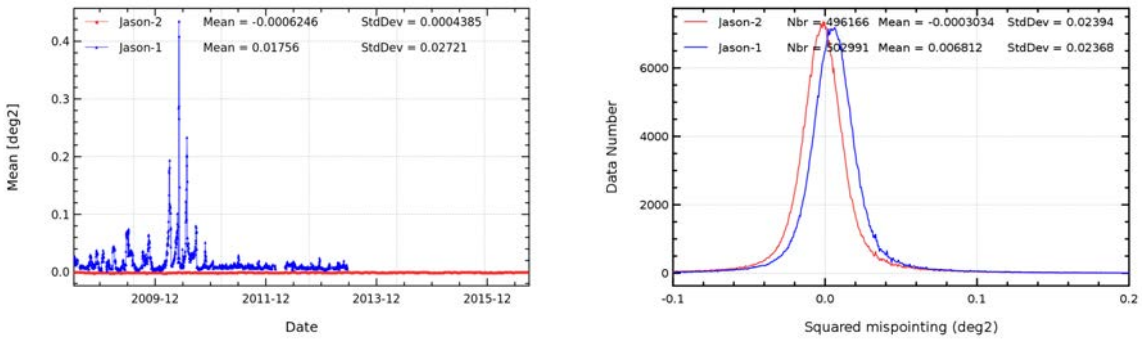

Figure 28 – Square of the off-nadir angle deduced from waveforms (deg^2) for Jason-1 and Jason-2: Daily monitoring (left), histograms for Jason-2 cycle 157 (Jason-1 cycle 513/514).

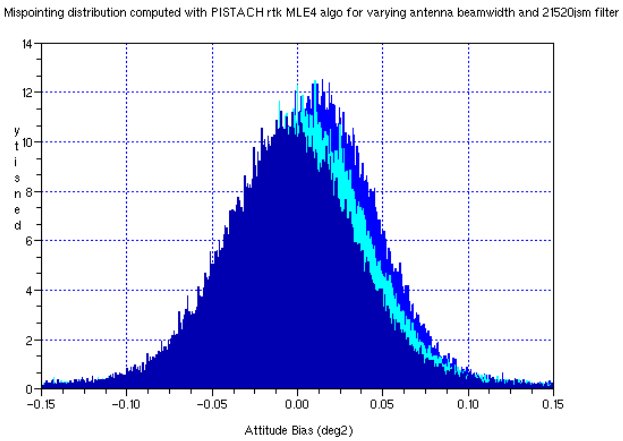

Figure 29 – Histograms of Jason-2 mispointing after retracking with different antenna beamwidth (from [101]): 1.26˚ (blue), 1.28˚ (light blue), 1.30˚ (dark blue).

4.4. Backscatter coefficient

The Jason-2 Ku-band and C-band backscatter coefficient shows good agreement with Jason-1 as visible for cyclic monitoring in figure 30 (top left and right). Left sides of figures 31 and 32 show daily monitoring of mean differences during the tandem phase. For Ku-band, a bias close to 0.29 dB is detected, it varies slightly ($\pm$ 0.05 dB). This slight variation ($\pm$ 0.05 dB) is related to Jason-1 backscatter coefficient which is slightly impacted by the higher off-nadir angles (due to low star tracker availability). Note that backscatter coefficients include instrumental corrections, which include also atmospheric attenuation which comes from the radiometer. Therefore differences between backscatter coefficients can also be partly due to differences between the atmospheric attenuation algorithms of Jason-1 and Jason-2. The main reasons for the differences (between Jason-1 and Jason-2 backscatter coefficients) are related to the antenna calibrations and to the internal calibrations of the altimeters (steps of numerical gain control).
The average standard deviation of both Sigma0 differences (measurement by measurement) is also very low around 0.15 dB rms. C-Band sigma0 differences indicate a small bias close to 0.16 dB. In the meantime, the map of mean differences (right side of figures 31 and 32) highlights very small differences. During the formation flight phase (from Jason-2 cycle 21 to 135), mean differences continue to be calculated but comparing only the global day per day statistics (see bottom of figure 30). Although the statistic is calculated less accurately, a similar bias is observed as during the tandem phase. After the last safe hold mode of Jason-1 (March 2013), a small jump is visible in the Jason-1 minus Jason-2 Sigma0 difference.

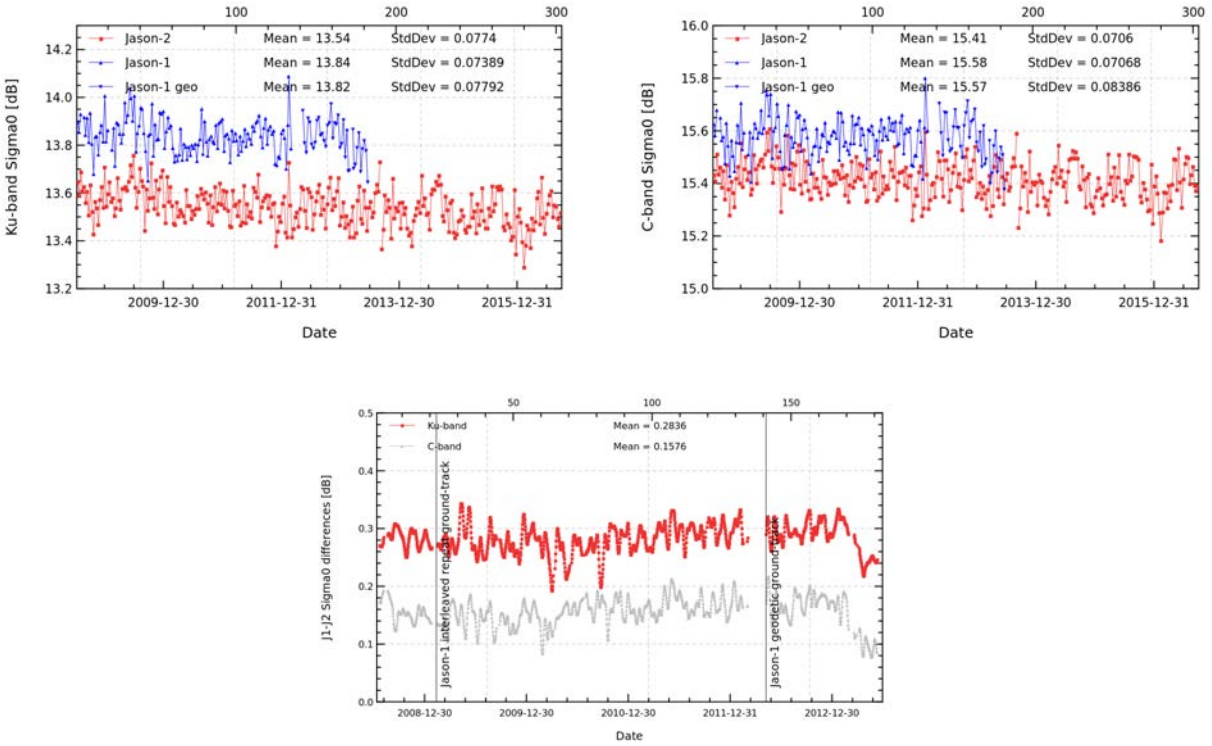

Figure 30 – Cyclic monitoring of Sigma0 for Jason-1 and Jason-2 for Ku-band (left) and C-band (right). Daily monitoring of Jason-1 - Jason-2 differences (bottom), a 10 day filter is applied.

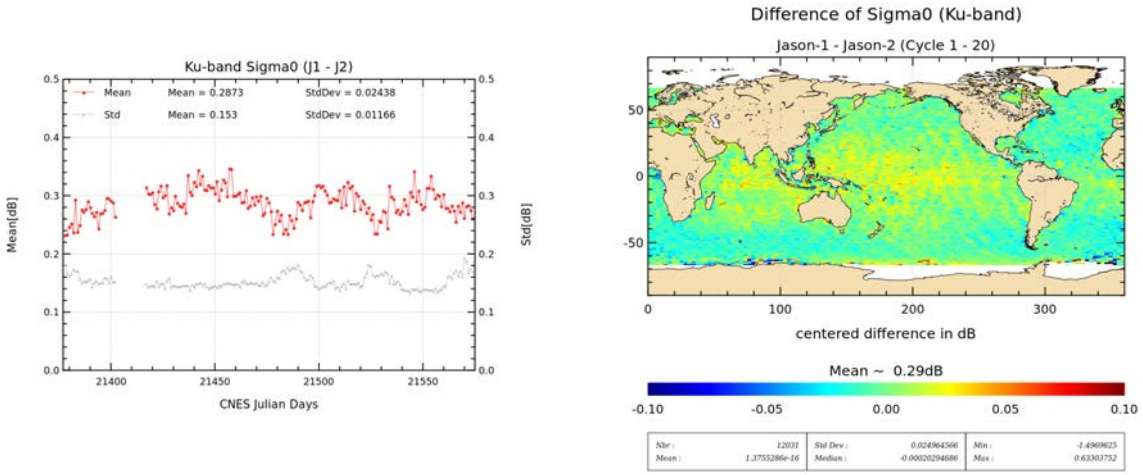

Figure 31 – Daily monitoring of mean and standard deviation of Jason-1 - Jason-2 differences for Ku-band Sigma0 (left) and map showing mean of Jason-1 - Jason-2 differences over cycles 1 to 20.

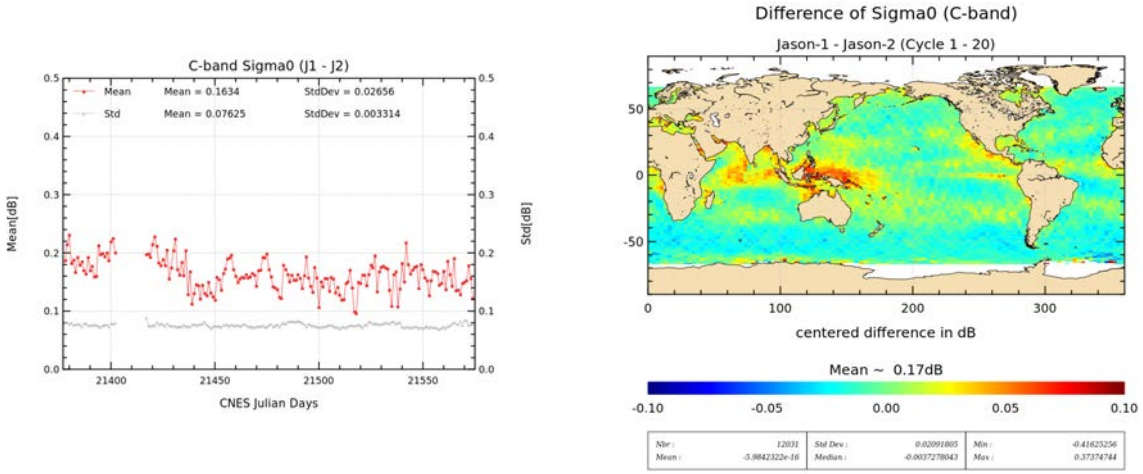

Figure 32 – Daily monitoring of mean and standard deviation of Jason-1 - Jason-2 differences for C-band Sigma0 (left) and map showing mean of Jason-1 - Jason-2 differences over cycles 1 to 20.

4.5. Significant wave height

As for Sigma0 parameter, a very good consistency between both significant wave height is shown (see top left and right of figure 33). A small bias close to around -1.3 cm is calculated over the tandem phase. It is close to -1.7 cm in C-band (see left side of figures 34 and 35). It is stable in time and space (see map of differences in right side of figures 34 and 35). These differences are too weak to impact scientific applications. They are probably due to ground processing differences between both missions. Differences are noisier for C-band. As previously, extending the monitoring of SWH bias during the formation flight phase (bottom of figure 33) highlights larger variations since both satellites do not measure the same SWH. However bias is still stable and no drift is detected.

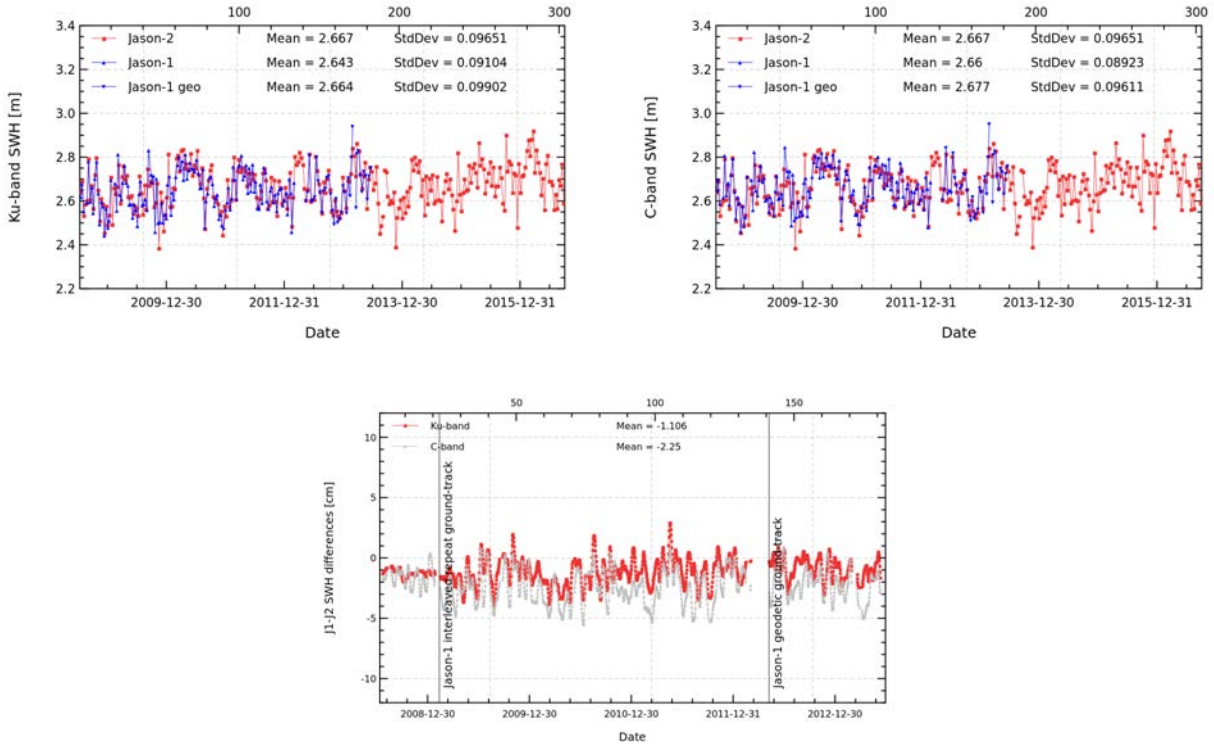

Figure 33 – Cyclic monitoring of SWH for Jason-1 and Jason-2 for Ku-band (left) and C-band (right). Daily monitoring of Jason-1 - Jason-2 differences (bottom), a 10 day filter is applied.

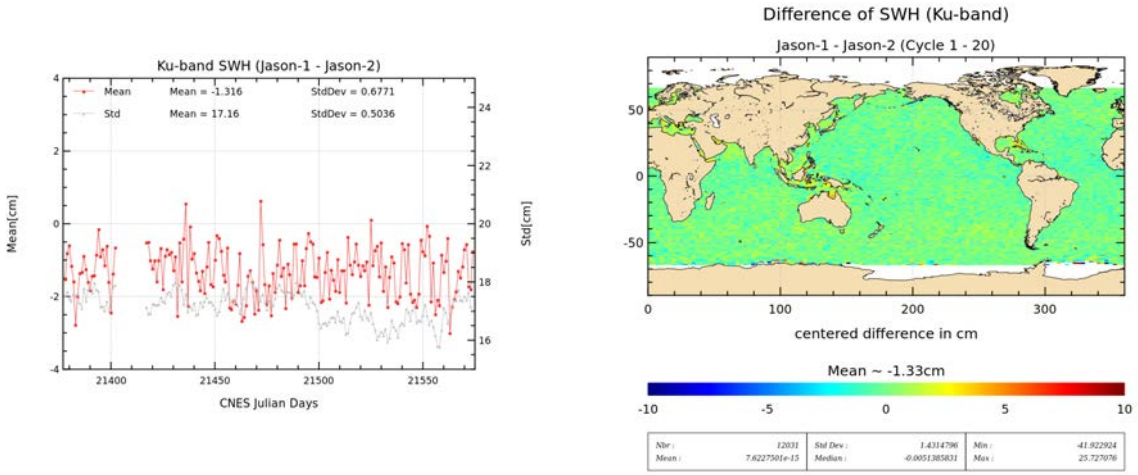

Figure 34 – Daily monitoring of mean and standard deviation of Jason-1 - Jason-2 differences for Ku-band SWH (left) and map showing mean of Jason-1 - Jason-2 differences over cycles 1 to 20.

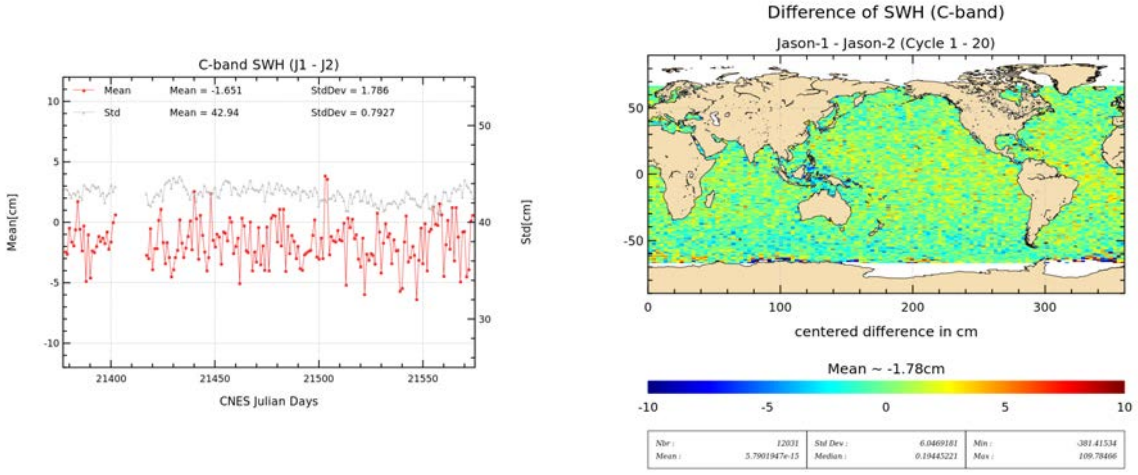

Figure 35 – Daily monitoring of mean and standard deviation of Jason-1 - Jason-2 differences for C-band SWH (left) and map showing mean of Jason-1 - Jason-2 differences over cycles 1 to 20.

4.6. Dual-frequency ionosphere correction

The dual frequency ionosphere corrections derived from the Jason-2 and Jason-1 altimeters show a mean difference of about +0.9 cm (figure 36 (left)), with cycle to cycle variations lower than 1 mm. This bias was -0.3 cm using Jason-1 GDR-C, due to the relative Ku-band (-7.0 cm) and C-band (-2.2 cm) range difference between Jason-1 and Jason-2, as well as the relative Ku-band (-2.8 cm) and C-band (-6.0 cm) sea state difference between Jason-1 and Jason-2. As the dual-frequency ionosphere correction is derived from a combination of Ku and C band ranges (corrected for the corresponding sea state bias), a bias of -3 mm between Jason-1 GDR-C and Jason-2 ionospheric corrections resulted, it is +9mm with Jason-1 GDR-E as bias on Jason-1 ranges have been modified (see [13] for more details). Apart from this bias, the two corrections are very similar and vary according to the solar activity. The map of local differences (figure 36 right) shows reduced regional differences compared to previous comparisons ([20]) thanks to Jason-1 reprocessing ([13]).

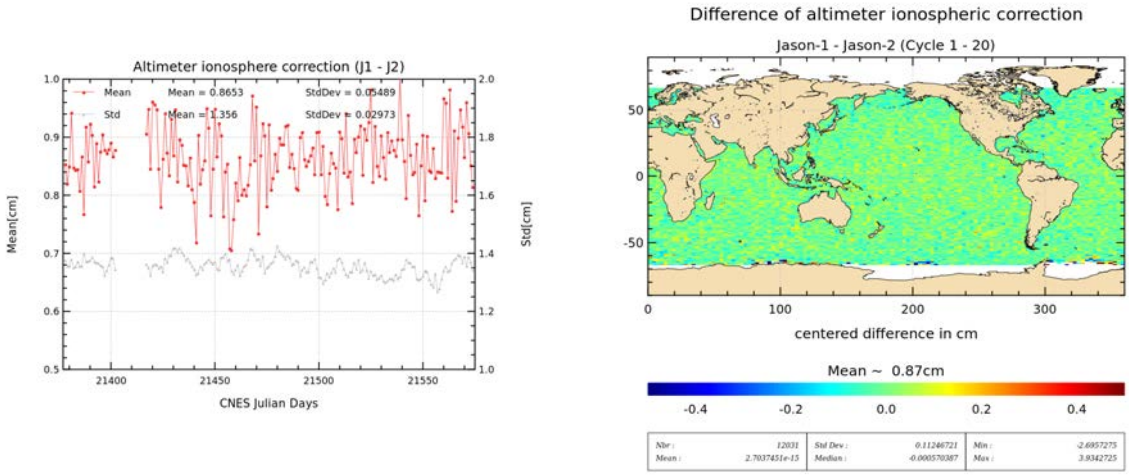

Figure 36 – Daily monitoring of mean and standard deviation of Jason-1 - Jason-2 differences for dual-frequency ionospheric correction (left) and map showing mean of Jason-1 - Jason-2 differences over cycles 1 to 20.

Notice that, as for TOPEX and Jason-1 (Le Traon et al. 1994 [77], Imel 1994 [72], Zlotnicky 1994 [106]), it is recommended to filter the Jason-2 dual frequency ionosphere correction before using it as a SSH geophysical correction (Chambers et al. 2002 [52]). A low-pass filter has thus been used to remove the noise of the correction in all SSH results presented in the following sections. Plotting difference of non-filtered ionospheric correction between Jason-1 and Jason-2 versus Jason-2 ionospheric correction shows an apparent scale error, which disappears when using filtered data (see figure 37). As in the beginning of the Jason-2 mission, ionosphere correction was very low, the ionosphere noise is of the same order of magnitude as the ionosphere correction itself. Therefore plotting the difference of non-filtered dual-frequency ionospheric correction versus dual-frequency ionospheric correction induces an apparent scale error.

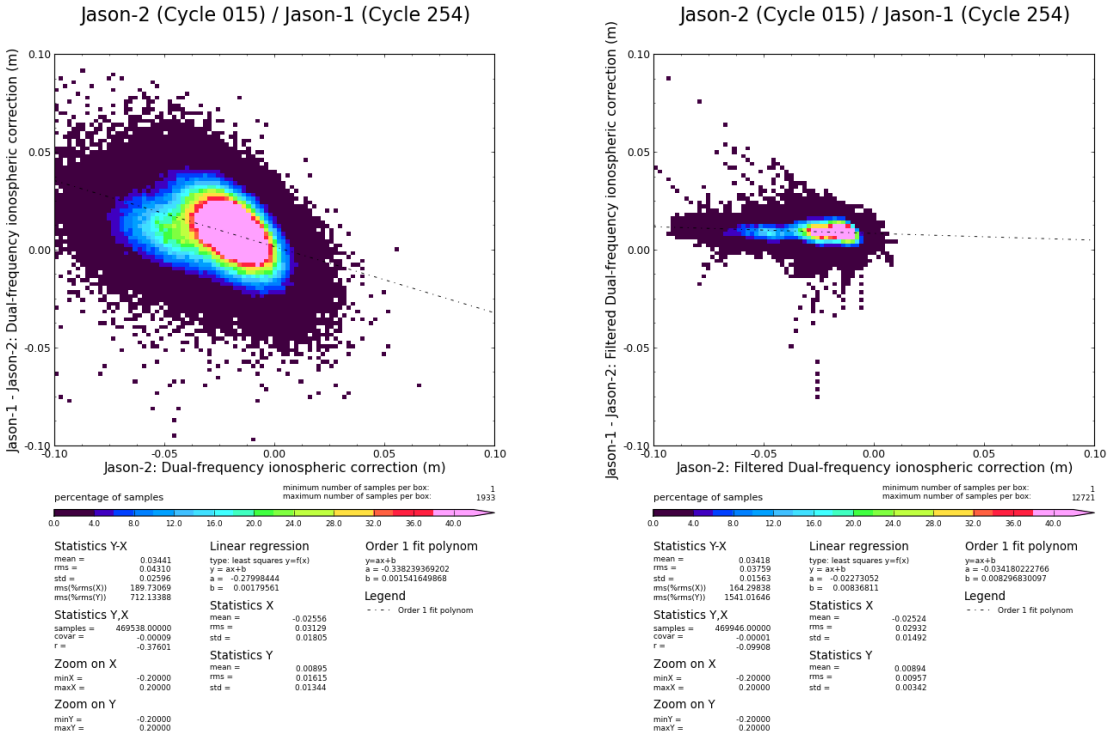

Figure 37 – Diagram of dispersion of Jason-1 (GDR-E) - Jason-2 versus Jason-2 dual-frequency ionosphere correction for Jason-2 cycle 15. Left: non-filtered, right: filtered.

During 2011, as at the end of 2013 and the beginning of 2014 solar activity has increased and therefore also the absolute value of ionosphere correction (right part of figure 38).

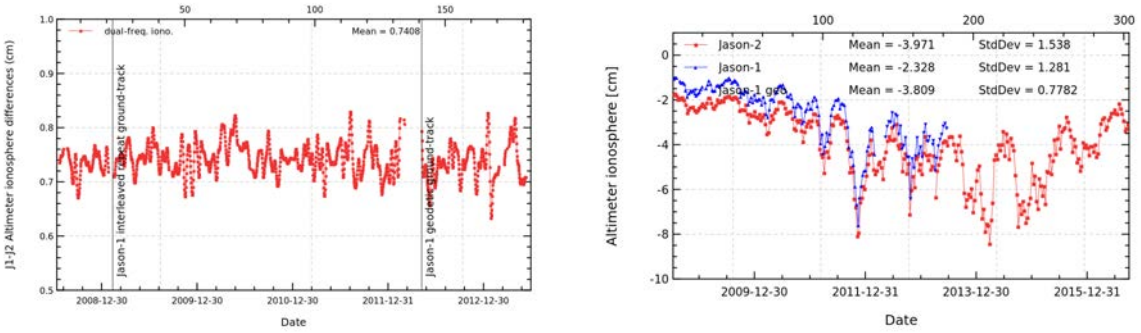

Figure 38 – Cyclic monitoring of dual-frequency ionosphere for Jason-1 and Jason-2 (right). Daily monitoring of Jason-1 - Jason-2 differences (left), a 10 day filter is applied.

When comparing altimeter ionosphere correction to GIM correction (figure 39), mean as well as standard deviation of this difference increases betwwen 2011 and 2015. This concerns both Jason missions (for 2011).

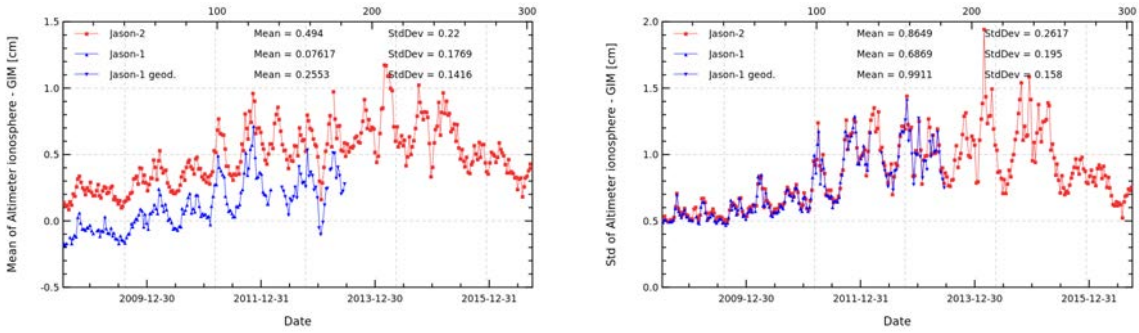

Figure 39 – Cycle per cycle monitoring of filtered altimeter ionosphere correction minus GIM ionosphere correction for Jason-1 and Jason-2. Left: Mean, right: standard deviation.

Figure 40 shows the mean difference between altimeter ionosphere and GIM correction after a one-year smooth for slots of local hours. Ionosphere differences between altimeter and GIM are higher for day time measurements than for night time measurements.

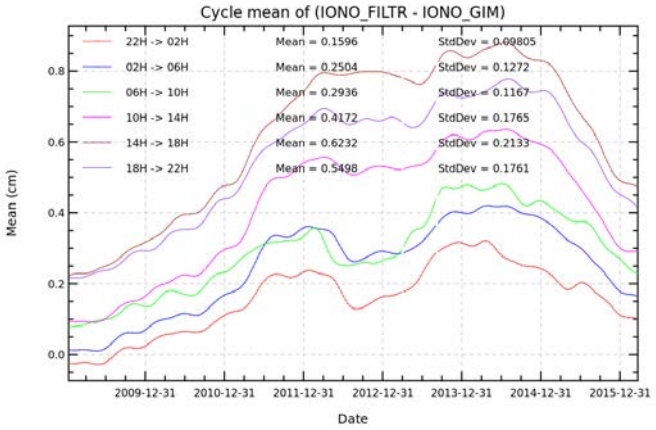

Figure 40 – Cycle per cycle monitoring of filtered altimeter ionosphere minus GIM correction computed per local hour time intervals. A one-year smooth is applied.

4.7. AMR Wet troposphere correction

4.7.1. Overview

The Jason-2 radiometer wet troposphere correction available contains an improved retrieval algorithm near coasts ([49]). Note that the product AMR radiometer wet troposphere correction has (according to S. Brown) several level of calibration:

- Cycles 1-113 - Climate data record quality calibration Cycles
- 114-140 - Intermediate quality calibration (somewhere between climate quality and operational(ARCS) quality)
- Cycle 141 onward - Operational(ARCS) quality calibration

Figure 41 shows on the left side the daily monitoring of the difference of radiometer wet troposphere correction between the two missions (JMR - AMR) during the tandem phase. Note that for Jason-1 the JMR GDR-E correction is used. AMR is globally slightly dryer than JMR (-0.13 cm). Note that both Jason-1 and Jason-2 correction use improved retrieval algorithm in coastal areas. The daily monitoring shows slight instabilities over this year 2008 (this is related to Jason-1 JMR instabilities).

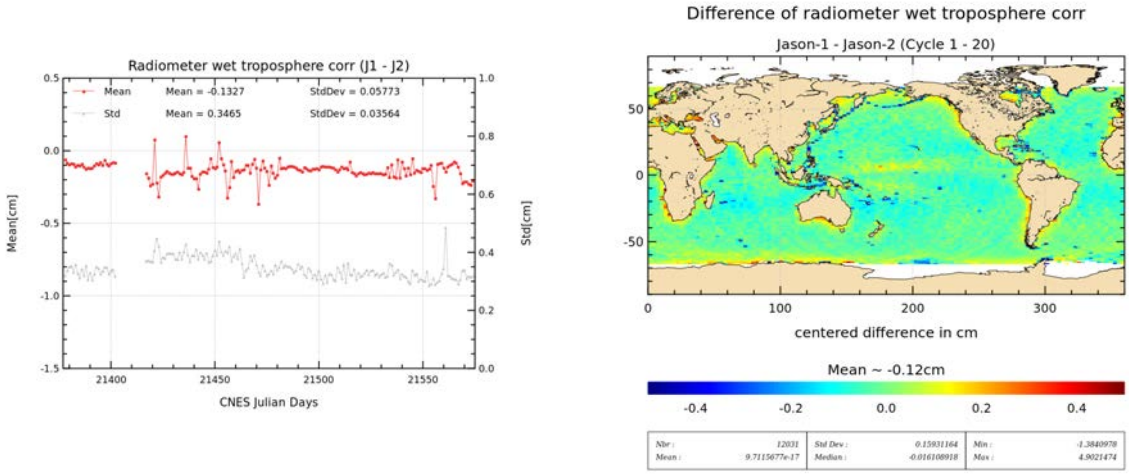

Figure 41 – Daily monitoring of mean and standard deviation (left) of Jason-1 - Jason-2 radiometer wet troposphere correction. Map showing mean of Jason-1 - Jason-2 differences over cycles 1 to 20.

Note that since 12 july 2016 (cycle 295), Jason-2 AMR have been recalibrated about every 2 months with cold sky calibration (as for Jason-3).

4.7.2. Comparison with the ECMWF model

The ECMWF wet troposphere correction has been used to check the Jason-1 and Jason-2 radiometer corrections. Daily differences are calculated and plotted in figure 43. It clearly appears (on left side of figure 43) that Jason-2 radiometer correction (AMR) from GDR products is much more stable than for Jason-1 (JMR). Now, thanks to the ARCS (Autonomous Radiometer Calibration System) (Brown et al. 2009, [48]) calibration system set up for Jason-2, AMR radiometer correction is calibrated at each GDR cycle and the calibration coefficients are modified if necessary. On right side of figure 43 the black lines indicate, each time a modification of the calibration coefficients were necessary. The lines are only drawn from cycle 114 onwards.
The AMR wet troposphere correction shows jumps and drifts in the IGDRs. The calibrations applied for the GDRs correct most of these anomalies, nevertheless small jumps persist. There can also be small drifts visible within a cycle, as the ARCS corrections apply a constant value over a whole cycle.

Finally, the cross-comparison between all radiometers and models available is necessary to analyze the stability of each wet troposphere correction. An overview of the wet troposphere correction importance for mean sea level is given in Obligis et al. [82].

Figure 42 shows mean and standard deviation for cycle per cycle differences between Jason-2 radiometer and ECMWF model wet troposphere corrections for several data types. Over year 2016, there were several changes of radiometer calibration coefficients. The radiometer minus ECMWF model wet troposphere differences for GDR is quite stable (less than 2 mm fluctuations over the year).
After the application of new calibration coefficients in GDR, the mean of IGDR and GDR radiometer minus ECMWF model wet troposphere differences are different as there is a roughly 1 to 2 month delay between GDR (black vertical lines) and IGDR (grey vertical lines) production, IGDR production was already a couple of cycles ahead. The standard deviation of OGDR and IGDR wet troposphere differences is higher for OGDR than for IGDR, as OGDR contain predicted model fields instead of analyzed model field (for IGDR and GDR products).

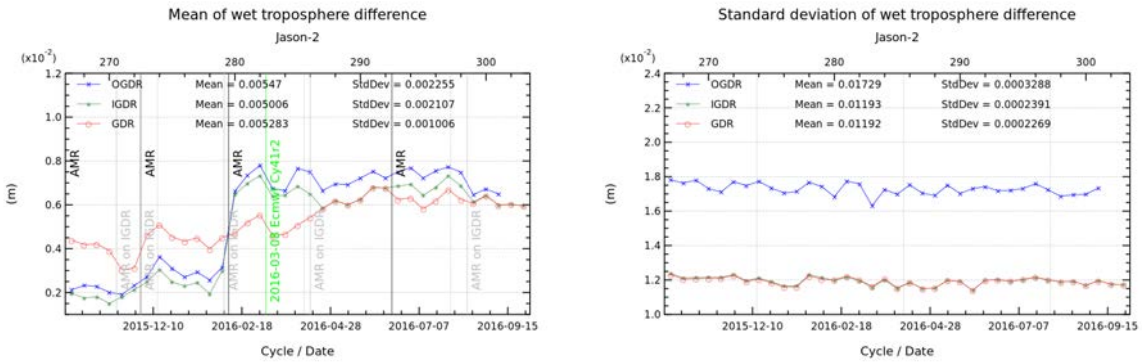

Figure 42 – Cycle per cycle monitoring of mean (left) and standard deviation (right) of radiometer minus ECMWF model wet troposphere correction over 2016 (until cycle 303) for Jason-2 O/I/GDR.

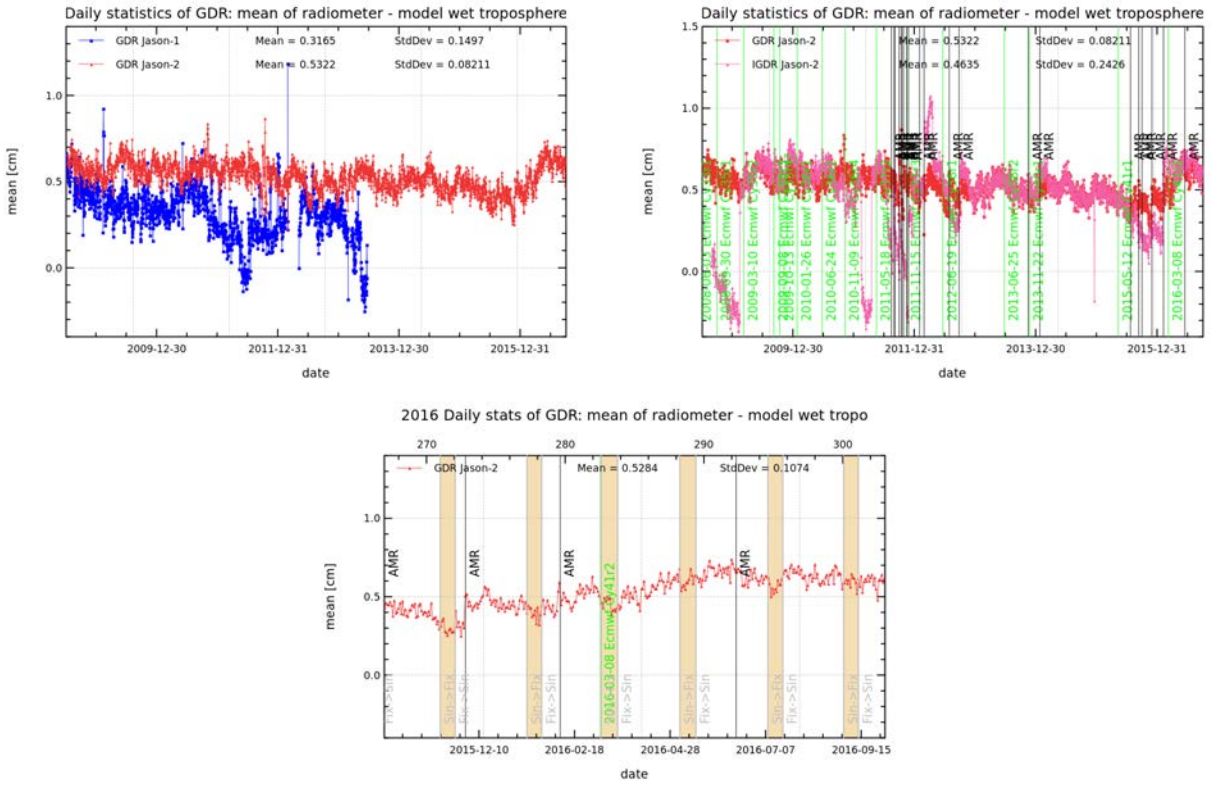

Figure 43 – Left: Daily monitoring of radiometer and ECMWF model wet troposphere correction differences for Jason-1 (blue) and Jason-2 (red). Right: daily monitoring for Jason-2 GDRs (red) and IGDRs (pink). Vertical green lines correspond to ECMWF model version changes, black lines correspond to AMR calibration coefficients changes on GDR products also impacting IGDR product (but later). Bottom: Daily monitoring for Jason-2 GDRs (red) for 2016. Vertical green lines correspond to ECMWF model version changes, black lines correspond to AMR calibration coefficients changes on GDR products. They impact also IGDR products (but later). Vertical gray bands correspond to yaw maneuvers on Jason-2.

4.7.3. Neural approach for wet tropospheric correction

In the frame of PEACHI-Jason-3 CNES contract, CLS performed a comparison between JPL and CLS/IPSL approaches for the wet tropospheric correction (WTC) retrieval ([112]).
JPL is in charge of the WTC retrieval NASA/CNES missions since Topex/Poseidon. Their algorithm is based on a statistical approach and a log-linear model parameterized through a comparison between radiosonde measurements and simulated brightness temperatures (TB).
CLS/IPSL method applied to Envisat, AltiKa and Sentinel-3 is based on a statistical approach and a neural network (NN) learned from a comparison between ECMWF surface and atmosphere analysis and simulated TB.
Then, the main differences between JPL and CLS/IPSL approaches are:

- log-linear (JPL) versus neural network (CLS/IPSL)
- NxM algorithms corresponding to N classes of wind and M classes of WTC (JPL) versus one

global algorithm (CLS/IPSL)

The main goal of this study is to defined a neural network / per classes approach, to compare the performance to the JPL WTC product and implement this solution in the PEACHI-J3 prototype. A comparison performed on Jason-2 products shows a small but significative improvement of the SSH variance at cross-over with a reduction of about 0.15 cm², that is of about 5% of the improvement of the radiometer WTC compared to ECMWF WTC.

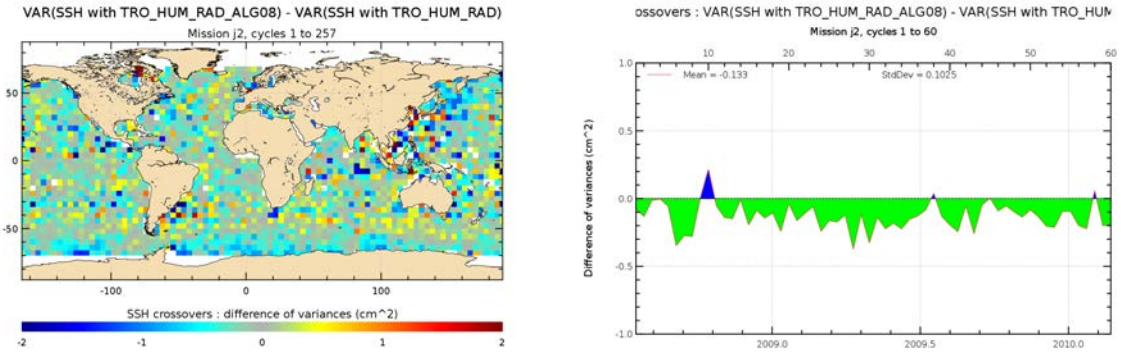

*Figure 44 – Map (**left**) and monitoring (**right**) of difference of variance at crossovers , neural approach for wet troposphere minus GDR product wet troposphere.*

4.8. Altimeter wind speed

Figure 45 shows on the left side the daily monitoring of the difference of altimeter wind speed between the two missions. Before the Jason-1 and Jason-2 reprocessing, there was a difference of about -0.4 m/s between Jason-1 and Jason-2. Finally the regional differences are also reduced. Locally (right side of figure 45), altimeter wind speed from Jason-1 is higher than from Jason-2. The signal visible on daily monitoring, is anti-correlated to the signal visible on daily monitoring of backscatter coefficient (see figure 31), as wind speed computation uses principally backscatter coefficient. This signal is related to events of high mispointing of Jason-1.

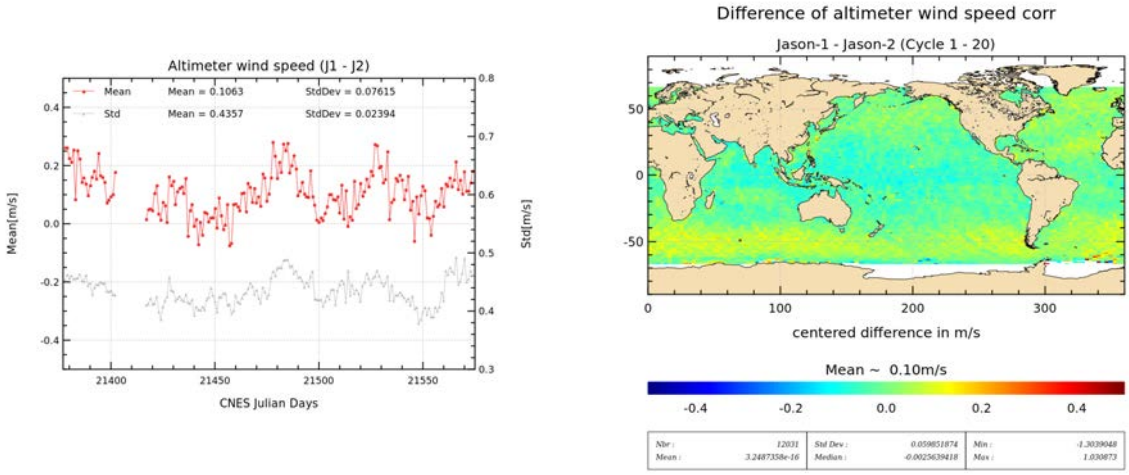

Figure 45 – Daily monitoring of mean and standard deviation (left) of Jason-1 - Jason-2 altimeter wind speed. Map showing mean of Jason-1 - Jason-2 differences over cycles 1 to 20.

Figure 46 shows mean and standard deviation for cycle per cycle altimeter wind speed for several data types of Jason-2. The altimeter wind speed of the different data types is coherent.

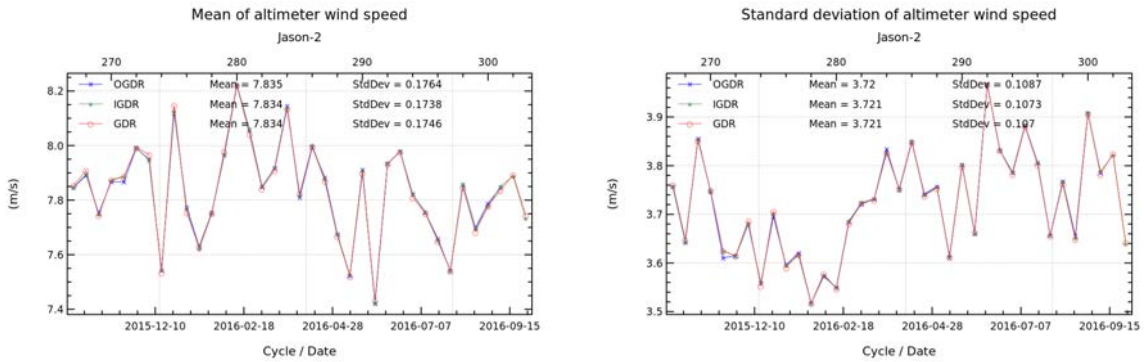

Figure 46 – Cycle per cycle monitoring of mean (left) and standard deviation (right) of altimeter wind speed over 2016 (until cycle 303) for Jason-2 O/I/GDR.

4.9. Sea state bias

The sea state bias look-up table used for GDR-D was computed using Jason-2 data from internal reprocessing which were as close as possible to the GDR-D standards. At OSTST 2012 meeting, Tran et al. [105] presented a new SSB model computed using one year of GDR-D data. This model seems better than the SSB model used for the GDR-D product, and as been used for Jason-1 GDR-E reprocessing (computed with GDR-E like Jason-1 data (see [13]). When using the updated sea state bias proposed by Tran et al. [105] for both missions, differences between Jason-1 GDR-E and Jason-2 GDR-D are about +0.3 cm (left of figure 47).

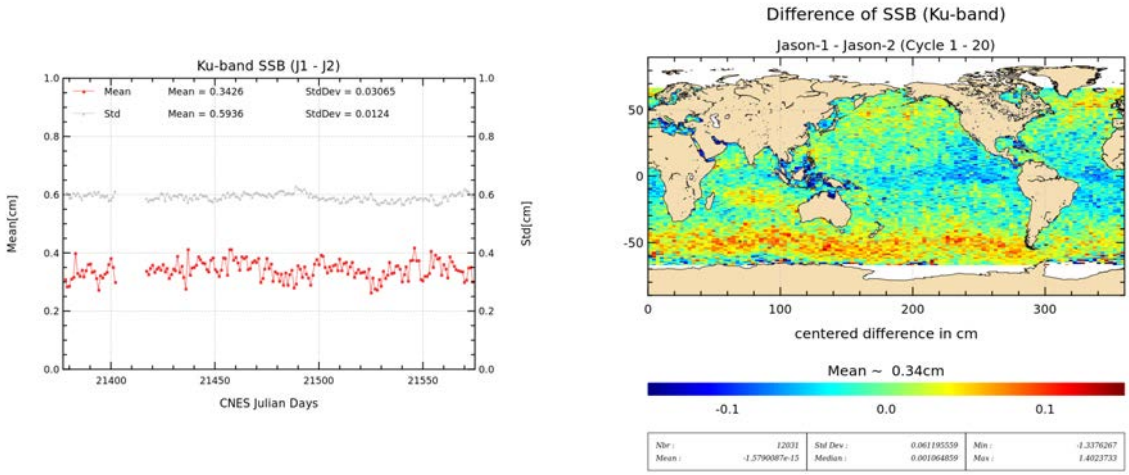

Figure 47 – Daily monitoring of mean and standard deviation (left) of Jason-1 - Jason-2 sea state bias over cycles 1 to 20. DMap showing mean of Jason-1 - Jason-2 sea state bias differences over cycles 1 to 20. using SSB from Jason-1 GDR-E and updated (2012) SSB for Jason-2 (map centered around +0.34 cm) (right).

5. SSH crossover analysis

5.1. Overview

SSH crossover differences are the main tool to analyze the whole altimetry system performances. They allow us to analyze the SSH consistency between ascending and descending passes. However in order to reduce the impact of oceanic variability, we select crossovers with a maximum time lag of 10 days. Mean and standard deviation of SSH crossover differences are computed from the valid data set to perform maps or a cycle by cycle monitoring over all the altimeter period. In order to monitor the performances over stable surfaces, additional editing is applied to remove shallow waters (bathymetry above -1000m), areas of high ocean variability (variability above 20 cm rms) and high latitudes ($> |50|deg$). SSH performances are then always estimated with equivalent conditions. The main SSH calculation for Jason-2 and Jason-1 are defined below.

$$SSH = Orbit - Altimeter\ Range - \sum_{i=1}^{n} Correction_i$$

with $Jason-1/Jason-2\ Orbit = CNES\ orbit$ for GDR products, and

$$\begin{aligned}\sum_{i=1}^{n} Correction_i &= Dry\ troposphere\ correction \\ &+ Dynamical\ atmospheric\ correction \\ &+ Radiometer\ wet\ troposphere\ correction \\ &+ Dual\ frequency\ ionospheric\ correction\ (filter\ 250\ km) \\ &+ Non\ parametric\ sea\ state\ bias\ correction \\ &+ Ocean\ tide\ correction\ (including\ loading\ tide) \\ &+ Earth\ tide\ height \\ &+ Pole\ tide\ height\end{aligned}$$

In 2016, Jason-1 GDR were available in version E. In order to allow better comparisons between Jason-1 and Jason-2, some standards of Jason-2 were updated (only when comparisons are done with Jason-1 GDR-E).

Note that from 7th of May 2012 (Jason-1 cycle 500, which corresponds to end of Jason-2 cycle 141) and until the end of the Jason-1 mission (21st of June 2013, during Jason-2 cycle 183), Jason-1 was on a geodetic ground-track.

5.2. Mean of SSH crossover differences

The cycle by cycle mean of SSH differences is plotted in figure 48 for Jason-2 and Jason-1 (using standards from Jason-1 GDR-E products). The curves are very similar and do not highlight any anomaly. However, a 120 day signal is visible for Jason-1 data (and also, but smaller on Jason-2 updated data).
Mean of SSH differences at crossovers for Jason-2 IGDR products (using MOE orbits) has noticeable negative values in average (-0.38cm over the last year versus -0.06cm in case of GDR), as can be seen

on left of figure 48. In addition, the IGDR data monitoring shows a 120 day signal that is reduced in case of GDR (right of figure 48). This difference of behaviour for IGDR and GDR is explained by the way the solar radiation pressure is taken into account in orbit solution computation (different for MOE and POE). Thanks to the orbit standard E (an identical modeling of solar radiation pressure is planned for MOE and POE) applied from cycle 254 onwards, the 120 day signal on IGDR is slightly reduced. In addition, even the remaining 120 day signal on GDR is reduced with POE-E (see bottom of figure 48).

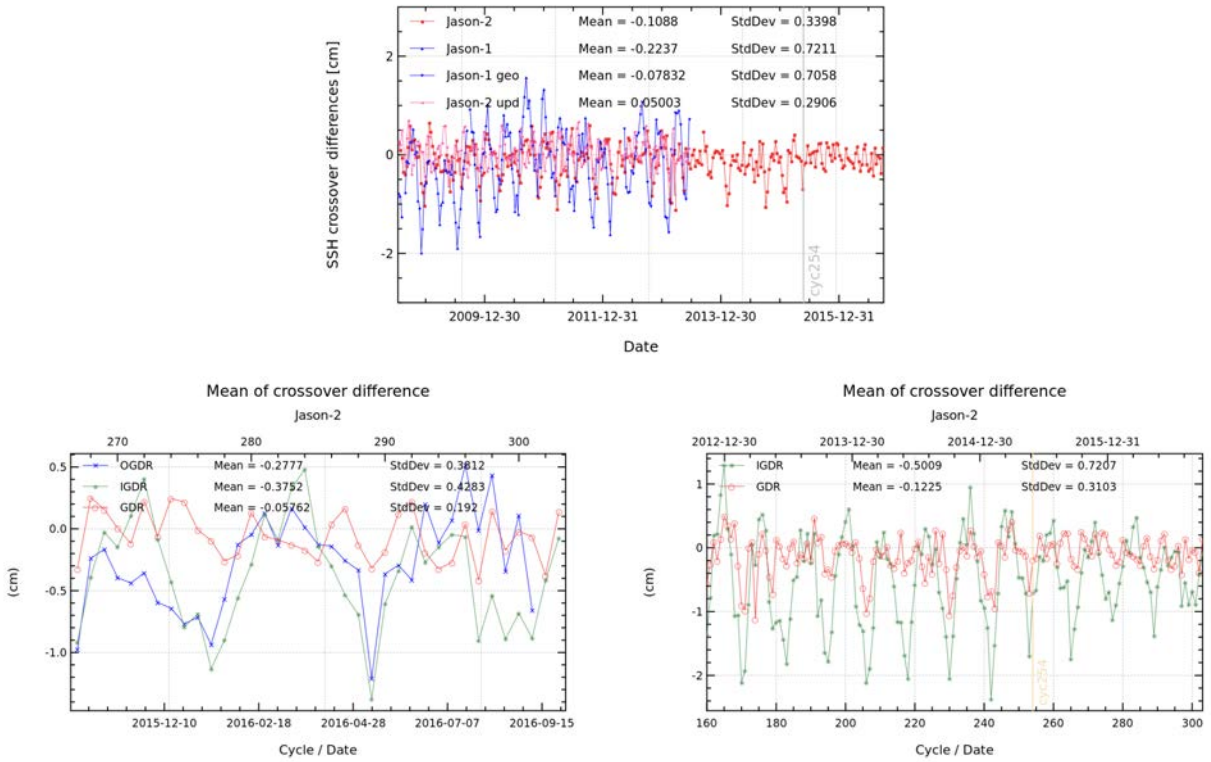

Figure 48 – Top: Monitoring of mean of SSH crossover differences for Jason-2 and Jason-1 using Jason-2 (red), Jason-1 GDR-E (blue), Jason-2 GDR-D Upd with GOT4.10 + POE-E + Tran2012 SSB (pink). Bottom: Monitoring of mean of SSH crossover differences for different data types of Jason-2: OGDR (blue), IGDR (green), GDR (red): over 2016 (left) and over 4 years (right).

The map of mean SSH crossover differences plotted in left side of figure 49 was calculated using Jason-2 GDR products, no strong geographically correlated patterns are detected. Nevertheless, there is a slight geographically correlated pattern on the map with GDR-D orbit solution (POE-D until cycle 253 and POE-E from cycle 254 onwards). This pattern disappears (right of figure 49) using only the final POE-E solution (see details about POE-E here [20] and [29]). This pattern might be related to the 120 day signal, as it disappears in the same time as the 120 day signal is reduced in the periodogram of the final POE-E solution (not shown here).

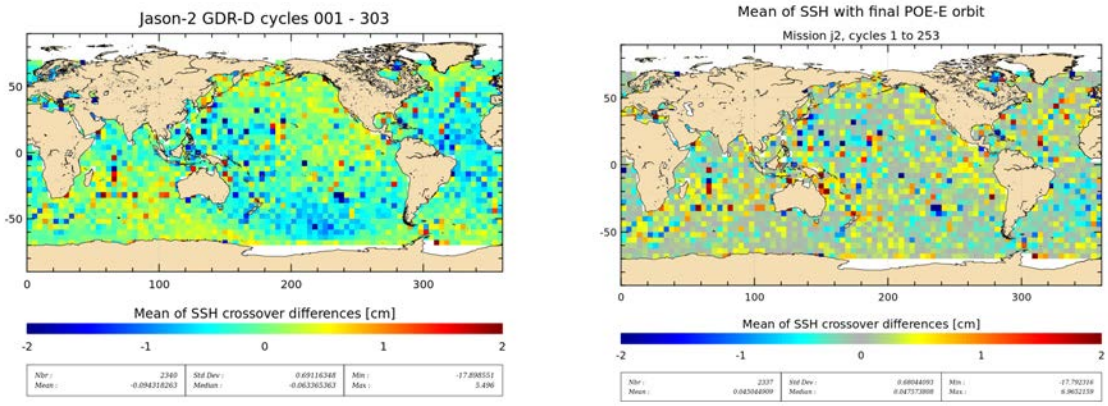

Figure 49 – Left: Map of mean of SSH crossovers differences for Jason-2 cycle 1 to 303. note that for cycles 1 to 253, GDR orbit is POE-D. GDR have been available with orbit POE-E since cycle 254. Right: Map of mean of SSH crossovers differences for Jason-2 cycle 1 to 253 using final POE-E orbit solution.

5.3. Standard deviation of SSH crossover differences

The cycle by cycle standard deviation of SSH crossovers differences are plotted for Jason-2 and Jason-1 in figure 50 after applying geographical criteria (bathymetry, latitude, oceanic variability) as defined previously (chapter 5.1.). Both missions show very good performances, very similar and stable in time. No anomaly is detected. The average figure is 5.0 cm rms for Jason-1, and 4.9 cm rms for Jason-2 data. Keeping in mind that during the Jason-1/TOPEX tandem phase in 2002, the same statistic using Jason-1 GDR-A products was close to 6.15 cm (see [61]). This illustrates the improvements performed in the altimetry ground processing since the Jason-1 launch especially thanks to new retracking algorithms, new geophysical corrections (oceanic tidal, dynamic atmospheric correction, ...) and new orbit calculations implemented first in GDR-B and later in GDR-C and GDR-E releases (see [91] concerning impact of GDR-B/GDR-A, [54] concerning impact of GDR-C/GDR-B, [13] concerning impact of GDR-E/GDR-C). The reprocessing of Jason-2 in GDR-D also improved the performance at crossover points compared to previous GDR-T. The variance of SSH crossover differences was reduced by 1.7 cm2 when switching from GDR-T to GDR-D standards, as shown on [15]. The main contributors to this improvement are the POE-D orbit standard and the GOT4.8 global ocean tide. Though Jason-1 and Jason-2 show very good performances and are within the mission specifications, their standard deviation of SSH differences at crossovers is sometimes higher than usual.

When comparing the performances of the different Jason-2 data types (OGDR, IGDR, GDR) over 2016 (right of figure 50), OGDR have the highest standard deviation with 6.1 cm, though this value is already extremely good considering that OGDR have a latency of about 3h, recalling that Jason-1 GDR-A products had a standard deviation of 6.15 cm. IGDR data have a standard deviation of 5.1 cm over the year.

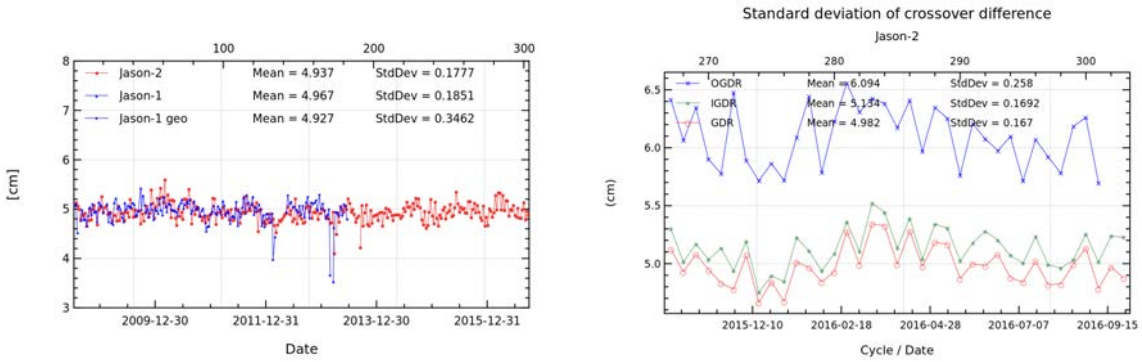

Figure 50 – Cycle by cycle standard deviation of SSH crossover differences for Jason-2 and Jason-1. Only data with abs(latitude) < 50°, bathymetry < -1000m and low oceanic variability were selected.

5.4. Estimation of pseudo time-tag bias

The pseudo time tag bias (α) is found by computing at SSH crossovers a regression between SSH and orbital altitude rate ($\dot{H}$), also called satellite radial speed:

$$SSH = \alpha \dot{H}$$

This empirical method allows us to estimate the potential real time tag bias but it can also absorb other errors correlated with $\dot{H}$. Therefore it is called "pseudo" time tag bias. The monitoring of this coefficient estimated at each cycle is performed for Jason-1 and Jason-2 in figure 51. Both curves are very similar highlighting an almost 59-day signal with almost no bias (close to -0.01 ms for Jason-1 and -0.02 ms for Jason-2).
Before the Jason-2 reprocessing the GDR-T showed a bias of -0.29 ms. The origin of constant part of the pseudo time tag bias was found by CNES [45] and so corrected in the Jason-2 GDR-D and Jason-1 GDR-E product (see also the Jason-2 [69] and Jason-1 [5] handbooks). The 59 day-signal is reduced for Jason-1 pseudo-datation bias thanks to the use of GOT4.10 ocean tide solution (see [13]).

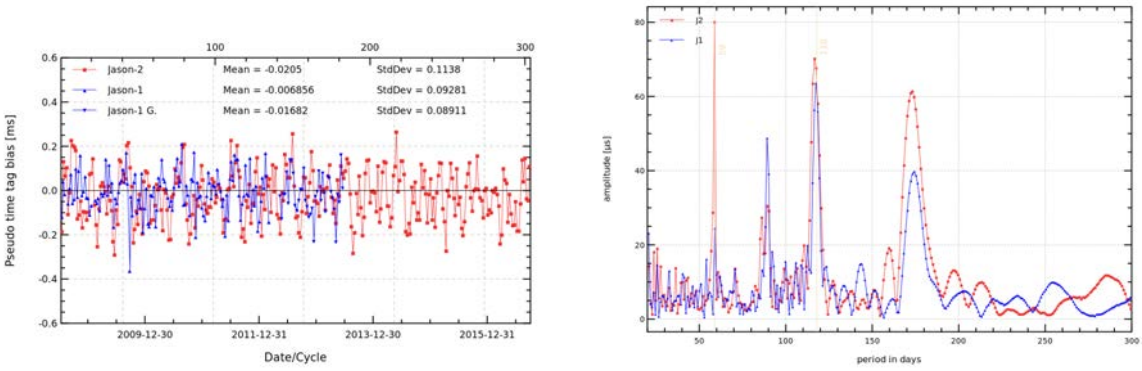

Figure 51 – Monitoring (left) and periodogram (right) of pseudo time-tag bias estimated cycle by cycle from GDR products for Jason-2 and Jason-1

6. Sea Level Anomalies (SLA) Along-track analysis

6.1. Overview

The Sea Level Anomalies (SLA) are computed along track from the SSH minus the mean sea surface with the SSH calculated as defined in previous section 5.1. :

$$SLA = SSH - MSS$$

Note that for better comparison with Jason-1, Jsaon-2 GDR-D are updated using GDR-E standards (POE-E orbit, Got4.10 ocean tide, MSS_CNES_CLS_2011 (with reference period of 20 years), Tran2012 sea state bias, and recomputed ionosphere correction (using Tran2012 ssb)).

SLA analysis is a complementary indicator to estimate the altimetry system performances. It allows us to study the evolution of SLA mean (detection of jump, abnormal trend or geographical correlated biases), and also the evolution of the SLA variance highlighting the long-term stability of the altimetry system performances. In order to take advantage of the Jason-2/Jason-1 tandem phase (cycles 1 to 20), we performed direct SLA comparisons between both missions during this period.

Corrections applied in SSH calculation are theoretically the same for Jason-1 and Jason-2 since both satellites measure the same ocean. Thus, it is possible to not apply them in order to obtain directly information on the altimeter range and the orbit calculation differences. However, as the stability of both ground passes is not exact (the ground track is maintained within a window of $\pm$ 1 km across-track distance from the theoretical ground track), SLA measurements have to be projected and interpolated over the Jason/TOPEX theoretical ground pass after applying the MSS in order to take into account cross-track effects on SSH.

$$\Delta SLA_{J1-J2} = [(Range_{Ku} - Orbite - MSS)_{J1}]_{\bar{T}} - [(Range_{Ku} - Orbite - MSS)_{J2}]_{\bar{T}}$$

This allows us also to select the intersection of both datasets and compare exactly the same data. After Jason-1 ground track change to its interleaved ground track, direct SLA comparisons are no more possible. Thus, global statistics computed cycle by cycle are just basically compared.

6.2. Mean of SLA differences between Jason-2 and updated Jason-1

The cycle by cycle monitoring of mean SLA differences between Jason-1 data and Jason-2 is plotted in figure 52 over all the Jason-2 period. During the tandem phase, the SSH bias is computed with and without the SSH corrections. During this period, both types of curves are very similar and stable in time with variations close to 1 mm rms, except that they are spaced out by a 1.1 cm bias (1.2 cm when using ECMWF model wet troposphere correction). This bias results from differences between Jason-1 and Jason-2 sea state bias model used, and to a small amount due to ionosphere correction differences. The global average SSH bias is close to -0.2 cm using SSH corrections (-0.3 cm when using ECMWF instead of radiometer wet troposphere correction) and 0.9 cm without (the 7.1 cm bias between Jason-1 GDR-C and Jason-2 GDR-D (see [20]) was corrected in Jason-1 data during the 2016 reprocessing [13]). However, the more crucial point for scientific applications is to insure that there is no drift between both missions, since the global bias can be corrected a

fortiori. The extension of the monitoring of the SSH bias after the Jason-1 ground track change is precisely a good way to check the long-term Jason-1 and Jason-2 stability. It is plotted over all common with Jason-1 cycles in figure 52.
When Jason-1 was moved to a geodetic ground track, a jump was visible with Jason-1 GDR-C data [20]. A part of this jump was understood. These explained part of the jump was corrected in Jason-1 data during the 2016 reprocessing [13]). Nevertheless, a small jump remains after Jason-1 safe hold mode in March 2013: it seems to be related to radiometer wet troposphere solution as it is not visible using model wet tropopshere correction (see [13] for more details).

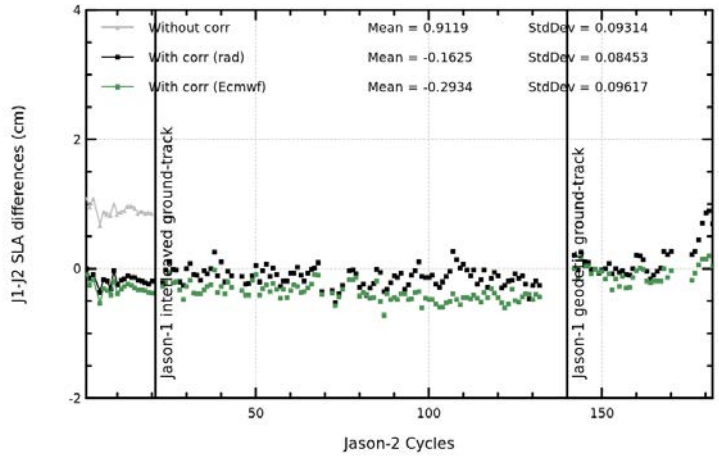

Figure 52 – Cycle by cycle monitoring of SSH bias between Jason-1 and Jason-2 before and after Jason-1 ground-track change (black curve and dots) and SSH bias without applying corrections in SSH calculation for both missions only during the tandem phase (gray curve).

Figure 53 shows the mean differences between Jason-1 and Jason-2 during tandem phase (cycles 1 to 20).

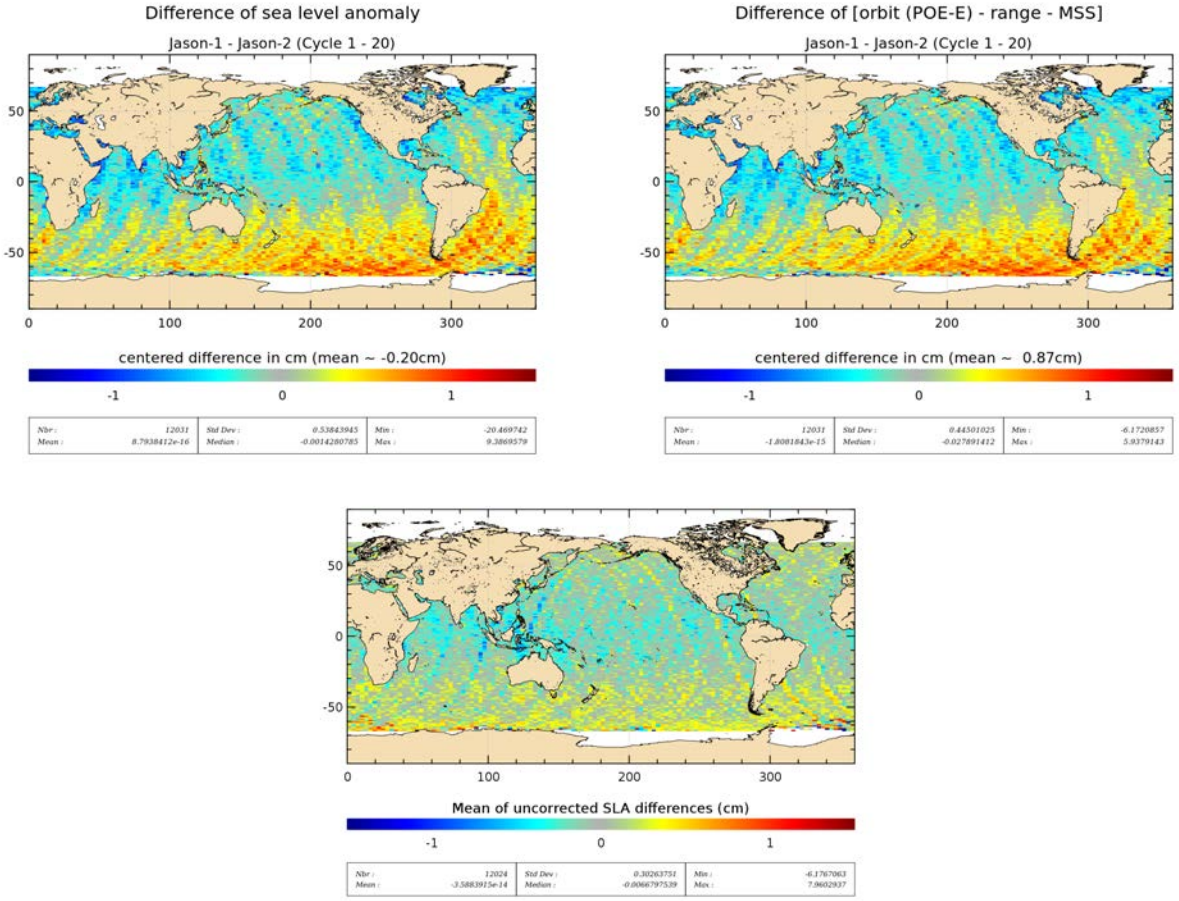

Figure 53 – ***Top left:*** *Maps of SLA (orbit (POE-E) - range - geophysical corrections - MSS 2011 (ref20)) mean differences between Jason-1 and Jason-2 during tandem phase (cycles 1 to 20), using Jason-2 updated GDR-D and Jason-1 GDR-E (the map is centered around the mean of 0.2 cm).* ***Top right:*** *without applying geophysical corrections.* ***Bottom:*** *using GSFC09 orbits without applying geophysical corrections*

Thanks to the update of sea state bias with the OSTST 2012 solution for both satellites Jason-1 and Jason-2 SLA are quite homogeneous. In order to obtain directly information on the altimeter range and the orbit calculation differences, spatial uncorrected SLA (orbit - range - MSS) differences (only during the Jason-1/Jason-2 tandem phase) between both missions is plotted in right side of figure 53. It shows a weak hemispheric bias lower than 1 cm. These differences are in relationship with orbit calculation differences. Though for both satellites POE-E was used, there are some differences between Jason-1 POE-E and Jason-2 POE-E, for Jason-1 orbit computation the GPS data are no longer available, whereas they are used for the Jason-2 POE computation. Jason-2 POE is therefore based on two orbit determination techniques (Doris and GPS, Laser is used for validation), whereas Jason-1 POE (over the Jason-2 period) is based on two orbit determination techniques (Doris and Laser). When using GSFC std 0905 orbits for both satellites (bottom of figure 53) the hemispheric bias disappears (the same result has been found using GSFC std 1204 orbit solution, but it is not shown here).

6.3. Standard deviation of SLA differences between Jason-2 and Jason-1

The monitoring of SLA standard deviation has been computed for both missions (plotted in figure 54). As concerned Jason-1, the blue curves are drawn using the standards that are in the GDR-E products (contain the MSS CNES/CLS 2011 referenced over 20years), whereas GDR-D standards are used to Jason-2 red curves (contain the MSS CNES/CLS 2011 referenced over 7years). Note that the standard deviation of GDR-E SLA is reduced compared to GDR-D thanks to GOT4.10 and $CNES/CLS2011_{with\ the\ reference\ period\ of\ 20\ years}$ MSS (see [13]). The change of reference period from 7 years to 20 years integrates the evolution of the sea level in terms of trends, but also in terms of interannual signals at small and large scales (e.g. Niño/Niña) in the additional 13 years: changing from a 7 to 20 years reference period leads to better interannual signals and oceanic anomalies (see [96] for more details about the change on reference period).
Cartography of standard deviation of spatial Jason-1 minus Jason-2 SLA differences (not shown here) does not show any anomaly. It varies indeed in function of noise on measurements, which is dependent on significant wave height. Therefore, standard deviation of SLA differences is higher in regions with important significant wave heights.
In addition to these results, a special investigation on SLA with 500km filtering is detailed in the investigation part about SLA in [18].

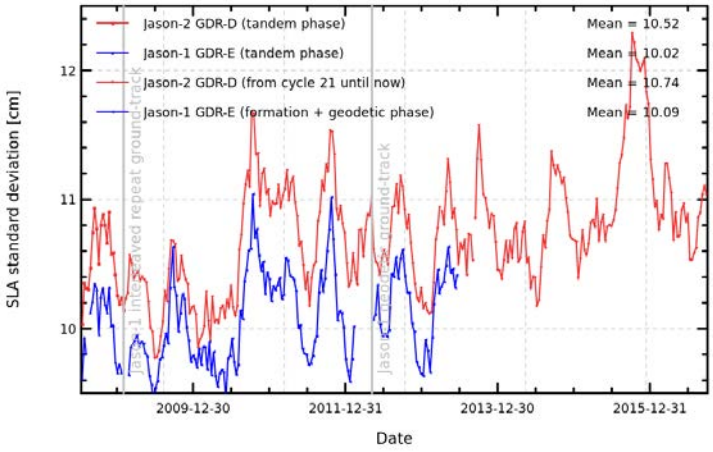

Figure 54 – Cycle by cycle monitoring of SLA standard deviation for Jason-1 and Jason-2.

6.4. Sea level seasonal variations

From Sea Level Anomalies computed relative to the Mean Sea Surface CNES-CLS 2011, the surface topography seasonal variations have been mapped in table 8 for the overall Jason-2 data set. Major oceanic signals are shown clearly by these maps: it allow us to assess the data quality for oceanographic applications. The most important changes are observed in the equatorial band with the development of El Niño. From mid 2009 to spring 2010 a moderate El Niño event occured (see [109]). In second half of 2010 a moderate to strong La Niña event developped (see [110]) until spring 2011. During 2015, conditions indicate an El Niño event of strong intensity (see [20]).

	Winter	Spring	Summer	Fall
2008			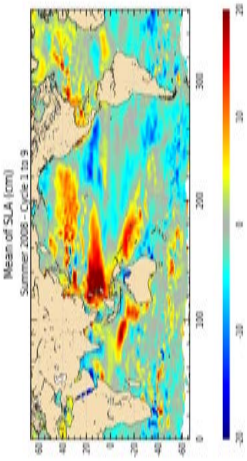	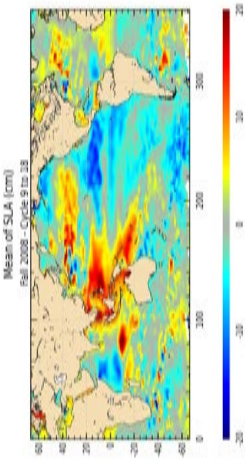
2009	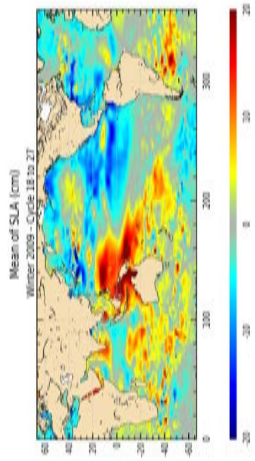	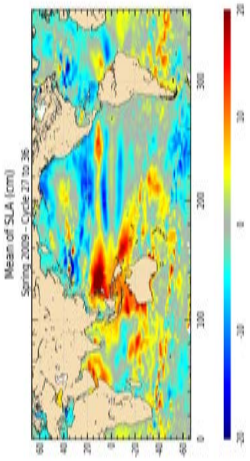	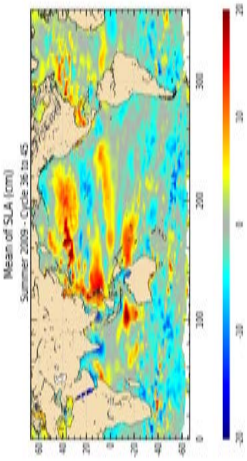	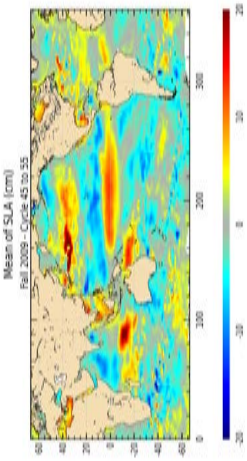
2010	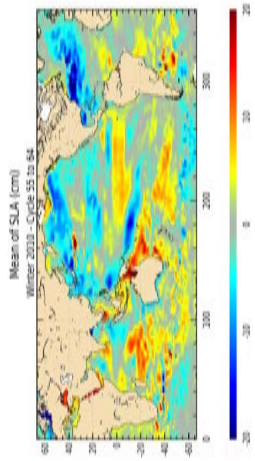	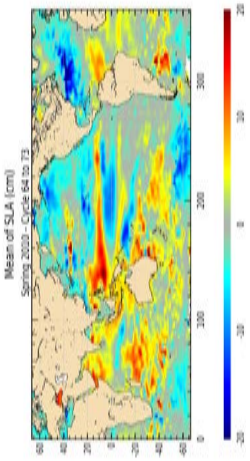	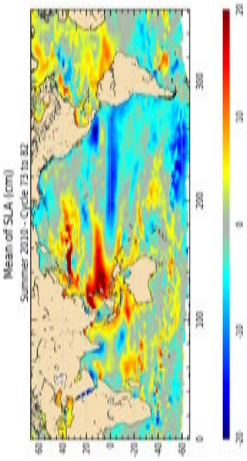	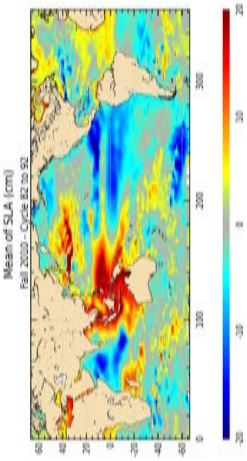

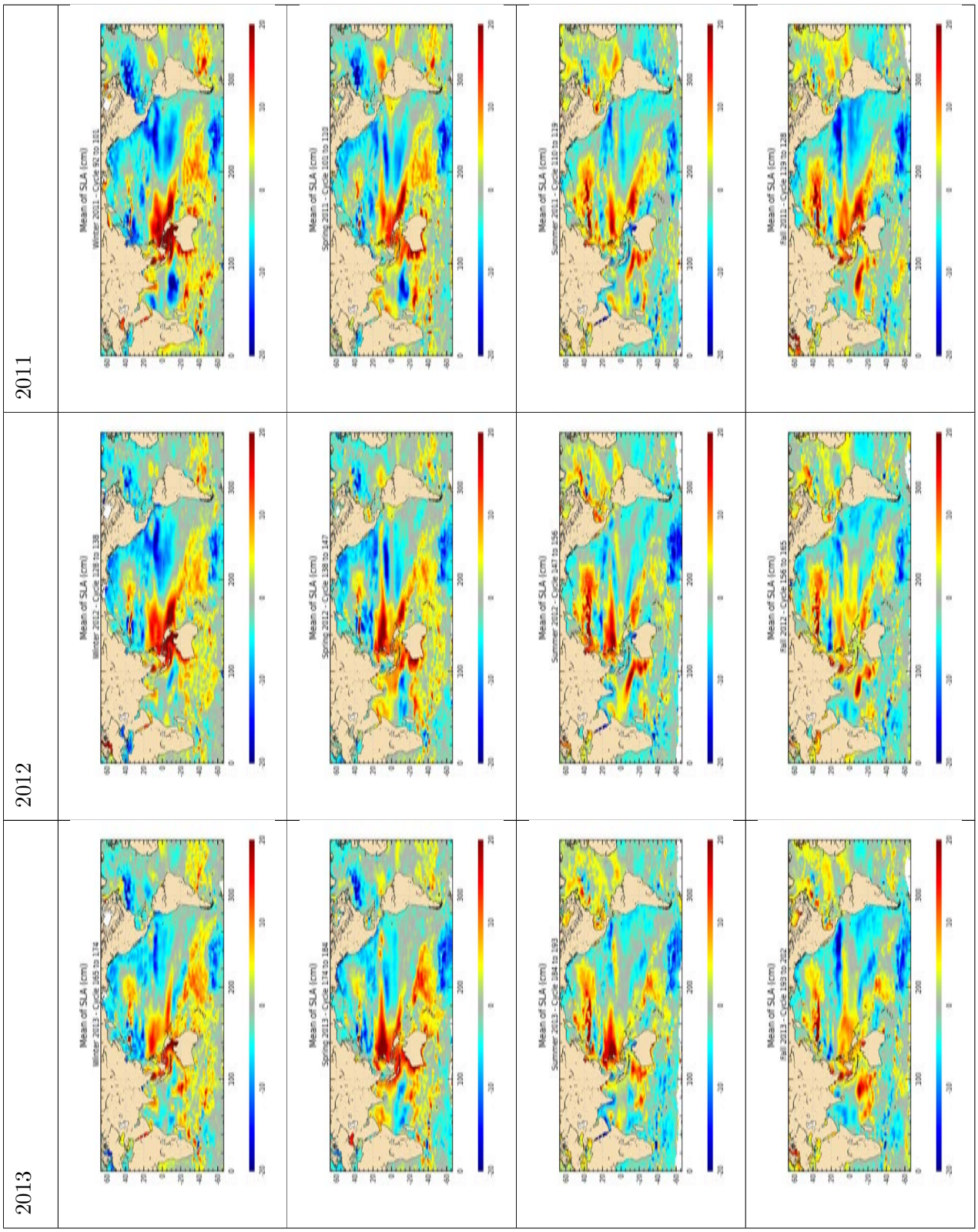
2011
2012
2013

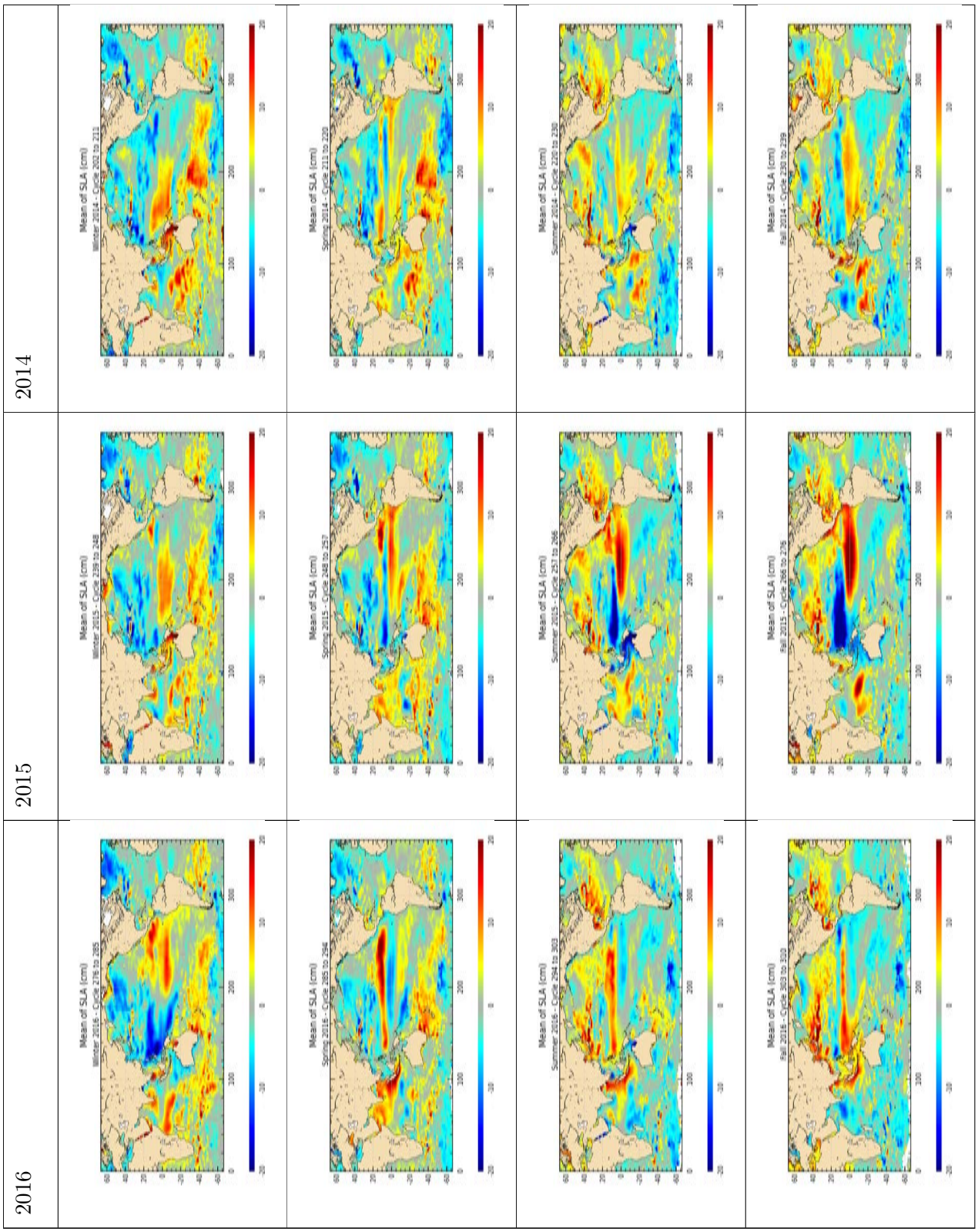

Table 8 – Seasonal variations of Jason SLA (cm) for years 2008 to 2016

7. Mean Sea Level (MSL) calculation

7.1. Altimeter Mean Sea Level evolution

7.1.1. Mean sea level (MSL) calculation of reference time serie

The global mean level of the oceans is one of the most important indicators of climate change. Precise monitoring of changes in the mean level of the oceans, particularly through the use of altimetry satellites, is vitally important, for understanding not just the climate but also the socioeconomic consequences of any rise in sea level. Thanks to the T/P, Jason-1, Jason-2 and now Jason-3 altimetry missions, the global MSL has been calculated on a continual basis since January 1993 (figure 55) highlighting a trend of 3.26 mm/yr (see http://www.aviso.oceanobs.com/msl). We connect Topex/Poseidon and Jason-1 at Jason-1's cycle 11 (May 2002) by subtracting a bias of -2.26 cm to Jason-1's MSL. We replaced Jason-1 by Jason-2 in the MSL time data series at Jason-2 cycle 11 (October 2008) by subtracting a bias of +3.9 cm to Jason-2's MSL as calculated previously (in addition to the bias between Jason-1 and Topex/Poseidon). The altimeter standards used are described on Aviso website (http://www.aviso.oceanobs.com/en/news/ocean-indicators/mean-sea-level/processing-corrections.html). To calculate a precise MSL rate, it is essential to link accurately time data series together. A study ([1]) showed the uncertainty on the global MSL trend resulting from the impact of MSL bias uncertainties between TOPEX-A and TOPEX-B (due to altimeter change in February 1999) and between TOPEX-B and Jason-1 (in May 2002) is close to 0.2 mm/yr from 1993 onwards. As we showed just previously, the SSH consistency between Jason-1 and Jason-2 is very good in space and stable in time during the tandem phase, the SSH bias uncertainty is consequently very weak and close to 0.5 mm. It is lower than between T/P and Jason-1 (estimated close to 1 mm ([1])). Its impact on global MSL trend error budget is thus very weak: lower than 0.05 mm/yr. Zawadzki et al ([108]) computed a confidence envelop of global MSL time-series deduced from Jason-1 and Jason-2 data, by tuning identified parameters (standards, data selection, average mesh grids, mission linking). The resulting envelop allowed to verify that AVISO and CU (University of Colorado) MSL stay within the confidence interval.
Notice, that MSL decreased in 2010/2011, similar, but much stronger to what was already observed in 2007. According to Boening et al. ([43] and [44]) the global mean sea level drop of 5 mm between beginning 2010 and mid-2011 is due to a decline of ocean mass coinciding with an equivalent increase in terrestrial water storage (primary over Australia, northern South America and Southeast Asia). The authors write, that this temporally shift of water from ocean to land is closely related to the transition from El Niño conditions in 2009/2010 to a strong 2010/2011 La Niña which affected precipitation patterns world wide. As these terrestrial water mass are not all directly linked to the ocean (thanks to rivers for example), they can only return to ocean thanks to evaporation. This process is long, which could explain the rise in GMSL in 2012.

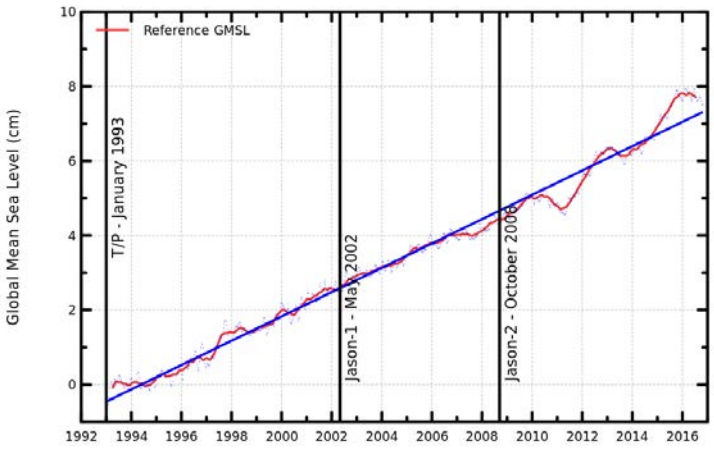

Figure 55 – MSL evolution calculated from T/P, Jason-1 and using Jason-2 data from October 2008 onwards. GIA (-0.3 mm/yr, [90]) is applied.

7.1.2. Regional and global mean sea level trend for Jason-2

Using radiometer wet troposphere correction increases for Jason-2 data the slope by around 0.2 mm/yr (left side of figure 56) compared to model wet tropopshere correction. Separating in ascending and descending passes, shows very similar slopes thanks to the POE-D standard (see right of figure 56). The amplitude of the MSL curve computed from descending passes is higher than for ascending passes. The difference between ascending and descending passes shows a signal of a period around 120 days (see also chapter 5.2.), that disappears when using POE-E final orbit solution.

The regional MSL trends over the Jason-2 period (figure 57) show an increase in eastern tropical pacific and a decrease in western tropical pacific. This is probably influenced by the El Niño conditions which occurred in 2015 ([111],[20]).

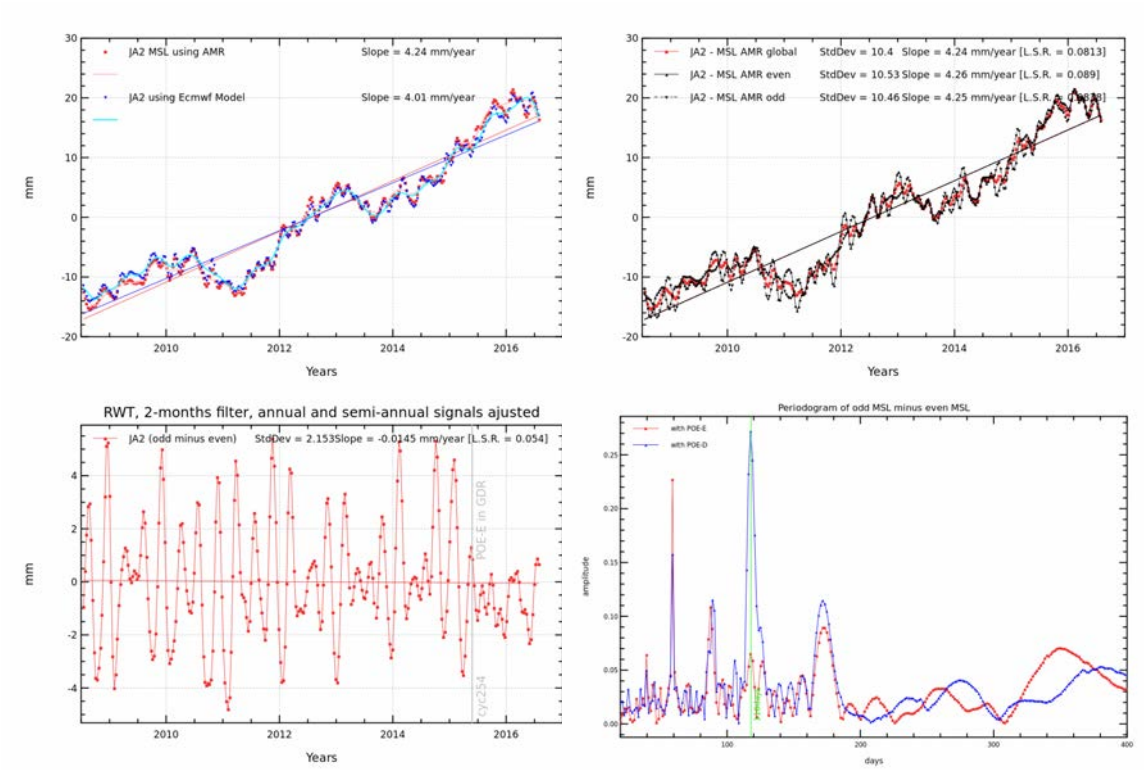

Figure 56 – Global MSL trend evolution calculated for Jason-2 (top left). MSL trend evolution when separating in ascending and descending passes (top right) , Seasonal signal (annual and semi-annual) is adjusted for top figures. Bottom: Difference of MSL slopes (MSL ascending passes - MSL descending passes) for Jason-2. Slopes are computed for 2 month filtered data. GIA correction is not applied. Bottom right: periodogram of MSL difference (MSL ascending passes - MSL descending passes)

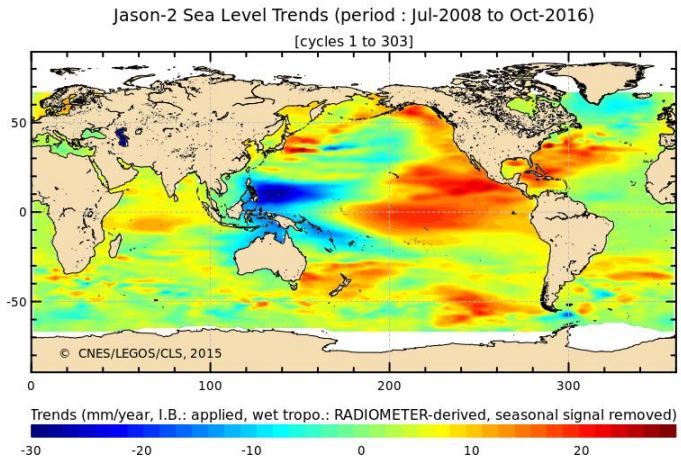

Figure 57 – Maps of regional MSL slopes for Jason-2 cycles 1 to 303, seasonal signal removed.

7.2. External data comparisons

In order to assess the global MSL trend, comparisons to independent in-situ datasets are of great interest. Two methods have been developed in the frame of in-situ Calval studies and thoroughly described in annual reports ([38] and [39]).

7.2.1. Comparison with tide gauges

Figure 58 displays the time series of global average differences between Jason-2 and tide gauges, either keeping (58a) or removing (58b) the seasonnal cycle. Considering both curves, the comparison with tide gauges measurements shows no long-term trend differences, around +0.1 mm/year. The formal adjustment error is low, close to 0.1/0.2 mm/yr, but we estimate that the total error of the method is larger, around 0.7 mm.yr [40].

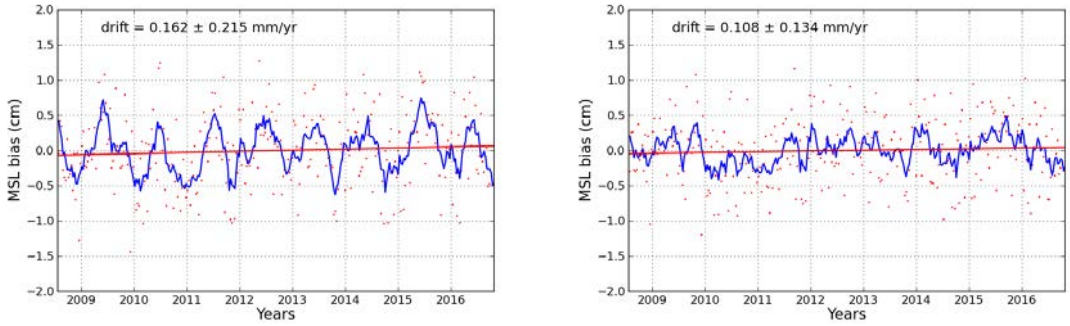

(a) with seasonnal signal *(b) seasonnal signal removed*

Figure 58 – Time series of global average differences between Jason-2 and tide gauges, with (58a) and without the seasonnal cycle (58b). The red points represent the raw data while the blue curve is obtained after applying a two months running mean filter

Figure 58 confirms the excellent stability of the Jason-2 mission with respect to tide gauges.

7.2.2. Altimeter calibration and validation by comparison with Argo in-situ measurements

Analyses comparing altimeter data with steric height derived from Argo profilers temperature salinity data have been used to compare the performances of altimeter standards and emphasize their improvment (e.g. pole tide altimeter correction as shown in the 2015 Alti TS report([37])). The 2016 Alti TS report ([39]) shows that the impact of evolving from standards 2014 to standards 2018 is not significant enough with respect to the accuracy of the SLA-DHA method to assess which standards offer the best performances for the Jason-2 products (table 9). Since standards accuracy is reaching the one of the method, new indicators have been developped. The 2016 Alti TS report ([39]) emphasizes that methods based on empirical orthogonal function analysis can be used to determine the trend of the SLA-DHA difference at regional scales. Using Jason-2 data and considering two orbit solutions differing in the use of different geocenter models, these exploratory methods showed promising results. As presented in figure 59, EOF decomposition allows to track the orbit solution differences and compute the SLA-DHA difference in these areas. As detailed

in the 2016 Alti TS ([39]) report the comparison of the drifts allows to determine the best orbit solution.

Global statistics DHA 900 dbar	**Correlation**	**rms diff**	**rms diff w.r.t rms DHA**
Jason-2 (Standards 2014)	0.75	5.5 cm	53.0%
Jason-2 (Standards 2018)	0.75	5.5 cm	52.9%

Table 9 – Correlation and rms of the differences between Jason-2 and Argo DHA referenced to 900 dbar over the period Aug. 2008 - Jul. 2016. Analyses performed for altimeter standards 2014 and 2018

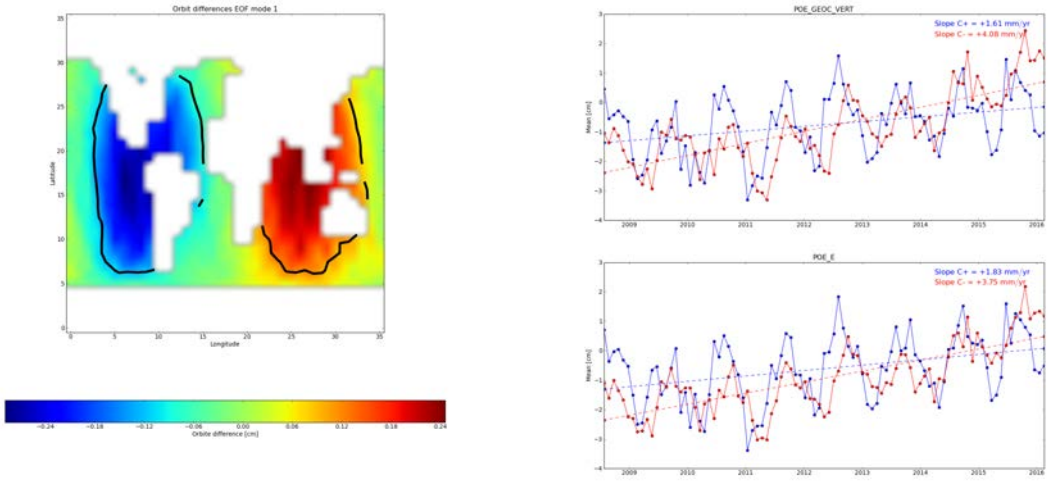

Figure 59 – Left : EOF mode 2 of the orbit differences and the contour defining areas of significant positive and negative difference. Right : SSH differences (cm) between altimeter and Argo data for Jason-2 computed with the GEOC-VERT (top) and POE-E (bottom) orbit solutions.

8. Investigations

8.1. Altimetry errors for submesoscale

8.1.1. Error Description

The sea level content provided by most of the conventional altimeters in low resolution mode (LRM) does not allowed the observation of ocean scales smaller than 80-100 km (Dibarboure et al.,2014 [60]). This limitation is mainly due to surface heterogeneities in the altimeter footprint (e.g. rain, sigma blooms) and the white noise level due to the instrumental noise and the measurement estimation. Hereafter, a quantification of these errors is presented.

A usual way to represent the error budget of altimeter missions at these small scales is to perform spectral analyses of sea-level anomalies. Such spectra based on Fourrier's transform are plotted in figure 60 for Jason-2, Jason-3 and SARAL/Altika at global scale and from high rate measurements. The noise level of each altimeter is easily deduced from the high frequency plateau of both missions. The white noise level is respectively estimated to 7.3 cm for Jason-2/Jason-3 and 5.4 cm for Altika, for significant wave height close to 2.7 m on average. This difference between both missions is mainly explains by the Altika high rate higher for Altika (40 Hz) than for Jason-2/Jason-3 (20 Hz). The noise level prevents the observation of small oceanic structures for distance (on average) close to 50 km for SARAL/Altika and 60 km for Jason-2/Jason-3. This distance is defined by the ratio between the oceanic signal slope and high frequency plateau equal to 1. This corresponds in figure 60 to the X-axis of the intersection between the high frequency plateau and the oceanic slope (Dufaut et al., 2016 [62]).

Furthermore, a large energy bump for wavelengths higher than few kilometers and lower than 100 km is observed as well as for Jason-2/Jason-3 as for SARAL/Altika (figure 60). Dibarboure et al., 2014 [60] described in details this signal and its origin. Basically, it is due to surface heterogeneities in the LRM footprint impacting altimetry measurements as for instance in areas impacted by rain cells or sigma bloom. The comparison of the observed SLA spectrum with the expected spectrum derived from the oceanic slope and the noise level (green, red and blue dash spectra in figure 60) allows the quantification of this error. At 80 km, about 50% of additional energy is measured. Therefore, the addition of this error and the white noise prevents the observation of small oceanic scales lower than 80-100 km (on average) for all the LRM missions.

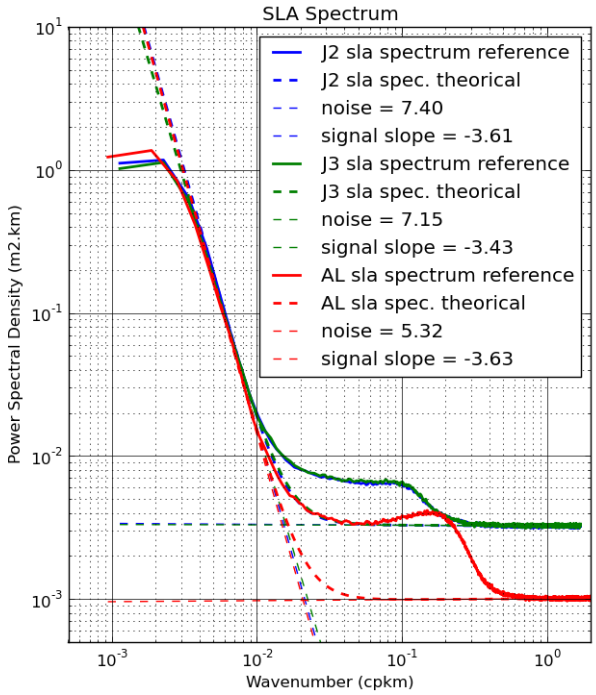

Figure 60 – SLA spectra for Jason-2/Jason-3 and SARAL Altika from respectively 20 Hz and 40 Hz measurements

8.1.2. Expected Improvements

The altimeter processing can have a strong impact on sea level performances at these small scales, as for instance the choice of retracking algorithms, empirical methods to reduce the altimeter noise or to remove spurious sea-level measurements. Furthermore, the improvements and benefits bring by Delay Doppler altimetry (or SARM) in terms of noise reduction and better across-track resolution allows avoiding this kind of artefact. In this way, the global SAR-mode coverage ensures by the recent Sentinel-3a mission (launched in February 2016), should significantly improve the observation and the understanding of small ocean scales. Hereafter, two methods have been further investigated to improve LRM measurements at small oceanic scales:

1. The development a better editing procedure adapted to the high rate measurements (20 hz or 40 hz). The schema below (61) gives the principle of the method.

2. The application of the empirical noise reduction method developed by (Zaron et al [107]), based on the correlation between the altimeter range and significant wave height noise : $\frac{\Delta SLA}{\Delta SWH} = \alpha + \beta SWH$.

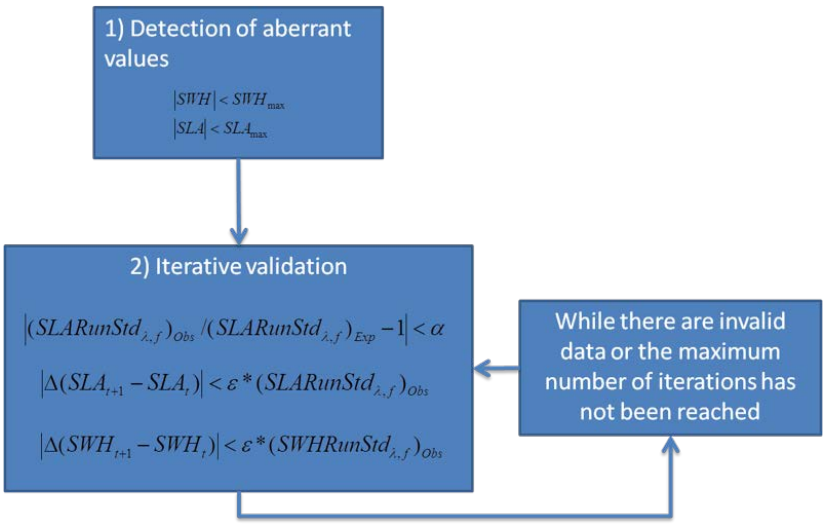

Figure 61 – Editing procedure adapted to high rate measurements for Jason-2/Jason-3 and SARAL/Altika missions

The impact of both new editing algorithm and Zaron's method (noted V1 hereafter) has been compared to Jason-2 data processed with a basic editing procedure (based on duplication of 1-Hz editing flag) and without any reduction flag (noted V0 hereafter).

Firstly, maps of variance reduction of SLA have been calculated filtering out along-track data lower than 200 km (figure 62). Significant SLA variance reduction is observed especially in areas where waveforms are disturbed by rain cells and sigma bloom events. On average, at global scale, the variance is reduced by about 2 cm^2. This statistic can reach 4-5 cm^2 in rain areas. The improvement in rain cells is mainly due to the new editing algorithm allowing a better detection of bad measurements. It is worth noting that about 3-4% of additional measurement have been removed (mainly in rain areas) compared to a classical 1-hz editing procedure.

Secondly, SLA spectra have been calculated for each V0 and V1 datasets (figure 63). A significant white noise reduction is observed by about 40% thanks to the Zaron's method. This allows the reduction of the Signal Noise Ratio (SNR) distance from about 60 to 50 km. A reduction of the spectral "bump" - characterizing the LRM errors at small oceanic scales - is also observed for distances lower than 30 km (figure 63 on right panel). However the spectral bump is just slightly modified for distances between 30 and 80 km. Unfortunately, these distances are of main interest for submesoscale studies. This means that the improvements described here do not really improved the observations of mesoscale structures on average at global scale. However, in specific areas with small altimeter range noise (i.e. small SWH), observations of smaller oceanic structures is likely possible. It is also worth noting that SLA spectrum analyses with classical Fourrier's transfom only reflect the altimer sea-level performances in areas with segment long enough (1000 km). In other words, this also means that SLA spectrum analyses are not adapted to measure the improvement in rain areas where segment are too short.

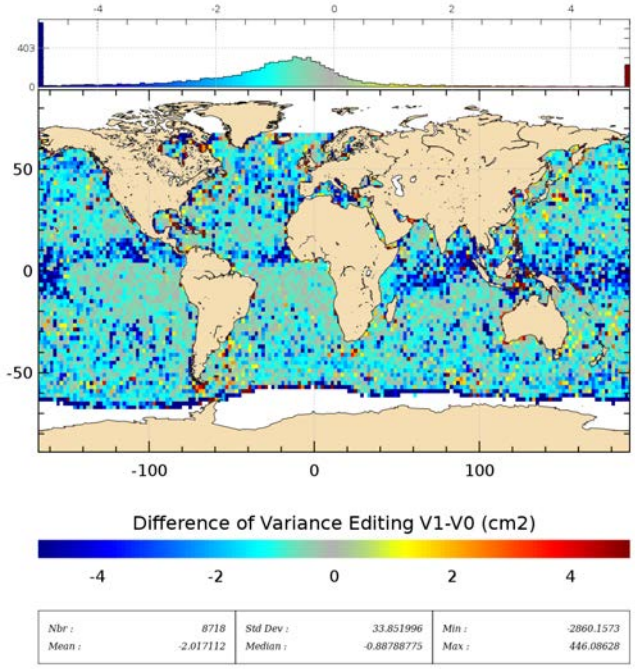

Figure 62 – Map of SLA variance reduction applying new editing and Zaron's method (V1) compared to data processed with classical 1-Hz editing procedure (V0), after filtering out along-track data lower than 200 km.

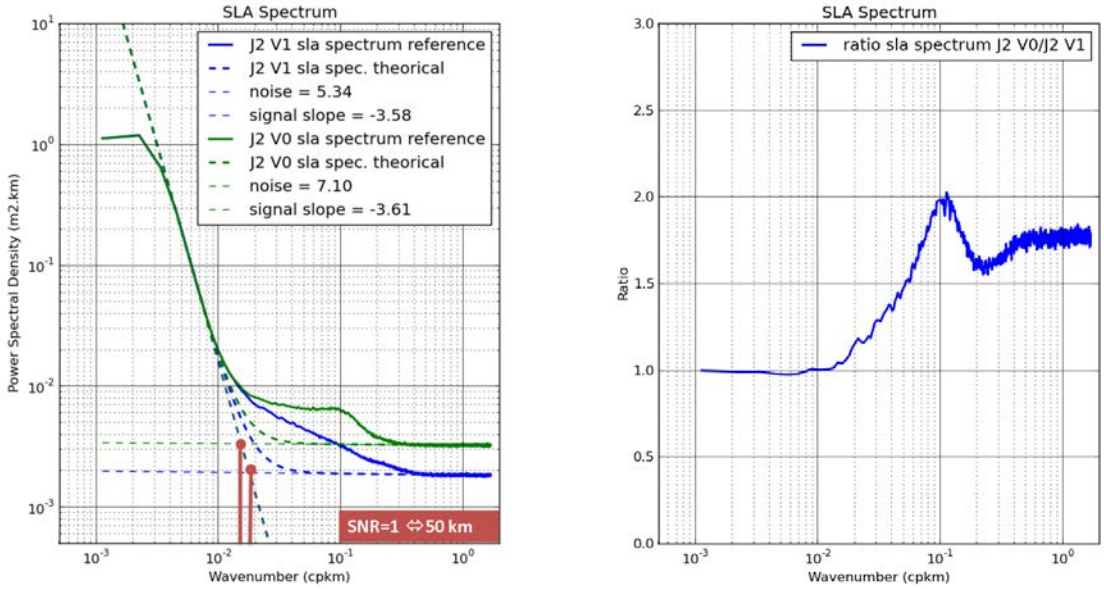

Figure 63 – SLA spectra applying new editing and Zaron's method (V1) compared to data processed with classical 1-Hz editing procedure (V0) : classical power spectral density spectra with theoretical spectra superimposed (dashed lines) on left and spectra differences between classical and theoretical spectra on right. Theoretical spectrum is defined from the oceanic slope (as observed by model) and the white noise level (plateau).

8.2. Assessment of orbit quality through the SSH calculation towards POE-E standards

For all nadir altimetry missions, the quality of the orbit ephemerides is crucial for the computation of the Sea Surface Height (SSH). Impacting mostly large scales, spatially and temporally, the errors attributed to the orbit are worse being quantified and analyzed precisely.

Conversely, to assess evolutions of the orbit computation, having a realistic knowledge of the impact on the SSH quality efficiently completes the intrinsic orbit based diagnosis. Indeed, it provides an external reference (the SSH) to benchmark different orbit solutions and to detect remaining weakness with a very fine precision.
All detailed results are present in the Annual report 2016 of activities of Orbit validation using altimetry [29]. The studies dedicated to Jason 2 mission are sumed up here after.

8.2.1. Quality of the current CNES POE orbits

Since end 2015 and during 2016, all prescise orbit ephemeris standards (POE) were upgraded from a GDR-D to GDR-E. It was necessary to evaluate the quality of new standard thanks to absolute diagnosis based on a direct estimation error of Sea Surface Height and by comparison with others standards.

Comparison with GDR-D standards shows that the upgrade to GDR E has no impact on MSL but improve scales below 10 days.

One of the most relevant absolute diagnosis to quantify orbital errors is the map of average difference of Sea Surface Height (SSH), plotted on Figure 64 with the new standard GDR E. It highlights the systematic discrepancies between coincident ascending and descending tracks separated by less than 10 days (insuring a good stability of ocean variability) and thus a potential error on the SSH estimation. Jason 2 mission has a very homogeneous and clean map of average difference of Sea Surface Height. In average, all the differences are below +/-1cm.

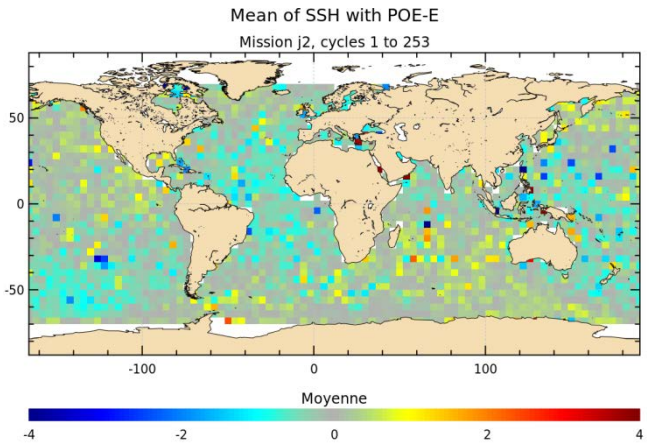

Figure 64 – Map of the mean difference of SSH at crossovers

8.2.2. Quality of the GSFC orbits

During this year, the new standard of GSFC (GSFC 15) was studied in comparison with the old one (GSFC 12) and the new standard of the CNES (GDR E) (see Figure 65).
This analysies show that for Jason 2 mission changing GSCF12 for GSFC15 gives more homogenous maps of the mean difference of Sea Surface Height at crossovers, has a strong impact on regional MSL trend but low impact on global MSL.

Finaly, the comparison between GSFC15 and POE E, evidences that the CNES orbit has better performances at crossovers as shown on Figure 65 .

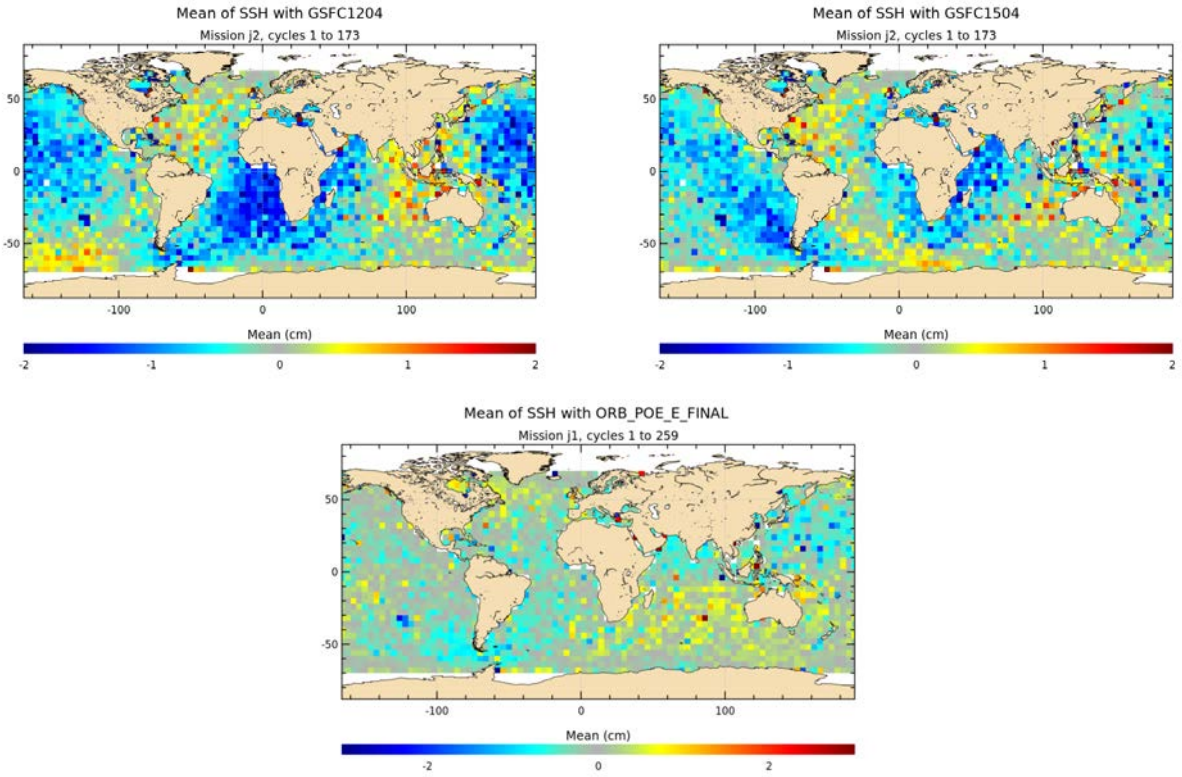

Figure 65 – On left : GSFC12 - Rigth : GSFC15- Bottom: GDR E

8.2.3. Impact on orbits of the geocenter position change

New GDR-E standards are reaching a very good quality.
Thanks to GRACE-based models, Gravity field errors are now much reduced. Smaller errors –considered as negligible before- are now observable.
This highlighted the fact that changing the geocenter position can induce millimetric variations on the orbits (order of magnitude of the precision required for climate studies) with a potential impact on climate scales.

A sensitivity study was performed this year on Jason-2 mission to analyze this point. It will be carried on in 2017.

9. Appendix

9.1. Jason-2 performance assessment: from meso-scale to climate

Jason-2 performance assessment: from meso-scale to climate

H. Roinard[1], S. Philipps[1], O. Lauret[1], M. Ablain[1], N. Picot[2], J.D. Desjonquères[2]

Contact: equipe-calval-jason@cls.fr

1. CLS, Toulouse, France
2. CNES, Toulouse, France

➢ **Cycle 303 is the last OSTM/Jason-2 cycle on the nominal ground track.**
➢ **Jason-2 in WAIT mode and collected no measurements until end of move of orbit maneuvers.**
➢ **Jason-2 has been moved to its interleaved orbit, with the first cycle 305 beginning on October 14th, 2016 (cycle 305 pass 164).**

Main performance metrics

Data availability

➢ Data availability over ocean is excellent with >99% of available data, SHM, calibrations and incidents included,
➢ After removing calibration and incidents, more than 99,9% of data over ocean are available.

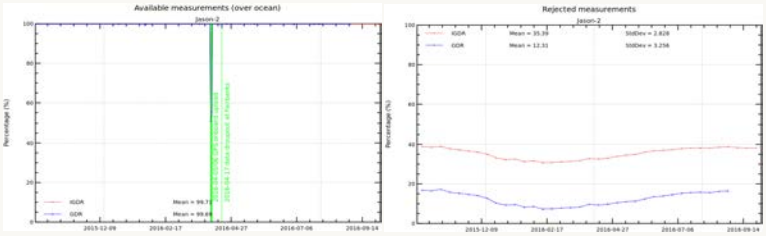

Percentage of available (left) and edited (right) ocean data, from 2015-10-01 onwards

Crossovers

➢ Sea Level performances: SSH error for Jason-2 is deduced from crossovers analyses using radiometer data (selecting |latitudes| < 50°, bathy<-1000m, oceanic variability < 20 cm)
  ➢ SSH error is close to **3.5 cm** for temporal scales < 10 days
➢ mean difference between ascending and descending tracks is near zero (-0.1 cm),
➢ Spatial distribution of mean SSH differences shows no geographically correlated patches with differences remaining below 1 cm,
➢ Crossovers analysis demonstrates the excellent performance of Jason-2

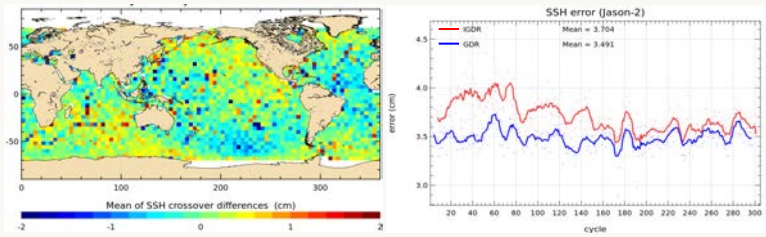

Performance at Xovers: [left] map of mean SSH differences (cycle 001 to 300)
[right] SSH error deduced from SSH crossovers

Other aspects

- Long-term evolution of Jason-1 and Jason-2 altimeter wind speed over ocean highlights a 3-4 cm.s-1/yr rise at global scale over a 15-year period.
- The very good altimeter stability for Jason missions gives a good confidence in its global indicator

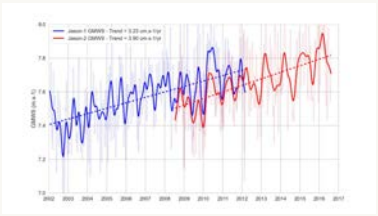

Long-term evolution of Jason-1 and Jason-2 altimeter wind speed over ocean

Global long-term sea level stability

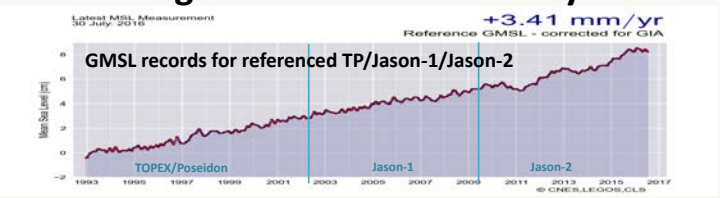

- MSL Jason-2 is used as the reference to compute the MSL from 2008 onwards
  [*see Aviso+ website, MSL* : http://www.aviso.oceanobs.com/msl/]
- Jason-2 GMSL stable with TG (within an uncertainty of 0.7 mm/yr)
- Better agreement between Jason-2 and Tide Gauge than with other missions

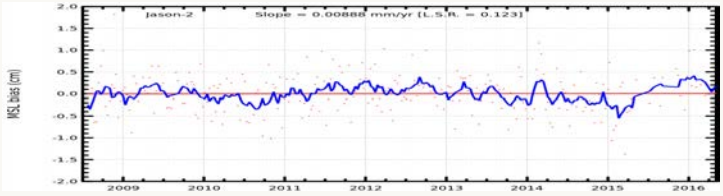

Jason-2 minus Tide Gauges differences

- Radiometer minus model wet tropospheric differences drifted over year 2015. During year 2016, some calibrations allowed to insure the correction stability.

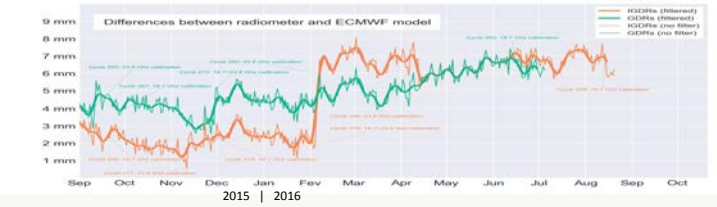

Radiometer minus model wet tropospheric differences for Jason-2: IGDR and GDR

High resolution capabilities

- Jason-2 measurements do not provide observable ocean small scales below 80-100 km due to the instrumental noise level and footprint contamination - rain cells, sigma blooms (Dibarboure et al., 2014)
- However post-processing algorithms can improve Jason-2 high resolution capabilities: new altimeter retracking, adapted method to edit spurious measurements at 20 hz, empirical method to reduce the reduction of retracker-related noise (Zaron et al, 2016)

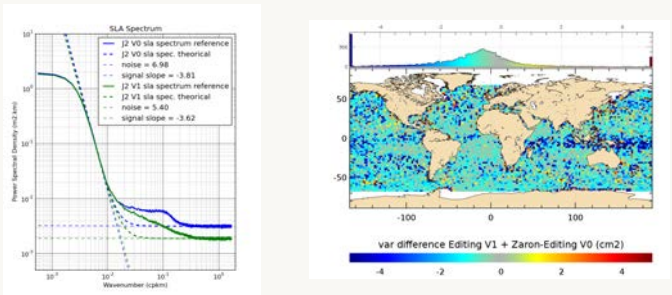

Reduction of Jason-2 sea level error bellow 100 km

Conclusions

- The Jason-2 mission gave data of excellent quality for more than 8 years on the historical TOPEX/Poseidon and Jason-1 ground track
- It flew for 8,5 months in a tandem phase with Jason-3, allowing the calibration of the new referenced mission.
- The mission has begun on October 14th a second life on an interleaved ground track (the same as TOPEX or Jason-1 in the past).
- Mission performance remains excellent
- All mission performance parameters are routinely checked by Cal/Val teams.
- Nevertheless improvements of Jason-2 products are possible:
  - ➢ For climate scales (orbit, radiometer wet troposphere correction, …)
  - ➢ For mesoscale (retracking (bump reduction), new editing strategies, …)
  - ➢ New geophysical corrections (ocean tides, sea state bias, …)
- CalVal activities on Jason-2 are still needed and useful:
  - ➢ Jason-2 is useful for validation activities for Jason-3
  - ➢ Once Jason-3 is reference mission, Jason-2 will continue to contribute to improvement of mesoscale during the interleaved phase

OST/ST meeting, Oct 31st- Nov 4th, 2016

10. References

References

[1] Ablain, M., A. Cazenave, G. Valladeau, and S. Guinehut. 2009 : A new assessment of the error budget of global mean sea level rate estimated by satellite altimetry over 1993-2008. *Ocean Sci*, **5, 193-201**. Available at http://www.ocean-sci.net/5/193/2009/os-5-193-2009.pdf

[2] Ablain, M., S. Philipps, 2006, Topex/Poseidon 2005 annual validation report, Topex/Poseidon validation activities, 13 years of T/P data (GDR-Ms).

[3] Ablain, M., S. Philipps, M. Urvoy, N. Tran, and N. Picot (2012) Detection of Long-Term Instabilities on Altimeter Backscattering Coefficient Thanks to Wind Speed Data Comparisons from Altimeters and Models, *Marine Geodesy*, **35:S1, 258-275**. Available at http://www.tandfonline.com/doi/pdf/10.1080/01490419.2012.718675

[4] Ablain, M., G. Larnicol, Y. Faugère, A. Cazenave, B. Meyssignac, N. Picot, J. Benveniste, 2012. Error Characterization of altimetry measurements at Climate Scales. Oral presentation at OSTST meeting, Venice, Italy, 27-28 September 2012. Available at: http://www.aviso.altimetry.fr/fileadmin/documents/OSTST/2012/oral/02_friday_28/04_errors_uncertainties_I/03_EU1_Ablain.pdf

[5] AVISO and PODAAC User Handbook. IGDR and GDR Jason-1 Products. Edition 4.1, October 2008. SMM-MU-M5-OP-13184-CN (AVISO), JPL D-21352 (PODAAC). Available at http://www.aviso.oceanobs.com/fileadmin/documents/data/tools/hdbk_j1_gdr.pdf.

[6] Beckley, B. D. , Zelensky, N. P. , Holmes, S. A. , Lemoine, F. G. , Ray, R. D. , Mitchum, G. T. , Desai, S. D. and Brown, S. T. (2010) Assessment of the Jason-2 Extension to the TOPEX/Poseidon, Jason-1 Sea-Surface Height Time Series for Global Mean Sea Level Monitoring, *Marine Geodesy*, **33:1, 447 - 471**. Available at http://pdfserve.informaworld.com/96442__925511460.pdf

[7] Bertiger, Willy , Desai, Shailen D. , Dorsey, Angie , Haines, Bruce J. , Harvey, Nate , Kuang, Da. , Sibthorpe, Ant and Weiss, Jan P. (2010) Sub-Centimeter Precision Orbit Determination with GPS for Ocean Altimetry. *Marine Geodesy*, **33:1, 363 - 378**. Available at http://pdfserve.informaworld.com/858128__925510150.pdf

[8] Bertiger, Willy , Desai, Shailen D. , Haines, Bruce J., R. DeCarvalho, and A. Dorsey (2010) Jason-2/OSTM Precision Orbit Determination with GPS *Oral presentation at OSTST meetting, Lisbon, Portugal*, Available at http://www.aviso.oceanobs.com/fileadmin/documents/OSTST/2010/oral/19_Tuesday/bertiger.pdf

[9] E. Bronner and G. Dibarboure, May 24th, 2012: Technical Note about the Jason-1 Geodetic Mission. *SALP-NT-MA-EA-16267-CNv1.0*. Available at: http://www.aviso.oceanobs.com/fileadmin/documents/data/duacs/Technical_Note_J1_Geodetic_Mission.pdf

[10] Valladeau, G., S. Philipps. Jason-1 validation and cross calibration activities (Annual report 2009).SALP-RP-MA-EA-21795-CLS, CLS.DOS/NT/10-005.

[11] Valladeau, G., S. Philipps. Jason-1 validation and cross calibration activities (Annual report 2010).SALP-RP-MA-EA-21903-CLS, CLS.DOS/NT/10-332.

[12] Roinard H., Philipps S., Ablain M., Valladeau G., and Legeais J.-F., Jason-1 validation and cross calibration activities (Annual report 2013). Reference: CLS.DOS/NT/13-226. Nomenclature: SALP-RP-MA-EA-22269-CLS. Available at http://www.aviso.oceanobs.com/fileadmin/documents/calval/validation_report/J1/annual_report_j1_2013.pdf.

[13] Roinard H., Philipps S.: Jason-1 GDR-E release. Global assessment over ocean. SALP-RP-MA-EA-22426-CLS. Available at http://www.aviso.altimetry.fr/fileadmin/documents/calval/validation_report/J1/Jason1_ReprocessingReport_GDR_E.pdf

[14] Philipps, S., M. Ablain, G. Valladeau, and J.-F. Legeais. Jason-2 validation and cross calibration activities (Annual report 2011). Reference: CLS.DOS/NT/12-005. Nomenclature: SALP-RP-MA-EA-22042-CLS. Available at http://www.aviso.oceanobs.com/fileadmin/documents/calval/validation_report/J2/annual_report_j2_2011.pdf.

[15] Philipps, S., M. Ablain, G. Valladeau, and J.-F. Legeais. Jason-2 validation and cross calibration activities (Annual report 2012). Reference: CLS.DOS/NT/12-223. Nomenclature: SALP-RP-MA-EA-22141-CLS. Available at http://www.aviso.oceanobs.com/fileadmin/documents/calval/validation_report/J2/annual_report_j2_2012.pdf.

[16] Roinard, H., Philipps S., Jason-2 reprocessing impact on ocean data (cycles 001 to 020). Comparison of Jason-2 Gdr-D with Gdr-T, as well as with Jason-1 Gdr-C. SALP-RP-MA-EA-22118-CLS. CLS.DOS/NT/12.138. Available at ftp://avisoftp.cnes.fr/AVISO/pub/jason-2/documentation/gdr_d_calval_report/JA2_GDR_D_validation_report_cycles1to20_V1_1.pdf

[17] Roinard, H., S. Philipps. Jason-2 reprocessing impact on ocean data (cycles 001 to 145). Comparison of Jason-2 Gdr-D with Gdr-T, as well as with Jason-1 Gdr-C and Envisat Gdr v2.1. SALP-RP-MA-EA-22140-CLS. CLS.DOS/NT/12.222.

[18] Philipps, S., H. Roinard, M. Ablain, G. Valladeau, and J.-F. Legeais. Jason-2 validation and cross calibration activities (Annual report 2013). Reference: CLS.DOS/NT/13-227. Nomenclature: SALP-RP-MA-EA-22270-CLS. Available at http://www.aviso.oceanobs.com/fileadmin/documents/calval/validation_report/J2/annual_report_j2_2013.pdf.

[19] Philipps, S., H. Roinard, M. Ablain, G. Valladeau, and J.-F. Legeais. Jason-2 validation and cross calibration activities (Annual report 2014).

[20] Philipps, S., H. Roinard, M. Ablain, G. Valladeau, and J.-F. Legeais. Jason-2 validation and cross calibration activities (Annual report 2015).

[21] Lauret O. Jason-3 validation and cross calibration activities (Annual report 2016). SALP-RP-MA-EA-23060-CLS.

[22] Ollivier A., M. Guibbaud. Envisat RA2/MWR ocean data validation and cross-calibration activities. Yearly report 2012. SALP-RP-MA-EA-22163-CLS, CLS.DOS/NT/12-292.

[23] A. Ollivier. M. Guibbaud. Envisat RA2/MWR ocean data validation and cross calibration activities (Yearly report 2013). Reference: CLS.DOS/NT/13-290. Nomenclature: SALP-RP-MA-EA-22293-CLS.

[24] M. Guibbaud. A. Ollivier. Envisat RA2/MWR ocean data validation and cross calibration activities (Yearly report 2014). Reference: CLS.DOS/NT/14-253. Nomenclature: SALP-RP-MA-EA-22396-CLS.

[25] S. Philipps. Saral/AltiKa validation and cross calibration activities (Annual report 2013). Reference: CLS.DOS/NT/13-228. Nomenclature: SALP-RP-MA-EA-22271-CLS.

[26] P. Prandi. Saral/AltiKa validation and cross calibration activities (Annual report 2014). Reference: CLS.DOS/NT/14-234. Nomenclature: SALP-RP-MA-EA-22418-CLS.

[27] P. Prandi. Saral/AltiKa validation and cross calibration activities (Annual report 2015). Reference: CLS.DOS/NT/15-064. Nomenclature: SALP-RP-MA-EA-22957-CLS.

[28] P. Prandi. Saral/AltiKa validation and cross calibration activities (Annual report 2016). Nomenclature: SALP-RP-MA-EA-23073-CLS.

[29] A. Ollivier Yearly report 2016 as parts as SALP activities (Annual report 2016).

[30] Valladeau, G.. Validation of altimetric data by comparison with tide gauge measurements for TOPEX/Poseidon, Jason-1, Jason-2 and Envisat. SALP-NT-MA-EA-22157-CLS, CLS.DOS/NT/12-259.

[31] Legeais J.-F. and S. Dupuy. 2012 annual report: Validation of altimeter data by comparison with in-situ T/S Argo profiles for T/P, Jason-1, Jason-2 and Envisat missions. CLS-DOS/NT/12-261. SALP-RP-MA-EA-22176-CLS.

[32] Valladeau G. and Prandi P., 2013:Validation of altimeter data by comparison with tide gauge measurements for TOPEX/Poseidon, Jason-1, Jason-2 and Envisat (Annual report 2013). [CLS.DOS/NT/13-262].

[33] Legeais J.F. and Ablain M., 2013: Validation of altimetric data by comparison with in-situ T/S Argo profiles (Annual Report 2013) [SALP-RP-MA-EA-22281-CLS, CLS.DOS/NT/13-256]

[34] Prandi P., Valladeau G., 2014:Validation of altimeter data by comparison with tide gauge measurements for TOPEX/Poseidon, Jason-1, Jason-2 and Envisat (Annual report 2014). [SALP-RP-MA-EA-22419-CLS, CLS.DOS/NT/15-020].

[35] Prandi P., Legeais J.F. and Ablain M., 2014: Validation of altimetric data by comparison with in-situ T/S Argo profiles (Annual Report 2014) [SALP-RP-MA-EA-22406-CLS, CLS.DOS/NT/15-007]

[36] Prandi P., Valladeau G., 2015:Validation of altimeter data by comparison with tide gauge measurements for TOPEX/Poseidon, Jason-1, Jason-2 and Envisat (Annual report 2015). [SALP-RP-MA-EA-22956-CLS, CLS.DOS/NT/15-062].

[37] Prandi P., Legeais J.F. and Ablain M., 2015: Validation of altimetric data by comparison with in-situ T/S Argo profiles (Annual Report 2015) [SALP-RP-MA-EA-22966-CLS, CLS.DOS/NT/15-068]

[38] Prandi P., Debout V.: Validation of altimeter data by comparison with tide gauges measurements: yearly report 2016 for TOPEX/Poseidon, Jason-1, Jason-2, ERS-2, Envisat and SARAL/AltiKa. SALP-RP-MA-EA-23082-CLS.

[39] Zawadzski L., Taburet N.: Validation of altimeter data by comparison with in-situ T/S Argo profiles (Annual Report 2016). SALP-RP-MA-EA-22966-CLS.

[40] Valladeau, G., J.F. Legeais, M. Ablain, S. Guinehut, and N. Picot, 2012: Comparing altimetry with tide gauges and Argo profiling floats for data quality assessment and Mean Sea Level studies. Marine Geodesy 2012, DOI: 10.1080/01490419.2012.718226.

[41] Legeais J.-F., P. Prandi, M. Ablain and S. Guinehut: Analyses of altimetry errors using Argo and GRACE data. Ocean Science Discussion, doi:10.5194/os-2015-111, in review, 2016.

[42] Bond, N. A., M. F. Cronin, H. Freeland, and N. Mantua (2015), Causes and impacts of the 2014 warm anomaly in the NE Pacific. *Geophys. Res. Lett.*, 42, 3414–3420. doi: 10.1002/2015GL063306.

[43] Boening, C., J. K. Willis, F. W. Landerer, R. S. Nerem, and J. Fasullo (2012), The 2011 La Niña: So Strong, the Oceans Fell, *Geophys. Res. Lett.*, doi:10.1029/2012GL053055, in press.

[44] John T. Fasullo , C. Boening, F. W. Landerer, R. S. Nerem (2013), Australia's Unique Infuence on Global Sea Level in 2010-2011, doi:10.1002/grl.50834, in press.

[45] Boy, François and Jean-Damien Desjonqueres. 2010. Note technique datation de l'instant de reflexion des échos altimètres pour POSEIDON2 et POSEIDON3 *Reference: TP3-JPOS3-NT-1616-CNES*

[46] Brown G.S., "The average impulse response of a rough surface and its application", *IEEE Transactions on Antenna and Propagation*, Vol. AP 25, N1, pp. 67-74, Jan. 1977.

[47] Brown S., S. Desai, and W. Lu "Initial on-orbit performance assessment of the advanced microwave radiometer and performance of JMR GDR-C", *Oral presentation at OSTST meeting, Nice, France, 9-12 november 2008*. Available at http://www.aviso.oceanobs.com/fileadmin/documents/OSTST/2008/oral/brown_calval.pdf

[48] Brown, S., S. Desai, W. Lu, and A. Sibthorpe. 2009. Performance Assessment of the Advanced Microwave Radiometer after 1 Year in Orbit. *Oral presentation at OSTST meeting, Seattle, USA*. Available at: http://www.aviso.oceanobs.com/fileadmin/documents/OSTST/2009/oral/Brown.pdf

[49] S. Brown. 2010. A Novel Near-Land Radiometer Wet Path-Delay Retrieval Algorithm: Application to the Jason-2/OSTM Advanced Microwave radiometer. *IEEE TGRS vol. 48 n ° 4*. Available at ftp://podaac.jpl.nasa.gov/allData/ostm/preview/L2/AMR/docs/Brown_TGARS_2010.pdf

[50] Cerri, L. , Berthias, J. P. , Bertiger, W. I. , Haines, B. J. , Lemoine, F. G. , Mercier, F. , Ries, J. C. , Willis, P. , Zelensky, N. P. and Ziebart, M. (2010) Precision Orbit Determination Standards for the Jason Series of Altimeter Missions, *Marine Geodesy*, **33:1, 379 - 418**. Available at http://pdfserve.informaworld.com/816985__925509111.pdf

[51] Cerri, L., A. Couhert, S. Houry, F. Mercier. 2011. Improving the long-term stability of the GDR orbit solutions. *Oral presentation at OSTST meeting, San Diego, USA*. Available at http://www.aviso.oceanobs.com/fileadmin/documents/OSTST/2011/oral/02_Thursday/Splinter3POD/05_Cerri.pdf.

[52] Chambers, D., P., J. Ries, T. Urban, and S. Hayes. 2002. Results of global intercomparison between TOPEX and Jason measurements and models. *Paper presented at the Jason-1 and TOPEX/Poseidon Science Working Team Meeting, Biarritz (France), 10-12 June.*

[53] Collard, F. (2005). Algorithmes de vent et période moyenne des vagues JASON à base de réseaux de neurons. BO-021-CLS-0407-RF. Boost Technologies.

[54] Commien, L., S. Philipps, M. Ablain and N. Picot. 2009. SSALTO CALVAL Performance assessment Jason-1 GDR "C"/GDR "b". *Poster presented at OSTST meeting, Seattle, USA*. Available at: http://www.aviso.oceanobs.com/fileadmin/documents/OSTST/2009/poster/commien.pdf

[55] Couhert, A., L. Cerri, F. Mercier, S. Houry. 2010. Status of Jason-1 and Jason-2 GDR orbits. *Talk presented at OSTST meeting, Lisbon, Portugal*. Available at: http://www.aviso.oceanobs.com/fileadmin/documents/OSTST/2010/oral/couhert.pdf

[56] DeCarvalho, R., S. Brown, B. Haines and S. Desai. 2009. Global cross calibration and validation of the Jason-1 and Jason-2/OSTM data products. *Oral presentation at OSTST meeting, Seattle, USA*. Available at: http://www.aviso.oceanobs.com/fileadmin/documents/OSTST/2009/oral/deCarvalho.pdf

[57] Desjonqueres, J.-D., G. Carayon, J.-L. Courriere, and N. Steunou "POSEIDON-2 In-Flight results", *Oral presentation at OSTST meeting, Nice, France, 9-12 november 2008*. Available at http://www.aviso.oceanobs.com/fileadmin/documents/OSTST/2008/oral/desjonqueres.pdf

[58] Desjonquères, J. D. , Carayon, G. , Steunou, N. and Lambin, J. (2010) Poseidon-3 Radar Altimeter: New Modes and In-Flight Performances, *Marine Geodesy*, **33:1, 53 - 79**. Available at http://pdfserve.informaworld.com/542982__925503482.pdf

[59] Dettmering, Denise and Bosch, Wolfgang (2010) Global Calibration of Jason-2 by Multi-Mission Crossover Analysis, *Marine Geodesy*, **33:1, 150 - 161**. Available at http://pdfserve.informaworld.com/315039__925510361.pdf

[60] - Dibarboure, G., F. Boy, J. D. Desjonqueres, S. Labroue, Y. Lasne, N. Picot, J. C. Poisson, and P. Thibaut, 2014: Investigating short-wavelength correlated errors on low-resolution mode altimetry. *J. Atmos. Oceanic Technol.*, **31**, 1337–1362, doi:10.1175/JTECH-D-13-00081.1

[61] Dorandeu.,J., M. Ablain, Y. Faugère, F. Mertz, 2004 : Jason-1 global statistical evaluation and performance assessment. Calibration and cross-calibration results. *Marine Geodesy* **27: 345-372.**

[62] - Dufau, C., M. Orsztynowicz,G. Dibarboure, R. Morrow, and P.-Y. Le Traon (2016), Mesoscale resolution capability of altimetry:Present and future, *J. Geophys. Res.Oceans*, **121**, doi:10.1002/2015JC010904.

[63] Faugère, Y. et al. 2009. The SLOOP project: preparing the next generation of altimetry products for open ocean. *Poster presented at OSTST meeting, Seattle, USA*. Available at: http://www.aviso.oceanobs.com/fileadmin/documents/OSTST/2009/poster/Faugere2.pdf

[64] Faugère, Y. et al. 2010. CROSS-CALIBRATION between ENVISAT and JASON-1/2. *Oral presentation at OSTST meeting, Lisbon, Portugal*. Available at: http://www.aviso.oceanobs.com/fileadmin/documents/OSTST/2010/oral/19_Tuesday/Tuesday_afternoon/faugere.pdf

[65] Jason-2 Version "T" Geophysical Data Records : Public Release, August 2009. Available at : http://www.aviso.oceanobs.com/fileadmin/documents/data/products/Jason-2_GDR_T_disclaimer.pdf

[66] Renaudie C., S. Philipps, 2014: Comparison of the latest GSFC SLR/DORIS std1204 orbits with current orbits for TP,J1 and J2. CLS Ramonville St Agne.

[67] Gourrion, J., Vandemark, D., Bailey, S., Chapron, B., Gommenginger, G.P., Challenor, P.G. and Srokosz, M.A., 2002: A two-parameter wind speed algorithm for Ku-band altimeters, *Journal of Atmospheric and Oceanic Technology*. **19(12) 2030-2048**.

[68] http://grgs.obs-mip.fr/grace/variable-models-grace-lageos/mean_fields

[69] Dumont, J.-P., V. Rosmorduc, N. Picot, S. Desai, H. Bonekamp, J. Figa, J. Lillibridge, R. Sharroo, 2011: OSTM/Jason-2 Products Handbook. CNES: SALP-MU-M-OP-15815-CN. EUMETSAT: EUM/OPS-JAS/MAN/08/0041. JPL: OSTM-29-1237. NOAA/NESDIS: Polar Series/OSTM J400. Available at http://www.aviso.oceanobs.com/fileadmin/documents/data/tools/hdbk_j2.pdf

[70] Hernandez, F. and P. Schaeffer, 2000: Altimetric Mean Sea Surfaces and Gravity Anomaly maps inter-comparisons. AVI-NT-011-5242-CLS, 48 pp. CLS Ramonville St Agne.

[71] Huffman, G. and D.T.Bolvin, 2009: TRMM and Other Data Precipitation Data Set Documentation. Available at ftp://precip.gsfc.nasa.gov/pub/trmmdocs/3B42_3B43_doc.pdf

[72] Imel, D.A. 1994. Evaluation of the TOPEX/POSEIDON dual-frequency ionospheric correction. *J. Geophys. Res.*, **99, 24,895-24,906**.

[73] Jalabert,E., A.Couhert, J. Moyard, F. Mercier, S. Houry, S. Rios-Bergantinos. 2015. JASON-2, SARAL AND CRYOSAT-2 STATUS. *Talk presented at OSTST meeting, Reston, USA, 20-23 October 2015.*http://meetings.aviso.altimetry.fr/fileadmin/user_upload/tx_ausyclsseminar/files/OSTST2015/POD-01-Jalabert.pdf

[74] Lemoine, F.G., Zelensky N.P., Chinn, D.S., et al. (2010), Towards development of a consistent orbit series for TOPEX, Jason-1, and Jason-2 Adv. Space Res., 46(12), 1513–1540, doi: 10.1016/j.asr.2010.05.007 (updated).

[75] Lemoine, F., N.P. Zelensky, S. Melachroinos, D.S. Chinn, B.D. Beckley, D.D. Rowlands, and S.B. Luthcke. 2011. GSFC OSTM (Jason-2), Jason-1 & TOPEX POD Update. *Oral presentation at OSTST meeting, San Diego, USA*. Available at http://www.aviso.oceanobs.com/fileadmin/documents/OSTST/2011/oral/02_Thursday/SplinterPOD/03Lemoine_etal_SWT2011_v01.pdf.

[76] Lemoine F., N.P. Zelensky, D.S. Chinn, B.D. Beckley, D.E. Pavlis, J. Wimert, O. Bordyugov. 2014 : New GSC POD Standards for TOPEX/Poseidon, Jason-1, Jason-2 (OSTM). *Oral presentation at OSTST meeting, Konstanz, Germany*. Available at http://www.aviso.altimetry.fr/fr/coin-utilisateur/equipes-scientifiques/sci-teams.html.

[77] Le Traon, P.-Y., J. Stum, J. Dorandeu, P. Gaspar, and P. Vincent, 1994: Global statistical analysis of TOPEX and POSEIDON data. *J. Geophys. Res.*,**99, 24619-24631.**

[78] MSEs (CNES, NASA, NOAA, EUMETSAT). 2011. GDR Status. *Oral presentation (by N. Picot) at OSTST meeting, San Diego, USA*. Available at http://www.aviso.oceanobs.com/fileadmin/documents/OSTST/2011/oral/03_Friday/Plenary/GDRProducts/02PicotGDR_status_2011.pdf.

[79] Aviso one-satellite-based Mean Sea Level reprocessing, http://www.aviso.altimetry.fr/fileadmin/documents/data/products/indic/msl/MSL_reprocessing_201402.pdf.

[80] Moyard J., E. Jalabert, A. Couhert, S. Rios-Bergantinos, F. Mercier, S.Houry. 2014 : Jason-2 POD status. *Oral presentation at OSTST meeting, Konstanz, Germany.* Available at http://www.aviso.altimetry.fr/fr/coin-utilisateur/equipes-scientifiques/sci-teams.html.

[81] Roinard,H., S.Philipps, O.Lauret, M.Ablain, E.Bronner, N.Picot. Jason-1 GDR-E reprocessing. *Talk presented at OSTST meeting, Reston, USA, 20-23 October 2015.* http://meetings.aviso.altimetry.fr/fileadmin/user_upload/tx_ausyclsseminar/files/Poster_OSTST15_JASON-1_GDR-E_Reprocessing.pdf.

[82] Obligis, E., L. Eymard, M. Ablain, B. Picard, J.F. Legeais, Y. Faugere and N. Picot, 2010. The wet tropospheric correction for altimetry missions: A mean sea level issue. *Oral presentation at OSTST meeting, Lisbon, Portugal.* Available at http://www.aviso.oceanobs.com/fileadmin/documents/OSTST/2010/oral/19_Tuesday/OBLIGIS.pdf.

[83] Ollivier A., Faugere Y., Granier N., 2008: Envisat RA-2/MWR ocean data validation and cross-calibration activities. Yearly report. Technical Note CLS.DOS/NT/09.10, Contract N° SALP-RP-MA-EA-21633-CLS http://www.aviso.oceanobs.com/fileadmin/documents/calval/validation_report/EN/annual_report_en_2008.pdf

[84] Ollivier A., Faugere Y., P. Thibaut, G. Dibarboure, and J.-C. Poisson, 2008: Investigation on the high frequency content of Jason-1 and Jason-2. CLS.DOS/NT/09-027

[85] Ollivier A., M. Guibbaud, Faugere Y. Envisat RA2/MWR ocean data validation and cross-calibration activities. Yearly report 2011. SALP-RP-MA-EA-22062-CLS, CLS.DOS/NT/12-021.

[86] Ollivier A., A. Couhert, V. Pignot, C. Renaudie, S. Phillips, N. Picot, 2014 : Assessment of orbit quality through the SSH calculation towards GDR-E standards. *Oral presentation at OSTST meeting, Constance, Germany.* Available at http://www.aviso.altimetry.fr/fr/coin-utilisateur/equipes-scientifiques/sci-teams.html

[87] Ollivier A., S. Philipps, M. Ablain, A. Edwell, L. Cerri, N. Picot, 2013 : Assessment of Orbit Quality through the Sea Surface Height calculation, New insight in resolving long term and inter-annual signal for climate studies. *Oral presentation at OSTST meeting, Boulder, USA.* Available at http://www.aviso.altimetry.fr/fr/coin-utilisateur/equipes-scientifiques/sci-teams.html

[88] Ollivier A., Dibarboure G., Picard B., Ablain M., OSTST2014, Konstanz - Germany, "Spectral analysis of altimetric signal and errors Towards a spectral error budget of Nadir Altimetric missions" http://meetings.aviso.altimetry.fr/fileadmin/user_upload/tx_ausyclsseminar/files/30Ball0900-2_Pres_OSTST2014_J2_ErrorBugdet_Spectra_Ollivier.pdf

[89] Otten M., C. Flohrer, T. Springer, and W. Enderle. 2011. Generating precise and homogeneous orbits for Jason-1 and Jason-2. *Oral presentation at OSTST meeting, San Diego, USA.* Available at http://www.aviso.oceanobs.com/fileadmin/documents/OSTST/2011/oral/03_Friday/Splinter6POD/01_Otten.pdf.

[90] Peltier, 2004, Global Glacial Isostasy And The Surface of The Ice-Age Earth: The ICE-5G (VM2) Model and GRACE. *Annual Review of Earth and Planetary Sciences*, May 2004, **Vol. 32, Pages 111-149**, doi: 10.1146/annurev.earth.32.082503.144359

[91] Philipps, S., M. Ablain, J. Dorandeu, P. Thibaut, N. Picot and J. Lambin. 2006. SSALTO CAL-VAL Performance assessment Jason-1 GDR 'B'/GDR 'A'. *Poster presented at OSTST meeting, Hobbart, Australia*. Available at: http://www.aviso.oceanobs.com/fileadmin/documents/OSTST/2006/ablain1.pdf

[92] Picot, N., P. Thibaut, N. Tran, S. Philipps, J.C. Poisson, T. Moreau, and E. Bronner. 2010. New Jason-2 GDR-C standards. *Oral presentation at OSTST meeting, Lisbon, Portugal*. Available at http://www.aviso.oceanobs.com/fileadmin/documents/OSTST/2010/oral/PThibaut_Jason2.pdf.

[93] Picot, N., P. Thibaut, N. Tran, S. Philipps, J.C. Poisson, E. Bronner, C. Garcia and many others. 2011. Jason-2 GDR-D standards. *Oral presentation at OSTST meeting, San Diego, USA*. Available at http://www.aviso.oceanobs.com/fileadmin/documents/OSTST/2011/oral/02_Thursday/Splinter5IP/05NPicot_et_al_OSTST_2011_J2-GDRD-Standards.pdf.

[94] Schaeffer, P., A. Ollivier, Y. Faugere, E. Bronner, and N. Picot. The new CNES CLS 2010 Mean Sea Surface. *Oral presentation at OSTST meeting, Lisbon, Portugal, 18-20 october 2010*. Available at http://www.aviso.oceanobs.com/fileadmin/documents/OSTST/2010/oral/19_Tuesday/Schaeffer.pdf.

[95] Schaeffer, P., Y. Faugere, J.-F. Legeais, A. Ollivier, T. Guinle, and N. Picot (2012). The CNES_CLS11 Global Mean Sea Surface Computed from 16 Years of Satellite Altimeter Data. *Marine Geodesy* **35: sup1, 3-19**. Available at http://www.tandfonline.com/doi/abs/10.1080/01490419.2012.718231

[96] DUACS/Aviso team 'A new version of SSALTO/Duacs products available in April 2014' http://www.aviso.altimetry.fr/fileadmin/documents/data/duacs/Duacs2014.pdf

[97] Scharroo, R., J. Lillibridge, and W.H.F. Smith, 2004: Cross-calibration and long-term monitoring of the Microwave Radiometers of ERS, Topex, GFO, Jason-1 and Envisat. Marine Geodesy, 97.

[98] Solar Radio Flux (10.7cm) (daily solar data). Available at http://www.swpc.noaa.gov/ftpmenu/indices/old_indices.html

[99] Thibaut, P. O.Z. Zanifé, J.P. Dumont, J. Dorandeu, N. Picot, and P. Vincent, 2002. Data editing: The MQE criterion. *Paper presented at the Jason-1 and TOPEX/Poseidon Science Working Team Meeting, New-Orleans (USA), 21-23 October*.

[100] Thibaut, P., J.-C. Poisson, A. Ollivier, S. Philipps, and M. Ablain: "Jason-2 waveforms, tracking and retracking analysis", *Oral presentation at OSTST meeting, Nice, France, 9-12 november 2008*. Available at http://www.aviso.oceanobs.com/fileadmin/documents/OSTST/2008/oral/thibaut.pdf

[101] Moreau, T., P. Thibaut, 2009. Etude dépointage Poseidon-3: optimisation de l'angle d'ouverture d'antenne. CLS-DOS-NT-09-028. 15 pp, CLS Ramonville St. Agne.

[102] P. Thibaut. Bilan des activités d'expertise altimétriques menées en 2009 : Lot 2D. SALP-RP-MA-EA-21808-CLS, CLS-DOS-NT-10-029.

[103] Tran, N. , Labroue, S. , Philipps, S. , Bronner, E. and Picot, N. (2010) Overview and Update of the Sea State Bias Corrections for the Jason-2, Jason-1 and TOPEX Missions, *Marine Geodesy*,**33:1, 348 - 362**. Avialable at http://pdfserve.informaworld.com/804727__925502357.pdf

[104] Tran, N., P. Thibaut, J.-C. Poisson, S. Philipps, E. Bronner, and N. Picot. Jason-1, Jason-2 and TOPEX Sea State Bias. Overview and Updates. *Oral presentation at OSTST meeting, Lisbon, Portugal, 18-20 october 2010*. Avialable at http://www.aviso.oceanobs.com/fileadmin/documents/OSTST/2010/oral/TRAN.pdf

[105] N. Tran, S. Philipps, J.-C. Poisson, S. Urien, E. Bronner, and N. Picot. Impact of GDR_D standards on SSB corrections. *Oral presentation at OSTST meeting, Venice, Italy, 27-28 September 2012*. Available at http://www.aviso.oceanobs.com/fileadmin/documents/OSTST/2012/oral/02_friday_28/01_instr_processing_I/01_IP1_Tran.pdf.

[106] Zlotnicky, V. 1994. Correlated environnemental corrections in TOPEX/POSEIDON, with a note on ionomospheric accuracy. *J. Geophys. Res.*, **99, 24,907-24,914**

[107] Edward D. Zaron , Robert deCarvalho, 2016. Identification and Reduction of Retracker-Related Noise in Altimeter-Derived Sea Surface Height Measurements. *Journal of Atmospheric and Oceanic Technology*, p201-210, doi:10.1175/JTECH-D-15-0164.1

[108] Zawaszki, L., M. Ablain, A. Cazenave, B. Meyssignac. 2014. Confidence envelop of the Global MSL time-series deduced from Jason-1 and Jason-2 altimetric missions. *Poster presentation at OSTST meeting, Constance, Germany, 28-31 October 2014*, Available at http://meetings.aviso.altimetry.fr/fileadmin/user_upload/tx_ausyclsseminar/files/Poster_OSTST14_GMSLUncertainty.pdf

[109] World Meteorological Organization, 2010: El Nino/ La Nina Update (30 March 2010). Available at http://www.wmo.ch/pages/prog/wcp/wcasp/documents/El_Nino_Mar10_Eng.pdf.

[110] World Meteorological Organization, 2011: El Nino/ La Nina Update (25 January 2011). Available at http://www.wmo.ch/pages/prog/wcp/wcasp/documents/El-Nino_Jan11_Eng.pdf.

[111] World Meteorological Organization, 2015: El Nino/ La Nina Update (16 November 2015). Available at http://www.wmo.int/pages/prog/wcp/wcasp/documents/WMO_ENSO_Nov15_Eng.pdf

[112] Correction Troposphérique Humide pour le radiomètre Jason-3 : approche neuronale. CLS-J3PROTO-15-0002. Projet CNES PEACHI-J3